THE EFFECTS OF ANNEALING ON PHASE TRANSFORMATION IN PLATINUM-MOLYBDENUM COATINGS

Dissertation presented for the degree of Master of Science in Department of Physics at the University of Cape Town.

By

Zakhelumuzi Mesuli Khumalo

KHMZAK001

Supervisor:

Prof. M. Blumenthal

Physics Department

University of Cape Town

Co-supervisors:

Emer. Prof. C. Comrie

Physics Department

University of Cape Town

Dr. M. Topić

Material Research Department

iThemba LABS, National Research Foundation

August 2012

DECLARATION

I know the meaning of plagiarism and declare that all of the work in the dissertation, save for which is properly acknowledged, is my own.

Signature: ……

Date: ……

ABSTRACT

The thermodynamic study of platinum binary systems has both fundamental and applied aspects. It is due to the fact that the formation of ordered phases increases the strength and surface hardness and could also have an impact on surface activity and chemical properties. The changes in mechanical, physical and chemical properties could be of significant importance in enhancing the performance of platinum-based systems in their respective applications, such as gas sensors, catalyst, fuel cells and superconductors.

In this investigation, the phase transformation in Pt-Mo coated systems induced by thermal annealing was studied by X-ray diffraction, scanning electron microscope, transmission electron microscope, energy dispersive X-ray emission and Rutherford backscattering spectrometry. The phase analysis showed the presence of several intermetalic phases, Pt_2Mo, PtMo and Pt_2Mo_3 which were observed to nucleate in sequence when the annealing time and temperature were extended. RBS analysis showed an increase in coating thickness after annealing which has been attributed to the formation of the Pt-Mo phases.

In addition Pt_2Mo phase was detected over a wide Pt compositional range of about 65 *at%* to 80 *at%*. It was also found that the stability of these phases depends on annealing time and coating thickness. The EDX analyses revealed the increase in molybdenum concentration on the surface of the coatings with increasing annealing time.

ACKNOWLEDGEMENTS

Firstly I would like to extend my gratitude to the almighty God for allowing me to complete this challenging work. I would also like to extend my appreciation to the following persons, without their honest assistance and motivation this work would not have been possible:

- Dr. M. Topić; iThemba LABS, Materials Research Department, for her honest Co-supervision throughout this research.
- Prof. C. Comrie; University of Cape Town, Physics department, for being my Co-supervisor and guiding me during RBS analysis.
- Prof. M. Blumenthal; University of Cape Town, Physics department, for being my supervisor.
- Dr. R. Bucher; iThemba LABS, Materials Research Department, for guiding me during XRD analysis.
- Prof. C. Pineda and Mr. P. Sechogela; iThemba LABS, Materials Research Department, for their help in RBS measurements.
- Dr. M. Nkosi; iThemba LABS, Materials Research Department, for guiding me during the preparation of coatings using electron beam evaporator.
- Prof. R. P. Vinci; Lehigh University, Materials Science and Engineering Department, for his help in the preparation of co-deposited samples.
- Mr. K. Kisslinger; Center for Functional Nanomaterials in Brookhaven National Laboratory (USA), for his help in the preparation of TEM sample.
- Prof. D. Aschman; University of Cape Town, the former head of Physics Department, for giving me the opportunity to further my studies at this university.

- Ms. M. Waldron; University of Cape Town, Electron Microscope Unit, for guiding me during SEM and EDX experiments.
- Dr. S. Botha; University of the Western Cape, Electron Microscope Unit, for helping in taking TEM images and EDX analyses.
- Dr. R. Nemutudi; iThemba LABS, the former head of Materials Research Department, for his help and encouragement throughout the project.
- Mintek, Department of Science and Technology (DST) and South African National Research Foundation (NRF) for financial support.
- The use of the facilities of iThemba LABS (Material Research Department), Center for Functional Nanomaterials (Brookhaven National Laboratory, USA), Materials Science and Engineering Department (Lehigh University, USA), Electron Microscope Unit (University of Cape Town) and Electron Microscope Unit (University of the Western Cape) is gratefully acknowledged.
- iThemba LABS, Materials Research Department staff and postgraduate students, for being a family to me.
- My deepest thanks extend to my late mother Gcinile Buthelezi-Khumalo whom I lost during the course of this work, may her soul rest in peace.
- My siblings; Thokozani, Scelokuhle, Nokwazi, Ntombi, Sengiphiwe and Ntombezinhle for their motivation and understanding throughout this research.
- My father Sukumisa Khumalo for his understanding and always wishing me well.
- Ms. T. Dlakude and my Sons, for their support and understanding during this long study.
- All my friends, even outside academic environment, for their friendship and encouragement.

- Ngibonga kini nonke boKhumalo, Mtungwa, Mbulaz'omnyama abathibedla umuntu bebe bemyega ngendaba, nina boMzilikazi kaMashobana, Mabaso owabas'entabeni kwadliwa ilanga lishona.

TABLE OF CONTENTS

LIST OF FIGURES

LIST OF TABLES

CHAPTER 1 INTRODUCTION AND LITERATURE REVIEW

1.1 Introduction

The study of the behaviour of materials under different environmental conditions such as temperature and time is of fundamental importance in the field of materials science. The structure of materials e.g. crystallite size, lattice parameters, atomic arrangement and the existence of defects has a significant influence on the mechanical, physical and electrical properties of various materials which in turn govern their performances into their respective applications**[1, 2]**. Hence the changes in the macrostructure, caused by environmental factors such as temperature and irradiation, are of significant importance for the application of platinum systems in many applications.

Platinum based systems are used in many applications including gas sensors, fuel cells, superconductivity, in glass industry and catalysts, wherein the surface properties, such as surface hardness and wear, corrosion and oxidation resistance play a significant role **[3]**. The current research is, however, restricted to the effects of annealing on the phase transformation in one Pt system, namely the Pt-Mo system. Recently the application of the inter-metallic phases of this system as cathode material for the production of hydrogen by electrolysis, to reduce energy consumption, has been reported **[4, 5]**. It has also been reported that products made of platinum coated molybdenum, such as stirrers, mandrels and electrodes, have useful lives at high temperatures up to 1200°C due to the excellent high temperature mechanical properties of the refractory metals and the outstanding oxidation resistance of the platinum metals **[3]**. However, it has also been reported that the appearance of a molybdenum rich phase (e.g. A15-type $PtMo_6$), formed at high temperatures above 1300°C, could develop high interfacial strains in the platinum

cladding of molybdenum which result in the failure of the product in harsh environment application **[6]**. The Pt-Mo phase transformation study is, therefore, believed to be of great importance in determining the limitations of the Pt-Mo products to be applied in harsh environments.

1.2 Aim of the research

The aim of this research is twofold. Firstly it is to study the phase transformation sequence in the Pt-Mo system. The phase formation sequence will be investigated by varying the annealing parameters as well as Pt coating thickness. The interest in the phase formation sequence is based on the fact that a particular phase or phases with desirable properties can be produced by controlling experimental parameters (temperature and time) in order to manufacture systems for specific applications. Secondly, the aim is to develop a better understanding of the Pt-Mo phase diagram, particularly in the Pt rich region. Pt rich compounds are known for their application as catalysts as well as jewellery alloys **[7, 8]**. The current existing phase diagram however, reveals only two Pt rich compounds, PtMo and Pt_2Mo phases, both of which can exist over a fairly wide compositional range. In the compositional range 70 *at%* to 80 *at%* Pt, the phase diagram indicates the presence of a two phase region, namely Pt_2Mo plus Pt-solid solution.

1.3 Literature review

1.3.1 The platinum-molybdenum system

The Pt-Mo phase diagram has been studied by many researchers **[9-16]**. Elliot **[9]** reported four Pt-Mo single phase regions: body centred cubic (b.c.c.) Mo-solid solution, hexagonal phase with Pt compositional range of about 30 to 55 *at%*, tetragonally distorted body centered structure with

concentration range between 65 and 80 *at%* Pt, and face centered cubic (f.c.c) Pt-solid solution. Two other Pt-Mo phases were reported by Rooksby *et al.* **[10]**. The compounds were Pt_2Mo with orthorhombic crystal structure and cubic A15-type $PtMo_6$ in the Mo rich of the phase diagram. The Pt_2Mo phase was reported to have unit cell lattice parameters *a=2.732 Å, b=4.900 Å, c=4.476 Å.* Dwight *et al.* **[11],** however, did not confirm the 2:1 stoichiometry of the orthorhombic (Pt_2Mo) phase and instead reported an orthorhombic PtMo (1:1) phase with lattice parameters *a′=4.475 Å (≈ c), b′=2.729 Å (≈ a), c′=4.918 Å (≈ b).* Sadagopan *et al.* **[12]** reported that the A15 phase is best represented by the formula Mo_3 ($Mo_{0.4}$, $Pt_{0.6}$) while Raub *et al.* **[13]** found, however, that the A15 phase is formed only in the presence of impurities such as oxygen. In addition there was no verification of a distorted tetragonal f.c.c (Pt_3Mo) phase, reported by other researchers **[9, 10]**, according to Maldonado *et al.* **[14]** when doing the study of the arc-melted polycrystalline samples of Pt-Mo system. They instead reported Pt_2Mo phase to be orthorhombic with unit cell parameters *a=2.748 Å, b=8.238 Å* and *c=3.915 Å.* Their findings were consistent with the work done by Ocken *et al.* and Flukiger *et al*. **[15, 16]** as the researchers also reported Pt_2Mo phase to be orthorhombic with lattice parameters *a=2.758 Å, b=8.270 Å* and *c=3.940 Å.* In addition the researchers also reported this phase (Pt_2Mo) to be an ordered form of the terminal f.c.c. Pt solid solution phase. Therefore the replacement of a tetragonal Pt_3Mo phase by orthorhombic Pt_2Mo phase was proposed after their observations.

The Pt-Mo phase diagram presently used was proposed by Brewer *et al.* **[17]**, Fig. 1.1, based mainly on the work of other researchers **[10-16]**. The phase diagram shows the existence of seven single phase regions: b.c.c. Mo-solid solution (α), A15 type $PtMo_6$ (β), disordered HCP Mg-type (ε) and ordered hexagonal Mg_3Cd-type Pt_2Mo_3 ($\acute{\varepsilon}$), orthorhombic PtMo (δ), orthorhombic Pt_2Mo (η) and f.c.c. Pt-solid solution (γ). The Pt-Mo compounds, as displayed on

the phase diagram, were later confirmed by Rechard *et al.* **[18]**. The researchers conducting tests on Pt-coated Mo-Ti-Zr (ZTM) alloy with and without diffusion barriers reported that Mo atoms, in the alloys with no diffusion barriers, diffused into the platinum coating to form two intemetallic compounds (Pt_2Mo and PtMo).

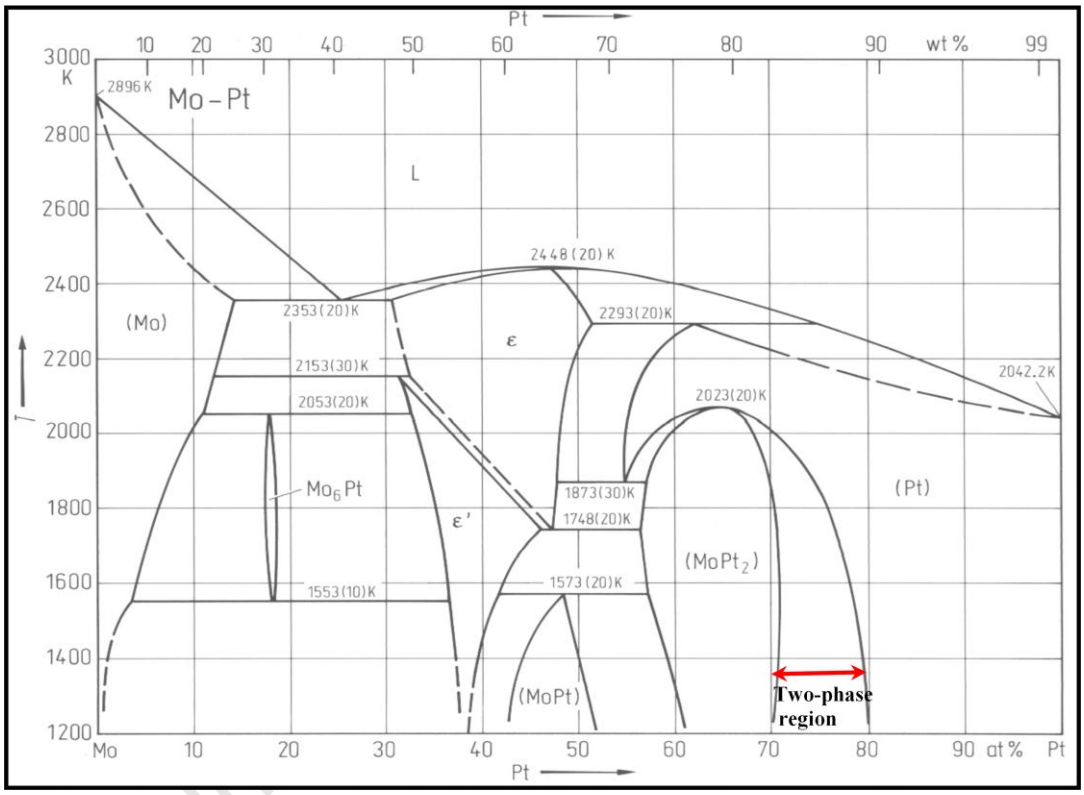

Figure 1.1: Platinum-Molybdenum phase diagram for bulk materials [17], showing the existence of seven single phase regions. The two–phase region in the Pt compositional range 70 *at %* to 80 *at%* is marked

Table 1.1 displays all the phases in the phase diagram with their symbol representations as well as their lattice parameters as suggested in the literature **[10-16]**. It has been noticed that the phase

diagram has a region left unmarked due to the unverified stoichiometric composition in the Pt rich region, currently indicated as two-phase region.

Table 1.1: Lattice parameters of Pt-Mo phases

Phase	Crystal structure	Lattice Parameters (Å)		
		a	***b***	***c***
Pt(Mo), γ	**f.c.c**	3.927	3.927	3.927
$MoPt_2$, η	**Orthorhombic**	2.758	8.270	3.940
MoPt, δ	**Orthorhombic**	4.475	2.729	4.918
Mo_3Pt_2(ordered),έ	**Hexagonal**	5.615	5.615	4.489
Mo_3Pt_2 (disordered), ε	**Hexagonal**	2.808	2.808	4.500
Mo_6Pt, β	**b.c.c**	4.989	4.989	4.989
Mo(Pt), α	**b.c.c**	3.147	3.147	3.147

It was, therefore, a subject of interest to pay attention in the region from about 65 to 80 *at%* Pt. In this region single phase Pt_2Mo has been reported to exist from 60 *at%* to 70 *at%* Pt compositional range and the other Pt rich region (70 *at%* to 80 *at%*) was left unmarked, Fig.1.1. It has been reported earlier in this chapter, that Pt_2Mo phase was reported by Ocken *et al.* **[15]** to be an ordered form of the terminal f.c.c. Pt solid solution, which refers to the phase that exists over composition ranges near the concentration extremities of the phase diagram. In addition, they also reported that the unmarked phase region should be considered tentative because of the challenges in distinguishing between single-phase Pt_2Mo and two-phase Pt_2Mo plus f.c.c. Pt solid solution, between 70 *at%* and 80 *at%* Pt. However Benarchid *et al.* **[19]** reported the

existence of a single phase of Pt-solid solution with rather smaller lattice parameters (3.908 Å) compared to that of pure Pt (3.924Å), at about 73.04 *at%* Pt composition. This observation did not agree with the two-phase Pt_2Mo plus Pt-solid solution reported by Ocken *et al.***[15]** and single phase Pt_3Mo reported by Rooksby *et al.* **[10]** at the same Pt composition. The phase formation in the Pt-Mo bulk system has also been studied quite extensively by many researchers **[4-5, 7-8, 14-16, 19-20]**. However our interest is focused on the phase formation sequence in Pt-Mo coated system.

1.3.2 Phase transformation and prediction in solid materials

The main objective of studying phase transformation in solids is to understand the thermodynamics and kinetics of phase formation, growth and their stability **[1-2, 21]**. This is often accomplished by subjecting the material to different environmental conditions e.g. heat treatment. Our study is based on the effects caused by annealing on the microstructure of the Pt coated Mo systems. Heat treating the material causes alteration in the microstructure through movement or diffusion of atoms making up the material **[1, 21-24]**. Diffusion almost always governs the phase transformation process which involves nucleation and growth of the new phase **[1]**. Nucleation is the formation of very small particles (nuclei) of the new phase at grain boundaries and other defects. This new phase will grow at the expense of the original phase.

The formation of the phases and the sequence of their formation in Pt-Mo coated system were of particular interest in this research. There has been considerable interest in the literature about the prediction of the first phase formation as well as the phase formation sequence in many systems **[25-33]**. The earliest model for predicting first phase formation and phase formation sequence was proposed by Walser and Bene´ **[25]**. There is also the Effective Heat of Formation model

(EHF), proposed by Pretorius **[28]**,which has been extensively used for first phase formation as well as phase sequence formation prediction **[29-33]**. The EHF model was successful in predicting first phase formation during the formation of silicides, germanides, aluminides and other metal-metal binary systems **[30-33]**. The formation of a new phase involves movement of atoms between the two solids involved in the reaction and consequently consists of the formation and growth of nucleus. The liquidus minimum composition was chosen as a measure of atomic mixing at the interface in both models. In addition, the EHF model takes into account the heat of formation of phases in comparison to Walser-Bene´ model. The EHF model can therefore predict the sequence of phase formation while Walser-Bene´ model has been most successful in predicting the formation of the first phase **[33]**.

1.3.2.1 Walser-Bene´model (W-B)

Solid state reactions in thin film are an example of non-equilibrium process whereby one phase is formed at a time. Walser-Bene´ model is the earliest model to predict the first phase formation in thin films. The primary predictions of Walser-Bene´ model were essentially for the prediction of the first phase formation upon annealing. The following Walser-Bene´ model rule was formulated for the prediction of the first phase formation in metal-silicon couples **[26, 28, 33]**:

"*The first compound nucleated in planar binary reaction couples is the most stable congruently melting compound adjacent to the lowest-temperature eutectic on the bulk equilibrium phase diagram*."

According to this model, the nucleation favours congruently melting phases and skips the non-congruently melting phases due to the higher energy barrier **[26-27]**.The model was also

extended to metal-metal systems **[27]** by relaxing the requirements of the first phase formation that needs to be congruently melting, the rule then stated:

"*The first phase nucleated in metal-metal thin-film reaction is the phase immediately adjacent to the low-temperature eutectic in the binary phase diagram*."

Due to the fact that the Walser-Bene´ model failed to reveal that there are phases that have an equal likelihood to form from a thermodynamic perspective, the EHF model which makes use of thermodynamic data was therefore proposed.

1.3.2.2 Effective Heat of Formation (EHF) model

The EHF model uses thermodynamic data to predict the first phase formation and the sequence of formation in thin film **[29-33]**. The model also allows the calculation of the heat of formation as a function of concentration of the reacting species and it has been applied in many systems. The principle that governs the EHF model during the prediction of the phase formation sequence is the change in Gibbs free energy given by the following expression **[33]**:

$$\Delta G^\circ = \Delta H^\circ - T\Delta S^\circ \qquad 1.1$$

Where: ΔH° is the change in enthalpy or heat of formation, T is the temperature, and ΔS° is the change in entropy.

Since the change in entropy is generally very small during solid state interaction, the heat of formation is a good measure of the change in free energy. It is, therefore, possible to use heat of formation ΔH° to predict phase formation when activation or nucleation barriers are neglected **[31-33]**. Phase formation at the interface is reported to be a non-equilibrium process which means therefore that equilibrium rules cannot be applied for the prediction of phase formation

during the solid state reaction at the interface **[31-33]**. In addition, one phase is expected to form at a particular interface. The EHF, defined as $\Delta H'$ with SI unit kJ (mol.at)$^{-1}$, is given by the following expression **[33]**:

$$\Delta H' = \Delta H^{\circ} \times \frac{effective\ concentration\ of\ the\ limiting\ element}{compound\ concentration\ of\ the\ limiting\ element} \qquad 1.2$$

It is of significant importance to know the effective concentration of the two elements involved in the reaction at a growth interface (e.g. effective concentration of the limiting element and concentration of the limiting element in the phase to be formed) in order to be able to predict the next phase to be formed using equation 1.2. It has been mentioned in the literature that, for the variety of systems with given structure and bond type, the activation energy for solid state diffusion is directly proportional to the melting point of the solid **[33, 34]**. From inter-diffusion perspective, the mobility is determined by the activation energy, hence, the smaller the activation energy the greater the mobility according to the equation 1.3 **[1, 21-23]**.

$$D = D_0 \exp\left(-\frac{Q}{RT}\right) \qquad 1.3$$

where: D_0 is a temperature- independent pre-exponential in m^2/s, Q is the activation energy in J/mol, R is the gas constant and T is absolute temperature in K.

It was reported therefore that the greatest mobility of the atoms and the most effective mixing at the growth interface is expected to be at the composition of the liquidus minimum **[33]**. As a result, the effective concentration was regarded to be the composition at the liquidus minimum of

the binary system. Based on this, the EHF model rule for the predicting the phase formation in metal-metal reaction couple, was formulated **[32]:**

"*The first compound to form during metal-metal interaction is the phase with the most negative effective heat of formation at the concentration of the liquidus minimum of the binary system*."

In addition, a general rule of the EHF model was also proposed **[32]**, which stated:

"*Phases will react with each other to form a phase, with a composition lying between that of the interacting phases, whose effective heat of formation, calculated at the concentration closest to that of the liquidus minimum within the composition range, is the most negative*."

With the help of equation 1.2, the EHF of any phase or compound could be calculated as a function of the reacting species concentration **[33]**.

In the case of the current investigation, the heat of formation ($\Delta H°$) data for Pt-Mo phases, determined by high temperature direct reaction synthesis calorimetry at a temperature between 1526K and 1768K, have been reported, see table 1.2, fourth column **[19]**.The heat of formation ($\Delta H°$) data was then used to calculate the effective heat of formation ($\Delta H'$) of Pt-Mo system phases using equation 1.2, (see table 1.2 fifth column). The information presented in the table was also used to plot the graph of the effective heat of formation for Pt-Mo compounds as a function of the concentration of the reacting elements, see Fig. 1.2.

Table 1.2: Calculated effective heat of formation $\Delta H'$ for Pt-Mo system based on high temperature direct reaction synthesis calorimetry data [19]

Phase	**at.% Pt [19]**	**at.% Mo**	**ΔH^o kJ/(mol.at.)**	**$\Delta H'$ kJ/(mol.at.)**
Pt solid solution	73.04	26.96	-27.1	-2.01
Pt_2Mo	63.64	36.36	-36.9	-2.02
PtMo	45.22	54.78	-27.7	-1.01
Pt_2Mo_3	36.64	63.36	-26.1	-0.82
$PtMo_6$	19.13	80.87	-13.0	-0.32

It was noticed from the Pt-Mo phase diagram given in Fig.1.1 that the liquidus minimum for the Pt-Mo system is the melting point of Pt, therefore, the effective concentration was arbitrarily taken as 98 *at%* Pt and 2 *at%* Mo as done in the other systems, Pt-Al, Pt-Cu and Au-In **[32]**. Therefore in the Pt-Mo system, Mo is the limiting element. The compound concentration of the limiting element was calculated based on the Pt concentration given by Benarchid *et al*. **[19]** as summarised in table 1.2. According to thermodynamic data given in table 1.2, the Pt rich phase (Pt_2Mo) is the first compound expected to nucleate during the metal-metal interaction in the Pt-Mo system because of its most negative effective heat of formation (EHF) value, -2.02 kJ/(mol.at), when compare to other compounds. The second phase expected to form in this system is PtMo compound with approximately 1:1 Pt to Mo ratio. The Mo rich phases, Pt_2Mo_3 and $PtMo_6$, are predicted to be the third and fourth compound to nucleate in Pt-Mo system, respectively.

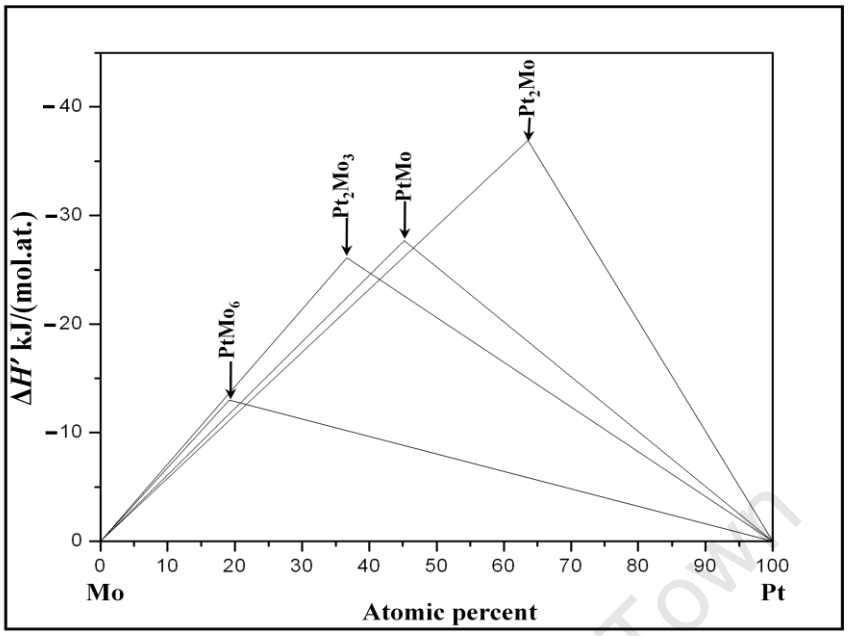

Figure 1.2: Effective Heat of Formation (EHF) of the Pt-Mo binary system plotted using data from table 1.2. Each triangle represents the energy released as a function of concentration during formation of each Pt-Mo phase

The EHF for the reported Pt-solid solution was also calculated and included in table 1.2, first row. It is interesting to note, however, that there is no significant difference between the EHF for Pt_2Mo (-2.02kJ/(mol.at.)) and Pt-solid solution (-2.01kJ/(mol.at.)). This could explain the difficulties encountered by Ocken *et al* **[15]** when trying to distinguish between one-phase Pt_2Mo and two-phase Pt_2Mo plus Pt-solid solution in the same Pt compositional range, as reported earlier in this chapter. Based on these observations, the Pt_2Mo phase and Pt-solid solution have almost equal probability to nucleate in Pt-Mo system.

1.4 Scope of Investigation

In this research project, Pt coatings (0.2 µm, 0.3 µm and 0.5 µm) deposited on 125 µm thick Mo substrates were heat treated in a vacuum furnace and subsequently characterised using different analytical techniques. The experimental approach and characterisation techniques used in this research work are discussed in **Chapter 2**. Several complimentary techniques, X-ray diffraction (XRD) for phase formation analysis, scanning electron microscopy (SEM) for surface morphology, transmission electron microscopy (TEM) for the microstructure of the coating's cross-section, energy dispersive X-ray emission (EDX) for the elemental composition and Rutherford Backscattering Spectrometry (RBS) for studying interfacial reaction, phase composition and coating thickness, were employed and the results are discussed in **Chapter 3** and **4**. The discussions and conclusion of this work are presented in **Chapter 5** and **Chapter 6**, respectively.

CHAPTER 2 SAMPLE PREPARATION AND CHARACTERIZATION TECHNIQUES

2.1 Preparation of Samples

The coating samples were prepared by using molybdenum as a substrate and platinum as a coating material. The molybdenum sheet (125 µm) was cut into small coupons (substrates) of approximately 1 cm × 1 cm. In order to eliminate any possible contamination during cutting, the substrates were cleaned in a sequence of several liquids (methanol, acetone, trichloroethylene, acetone, methanol and de-ionized water) for the duration of 10 minutes for each step prior to the 0.2 µm, 0.3 µm and 0.5 µm Pt layer deposition using either electron beam evaporator or sputtering techniques.

2.1.1 Electron Beam Evaporation and Sputtering techniques

Electron beam evaporation (EBE) and sputtering are the coating techniques used to prepare coating materials and the depositions are carried out under high vacuum. During EBE experiment, the target material is bombarded with high energy electrons causing the target to be heated up which results in the evaporation of target atoms into a vapour. The vapour then condenses onto the substrate surface where the coating of interest is produced. The evaporator equipment used in this study consists of a copper crucible with three holders where target materials to be evaporated can be placed, Fig. 2.1. Since three target materials can be mounted in this crucible, contamination of material during evaporation is possible. Therefore, materials to be evaporated are separated from each other by the dividing walls of about 20 mm high, Fig. 2.1. In addition, the molten material may form a crust near the crucible walls, so that the material itself acts as its own crucible. Since only the central part of the exposed surface of this metal is heated,

the evaporation of copper crucible and contamination of target material are avoided. Single platinum coating samples, 0.2 μm, were deposited onto cleaned molybdenum substrates. During the preparation of the coatings, a quartz thickness monitor was used to track the coating thicknesses.

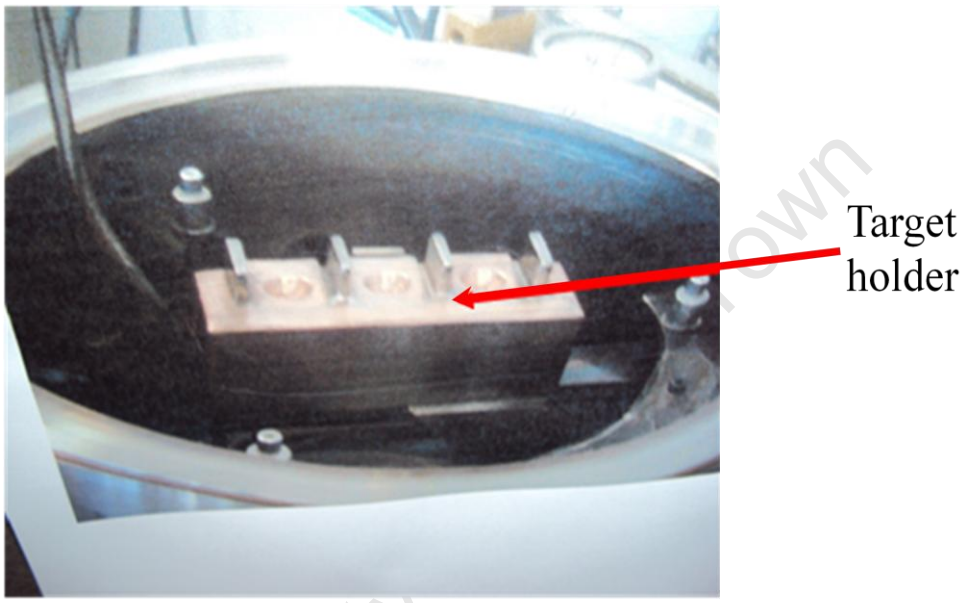

Figure 2.1: Electron beam evaporator chamber used for the deposition of Pt onto Mo substrate showing a Copper crucible with three target holders

The pressure was between $1x10^{-5}$and 2 $x10^{-6}$ mbar during deposition while the deposition rate was controlled by changing the filament current. The rate at which coatings were deposited was between 0.6-1.2 Å/s using current ranging between 30 to 130 mA. The thick platinum coatings, 0.3 μm and 0.5 μm were deposited on the Mo substrate using sputtering coating technique, Fig. 2.2, at the Centre for Functional Nanomaterials (USA) after a day of successful training on the sputtering (Kurt Lesker PVD 75) instrument. The sputtering technique was used to deposit thick

coatings because EBE could not get these coatings well prepared onto substrate surface as the coatings would always peel. The peeling of the thick Pt layer when using EBE was believed to be due to the fact that the evaporated atoms arrived at the surface of the substrate with less energies than the sputtered ones **[35]** resulting in the formation of a coating layer which does not bond firmly to the substrate. The difference in the coefficient of thermal expansion of Pt and Mo, $9.1\times10^{-6}/^{\circ}C$ and $4.9\times10^{-6}/^{\circ}C$, respectively **[1]**, could lead to the increased strain in the thin film, and with poor bonding between the substrate and the coating, the peeling of the thick coatings is therefore possible. The parameters used for deposition of the thick coatings by sputtering method were as follows: deposition rate 3.8 Å/s, base vacuum pressure was $1x10^{-5}$ mbar and the coatings were prepared at 300W power (dc) using argon gas. The process pressure was set to a desired pressure set point ($6.5x10^{-3}$ mbar).

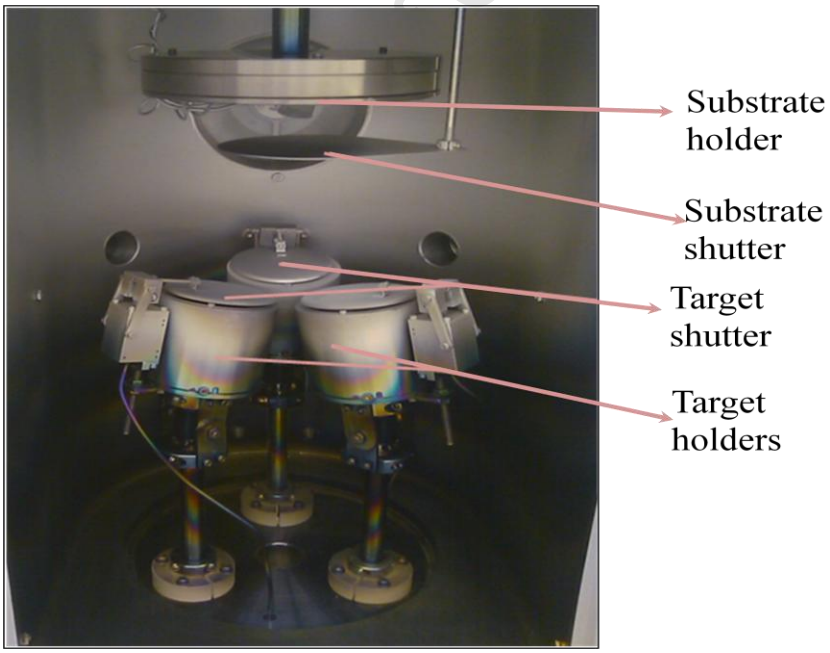

Figure 2.2: Photograph showing the sputtering (Kurt Lesker PVD 75) coating instrument used to deposit thick coating samples

The sputtering, at Lehigh University (USA), was also used to co-deposit Pt and Mo of approximately 1 µm without breaking vacuum. The process pressure was set to $5x10^{-3}$ mbar and the base vacuum pressure was $6.65x10^{-7}$ mbar. The systems were deposited to have different compositional ratios of about 3:1 and 2:1 Pt to Mo. All coated samples were heat treated at elevated temperatures, ranging from 800°C to 1200°C, for different annealing periods. The annealing process was carried out in a gauge pressure of $1x10^{-7}$ mbar, using an Elite Thermal System Limited furnace at iThemba LABS, Fig. 2.3. The samples were placed in ceramic boats and loaded into the quartz tube of the furnace.

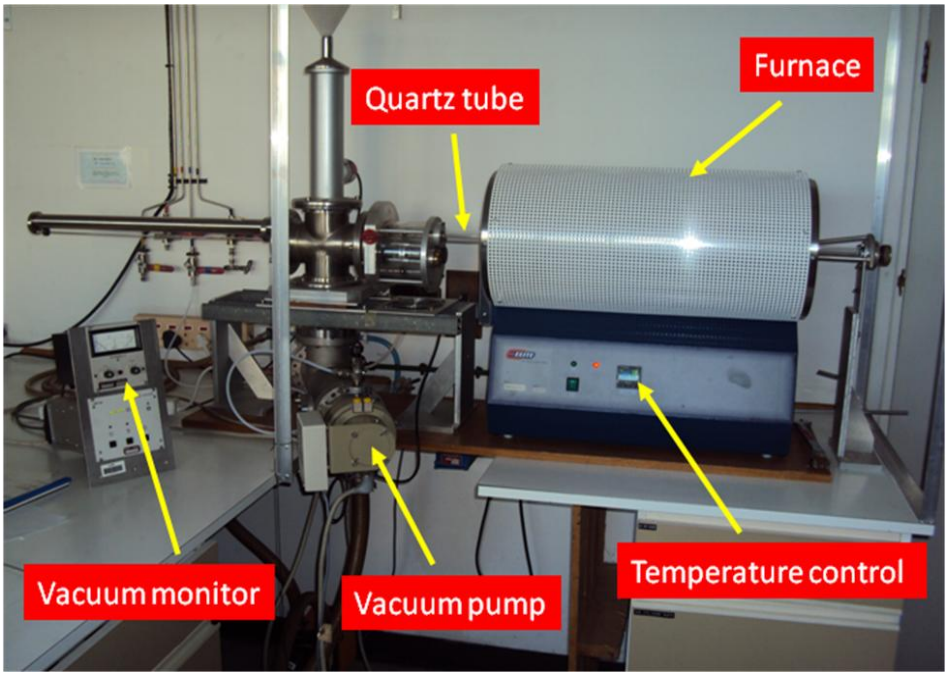

Figure 2.3: Photograph showing parts of the Elite Thermal System Limited furnace used for annealing

After annealing, the samples were removed from the furnace and allowed to cool in the vacuum. The as-deposited and annealed samples were characterized using complementary analytical techniques describe in section 2.2.

2.1.2 Preparation of TEM specimen by FIB

A selected annealed Pt-Mo coating was prepared for transmission electron microscopy (TEM) analysis. The sample was prepared by Mr. Kim Kisslinger using Focused Ion Beam (FIB) milling technique, Fig. 2.4, at the Centre for Functional Nanomaterials, USA. During sample preparation, the spongy looking region (region of interest) was selected, as shown in figure 2.5.

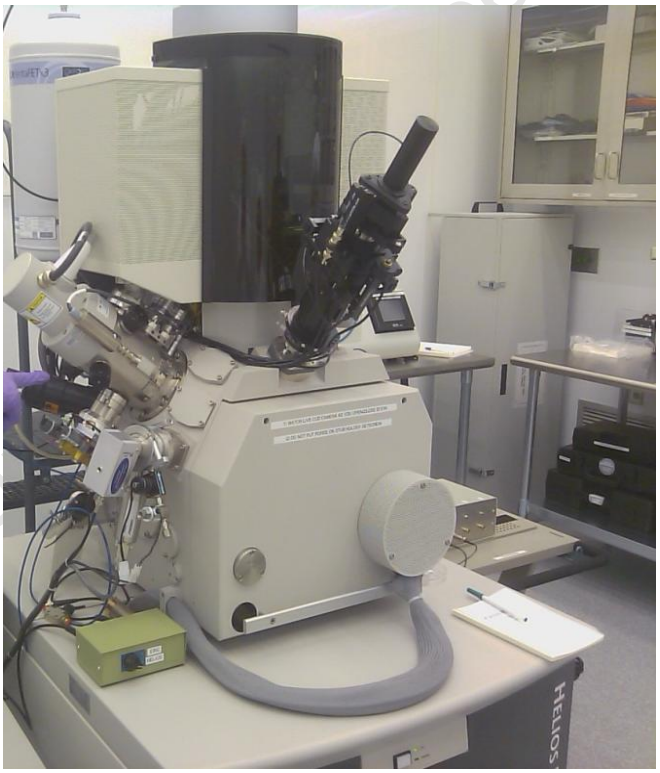

Figure 2.4: Photograph showing FEI Helios NANOLAB 650 FIB-SEM used to prepare TEM specimen

FIB is the sample preparation technique used to directly remove an electron-transparent thin foil sample from bulk specimen without mechanical polishing **[36, 37]**. The advantages of using FIB than the standard procedure, for TEM sample preparation, is that **[37]**: (i) the area of interest can be precisely chosen, (ii) The sample preparation by FIB is fast and reliable and (iii) FIB sample preparation techniques are independent of the nature of the material. In this research project, FIB was used to obtain the cross-section of the coating material in order to determine the compositional gradient of Pt and Mo across the coating through the substrate.

During FIB milling of Pt-Mo coating, the surface of the chosen area of interest was protected from sputtering damage, such as Ga implantation and surface amorphization **[38, 39]**, by depositing a layer of Pt prior to milling process. The deposited Pt layer as shown in Fig. 2.5 (a) also helps to minimum uneven milling **[38]**.

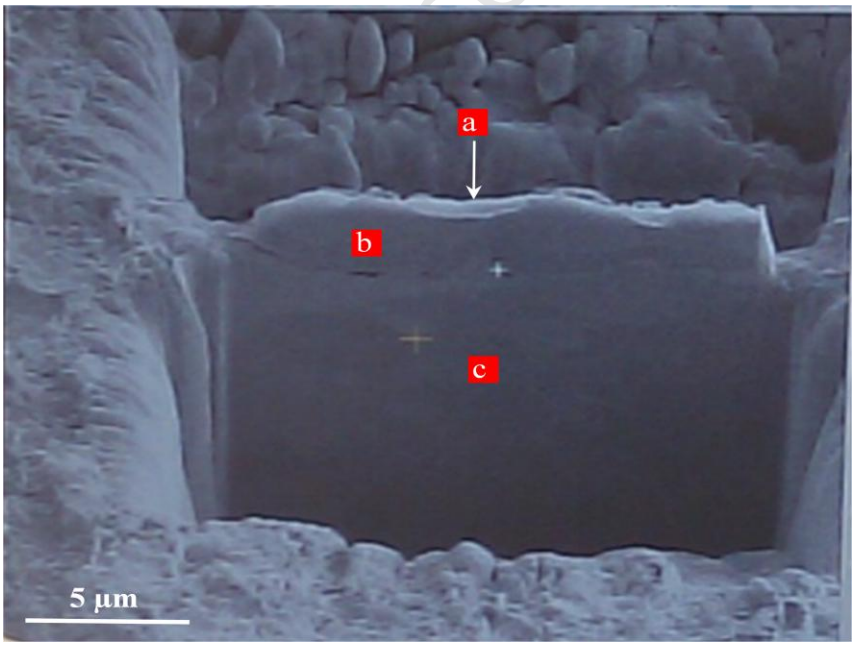

Figure 2.5: SEM image of Pt-Mo coating during milling process: (a) Pt surface damage protection layer (b) Pt-Mo coating region and (c) Mo substrate

Figure 2.5 shows the image of the Pt-Mo coating taken during the milling process. The cross-section of the sample was cut and afterwards milled out using a (Ga) beam in the FIB operating at 30 keV. The milled section was lifted out of the sample by attachment to an Omniprobe needle and transferred to a Cu grid. Final polishing of the sample was done at 500V to a thickness of 50 nm. High resolution imaging and elemental composition (line scanning mode) were obtained using transmission electron microscope (TEM), scanning transmission electron microscope (STEM) and JEM 2100F JEOL scanning electron microscope at an accelerating voltage of 200 kV. The elemental line scans were obtained across the interface between the coating and the substrate.

2.2 Characterization techniques

The coated and annealed specimens were characterized using scanning electron microscopy (SEM), transmission electron microscopy (TEM), energy dispersive X-ray spectroscopy (EDX), Rutherford Backscattering Spectrometry (RBS), and X-ray diffraction (XRD). The basic principles of these complementary techniques are described in this section.

2.2.1 Electron Microscopy

2.2.1.1 Scanning Electron Microscopy (SEM)

Scanning electron microscopy is the microscopic technique used to provide images detailing the arrangement of atoms on the surface of the sample by scanning it with a high energy beam of electrons **[40-42]**. SEM consists of electron gun (source of electrons), column, scanning system, sample holder and detector. A focused beam of electrons generated from the injector is directed towards the external surface of the sample. The movement of the beam, before reaching the

sample, is controlled in the column which consists of two types of electromagnetic lenses: condenser and objective lenses. These lenses govern the path of the beam to the sample by reducing its size before passing through the lenses aperture to the surface of the sample. Therefore, a small part of the beam passes through the aperture to the analysed sample. In addition, the stigmator gives the beam a circular cross section by creating a magnetic field around the beam **[40]**. In the time of the interaction of the beam with the atoms present on the surface of the sample, several signals are generated as schematically shown in Fig. 2.6 **[40, 41]**.

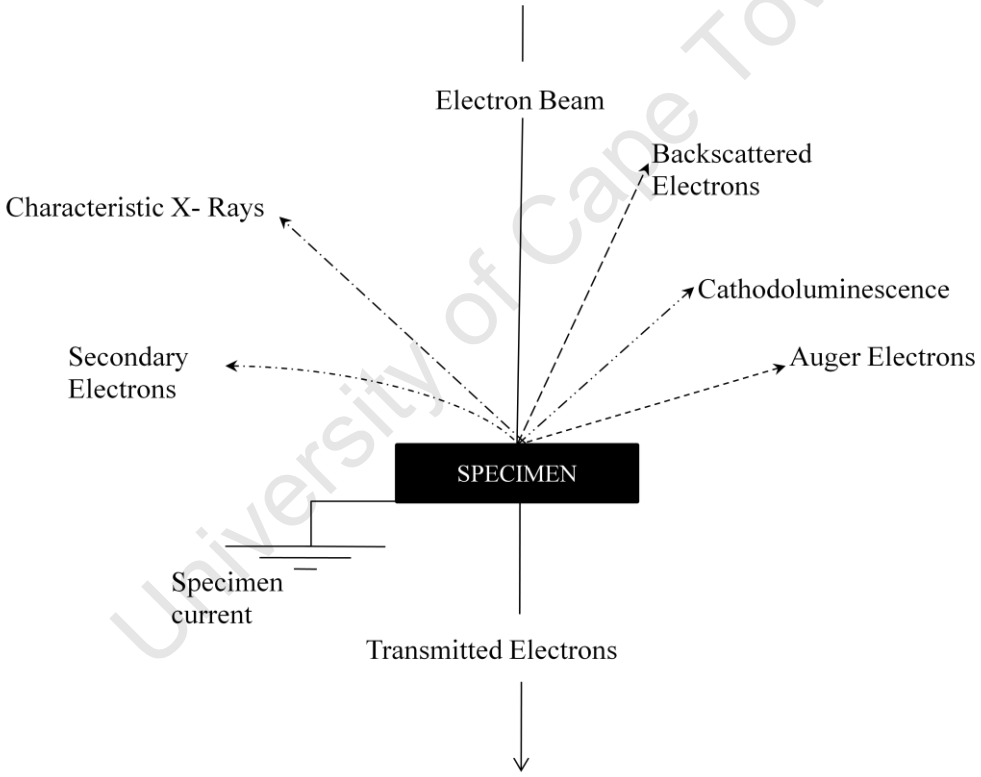

Figure 2.6: **Schematic diagram showing possible signals generated during the interaction of the electron beam with the sample [40, 41]**

These signals reveal information about crystalline structure, external morphology and chemical composition of the sample under investigation. The interest was in the secondary electron signal and characteristic X-ray. These signals reveal the surface morphology of the analysed sample and average elemental composition on the coating **[40, 41]**. The secondary electron signal takes place when a beam of electron inelastically collides with the atoms of the sample. The amount of beam energy is transferred to the atom of the sample causing it to ionize and emit electrons. The emitted electrons are detected to reveal the surface morphology of the sample **[40-42]**. The detection of characteristic X-ray signal is possible in both SEM and TEM analytical techniques and is described in section 2.2.1.3. In this research work the surface morphology of the coatings (as-deposited and annealed) was studied using a Nova NanoSEM 230 scanning electron microscope, Fig. 2.7, under the supervision of Ms. M. Waldron, at the Electron Microscope Unit, University of Cape Town. The Nova Nano**SEM** 230 scanning electron microscope instrument is equipped with EDX analytical technique which was also used for elemental analyses of Pt-Mo coatings. Tungsten filament was used as a source of electrons. The SEM micrographs were acquired at an accelerating voltage of 20 keV in secondary electron (landing) mode.

Figure 2.7: **Photograph showing the scanning electron microscope (Nova NanoSEM 230) used for image acquisition**

2.2.1.2 Transmission Electron Microscopy (TEM)

Transmission electron microscope technique is used to analyse the microstructure of materials with atomic scale resolution **[40, 41]**. The technique contains the electron gun which is capable of accelerating the electrons through a selected potential difference. The appropriate electron energy for a TEM experiment depends on the nature of the specimen and the information required **[41]**. The electrons travel in vacuum through condenser lenses whose main functions are to de-magnify the beam and to control its diameter and convergence angle as it hits the specimen. The high energetic electrons then interact with a very thin specimen under investigation and are transmitted through. After the beam interacted with the specimen, depending on the density of the analysed material, some of the electrons are scattered and disappear from the beam **[41]**. The transmitted electrons then pass through an objective lens where the first intermediate image and diffraction pattern is formed.

The micrograph of the cross-section of the selected coating and elemental composition across the cross-section of the coating were acquired by Dr. S. Botha using the EDX equipped Tecnai G2 F20 X-Twin instrument, Fig. 2.8, (Electron Microscope Unit, University of the Western Cape) operated at an accelerating voltage of 200 kV. Si(Li) EDAX detector and Schottky Field Emission Gun, as a source of electrons, were used during experiment. The regions of interest were chosen during the measurements for compositional gradient analysis followed by the data interpretation as presented in this thesis.

Figure 2.8: **Photograph showing the Tecnai G2 F20 X-Twin Mat 200 kV Field Emission TEM used to obtain coating cross-section and compositional gradient**

Prior to the TEM experiment, the specimen was prepared by means of Focus Ion Beam (FIB) technique at Brookhaven National Laboratory (BNL, USA).

2.2.1.3 Energy Dispersive X-ray Spectroscopy (EDX)

The EDX analysis is an integrated feature of both scanning electron microscope (SEM) and transmission electron microscopy (TEM). EDX is used to analyse the elemental composition of the materials. The technique is based on the spectral analysis of the characteristic X-rays which are emitted from the atoms of the analysed sample **[40-42]**. The X-rays are emitted during the interaction of the focused electron beam with the sample. During EDX analysis the beam of electrons interacts with the bound electrons of the analysed sample as shown in Fig. 2.9.

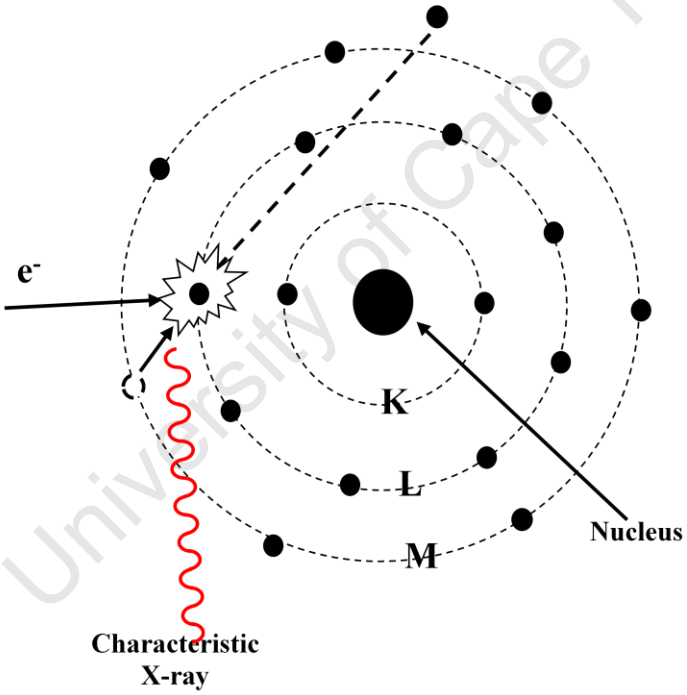

Figure 2.9: Schematic representation of electrons interacting with atoms of the element present in the sample and the emission of the characteristic X-ray (L line) [41-43].

The electrons are ejected from their shells resulting in the formation of unoccupied states within the atoms **[40-43]**. Electrons from an outer, higher-energy, shell fill the gap left by ejected electrons. The energy difference between the shells involve in the transition (outer and inner shells) is released in the form of X-rays. The released X-rays create a spectrum with different peaks corresponding to distinct atomic transition of the elements present in the analysed sample. Energy dispersive X-ray spectroscopy (EDX) attached to the SEM was used to analyse the average elemental composition of the Pt-Mo coatings in the selected area of approximately 30 μm^2 while the EDX attached to the TEM was used for elemental composition across the cross-section of the coating material. The operational parameters for the EDX attached to SEM were as follows: Spot size was 3 micros, which is equivalent to a beam current of 56 pico amps (pA). The data was collected using Oxford 20mm^2 detector which uses INCA software. The spectrum was acquired for 30 seconds at 20 kV. In the case of the EDX attached to TEM, the following operational parameters were used: The beam source and spot size were Schottky Field Emission Gun and 1 micron, respectively. The instrument was operated in STEM (using High Angle Angular Dark Field detector) and TEM (using Si(Li) EDAX detector) modes. The STEM mode was used to perform drift corrected spectrum profiles (line scans) while TEM mode was used to analyse the data.

2.2.2 X-Ray Diffraction (XRD)

After annealing the Pt-Mo coated samples at different temperatures and times, XRD technique was used to study the formation of intermetallic compounds. X-ray diffraction is a characterization technique which makes use of the interaction between X-rays and the periodic

arrangement of atoms in a crystalline sample. Consequently, any phase present in solid materials can be identified **[44-49]**.

X-rays are part of the electromagnetic spectrum and are generated when high energy electrons interact with the atoms of a solid material. Three requirements are needed to produce X-rays **[45]**: (i) source of electrons (cathode), (ii) high voltage to accelerate electrons to high speed and (iii) a target material (anode). Electrons originate from a wire (filament) in the X-ray tube under high vacuum. They accelerate towards the anode (target) by a large potential difference and collide with the target atoms at high kinetic energy.

In the X-ray diffraction principle, the interaction of monochromatic X-rays with the periodic arrangement of atoms in a crystalline sample, see Fig. 2.10, leads to the coherent scattering by the electrons of the atomic planes **[44, 45]**.

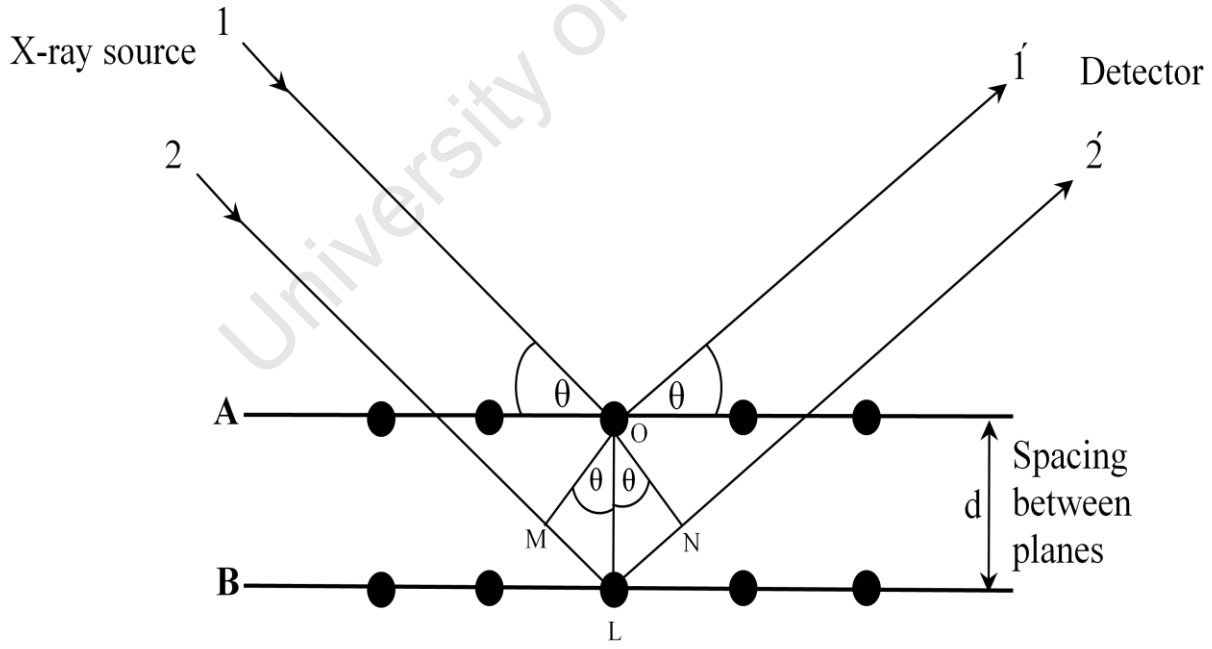

Figure 2.10: **Schematic diagram of X-ray interacting with atomic planes of the crystalline sample [45]**

A diffracted beam is only produced when some geometric conditions given by the Bragg law, equation 2.1, are satisfied **[44-49]**.

$$n\lambda = 2d\sin\theta \qquad 2.1$$

where: d represent the separation of the periodical arrangement of atoms making up the sample, λ-wavelength of the incident X-ray beam, n-whole number of wavelengths and θ-diffraction angle.

Figure 2.10 shows two parallel X-rays (1 and 2) interacting with the atoms of adjacent planes in a crystal sample. To satisfy Bragg's law conditions and for diffraction to take place the scattered X-rays must continue travelling parallel to each other when they leave the crystal to the detector (constructive interference) **[44-49]**. Bragg's Law is satisfied by varying the angle θ which then gives different d-spacing corresponding to different planes present in the crystalline sample under investigation. X-ray diffraction pattern, which is the finger print of the analysed sample, is produced by plotting the angular positions and intensities of the resultant diffraction peaks. The obtained X-ray pattern is then compared to a database containing reference diffraction patterns for thousands of elements and compounds whereby the identification of phases present in the analysed sample is possible. The Pt-Mo phase analysis was carried out at room temperature using a D8 Advance Bruker diffractometer at iThemba LABS, Fig. 2.11.

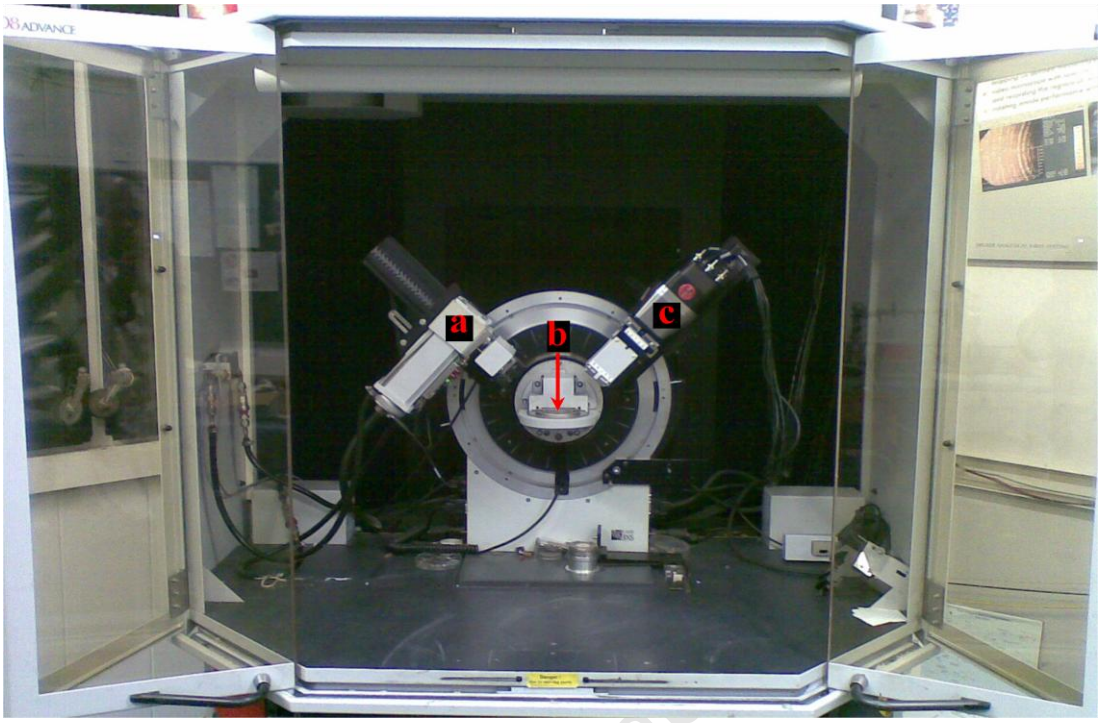

Figure 2.11: D8 Advance Bruker diffractometer showing (a) X-ray tube (b) sample stage and (c) Vantec X-ray detector

The configuration of this diffractometer is in such a way that the detector and the X-ray tube move in a locked coupled mode, called θ-θ scan mode. This means that the detector move angle θ (also called step size or increment, which is determined based on the nature of the measurement) for every θ that the X-ray tube moves. During this process, the analysed sample remains at a fixed position. The diffractometer was equipped with Cu target, as a source of X-ray, which was capable of giving CuKα radiation (λ≈ 1.54Å) and the X-ray tube was operated at 40 kV and 40 mA. In addition, the X-ray beam was collimated by a Göbel mirror while the V-groove germanium crystal compressed and filtered the X-ray beam so that only CuKα radiation

is present in the controlled beam. The calibration was performed using aluminium oxide (Al_2O_3) standard prior XRD measurements. Data were collected between 15° and 90° in 2θ with a step size and time per step of 0.03 and 1 second, respectively, using a position sensitive (Vantec) detector. Therefore, each measurement took approximately 45 minutes. The X-ray diffraction patterns were then compared to the reference diffraction patterns contained in the XRD database (Eva. software) in order to identify the phase present in the Pt-Mo coating samples followed by the plotting of the XRD data using Origin 6.0 software.

2.2.3 Rutherford Backscattering Spectrometry (RBS)

The interfacial reaction of Pt and Mo as well as compound composition in Pt-Mo coatings were studied by Rutherford backscattering spectrometry (RBS). In RBS experiment, energetic ion beam of particles, $4He^+$, collide with the target atoms and are scattered in a backward direction into the detector which measures the energy of the backscattered particles **[50]** as shown in Fig. 2.12. The incident particles, having mass (M_1) different to the mass of the target atom under study (M_2), can have energy ranging between 1 to 3 MeV. The analysed samples are placed in the vacuum chamber ($\approx 1\times10^{-6}$ mbar) while being tested and normally titled at -10° with respect to the ion beam. The backscattered particles at 165 degrees (θ) are detected for compound composition and target thickness analyses. The scattering event occurs between the nucleus of the incident ion and the nucleus of the target atom in which the energy is transferred from the incident ion to the stationary target atom **[50, 51]**.

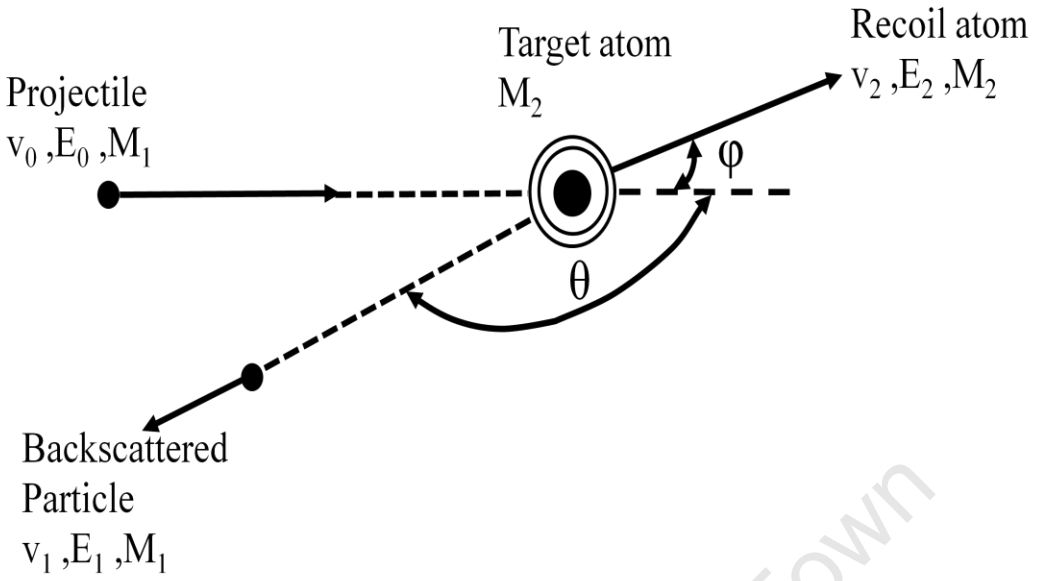

Figure 2.12: Schematic of RBS principle showing beam of particle incident on the sample and the back scattered particles to a particle detector [51]

After the collision, the measured energy E_1 of the particles scattered at angle θ depends on both masses of incident beam (M_1), with energy E_0, and target atoms (M_2) according to the following expression **[50, 51]**:

$$\frac{E_1}{E_0} = K = \left[\frac{(M_2^{\,2} - M_1^{\,2}\sin^2\theta)^{1/2} + M_1\cos\theta}{M_2 + M_1} \right]^2 \qquad 2.2$$

Where: K is the kinematic scattering factor, which is defined as the energy ratio of the particles before and after the collision.

The detected particles provide the signature of the target atoms which includes the compound composition, the thickness of the thin film, depth profiles of the impurities and dopants in the solid **[50, 51]**. During the RBS experiment, the detector counts each particle scattered in the differential solid angle $d\Omega$, Fig. 2.13. The differential scattering cross-section $d\sigma/d\Omega$ is defined by the following expression **[50, 51]**:

$$\frac{d\sigma}{d\Omega} = \frac{1}{Nx}\frac{1}{d\Omega}\frac{dQ}{Q} \qquad 2.3$$

Where: Q is the total number of particles impinging on the area of the sample exposed to the beam (S_A) and dQ is the number of particles recorded by the detector.

The other parameters in the expression above, N and x, represents the volume density of atoms in the target and the thickness, respectively. Therefore, the Nx represents the number of target atoms (composition) per unit area.

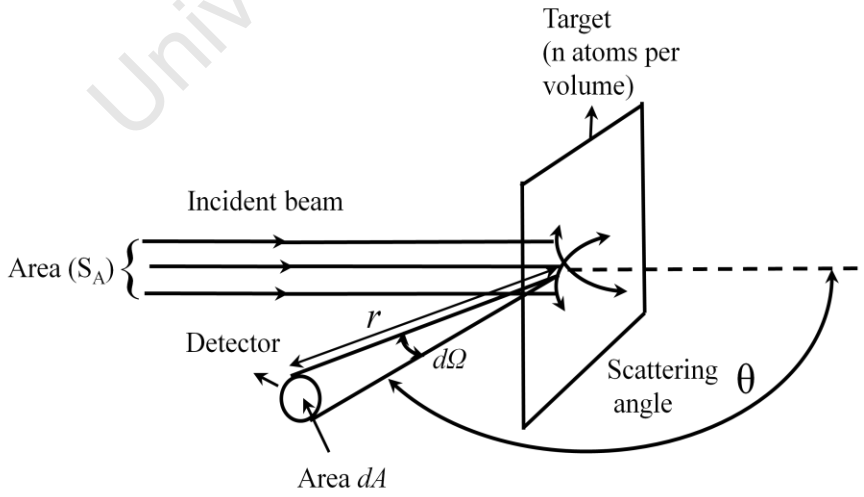

Figure 2.13: Schematic diagram of a scattering experiment [51]

During the interaction of the incident particle with a target material the beam loses its kinetic energy as it penetrates the target **[50, 51]**, Fig. 2.14. The amount of the energy loss during the interaction with the target depends on the nature of the incident beam, density and composition of the target material which is expressed as a stopping power $\frac{dE}{dx}$ **[50].** The detected energy losses, by particle detector, can be used to determine the thickness of the target material. If a constant value of the energy loss $\frac{dE}{dx}$ along the inward and outward paths is assumed, then there exists a relation between energy loss (ΔE) and depth (x) that can be expressed as $\Delta E = [S]x$ where the proportionality factor $[S]$ is called the backscattering energy loss factor or S factor **[50, 51]**.

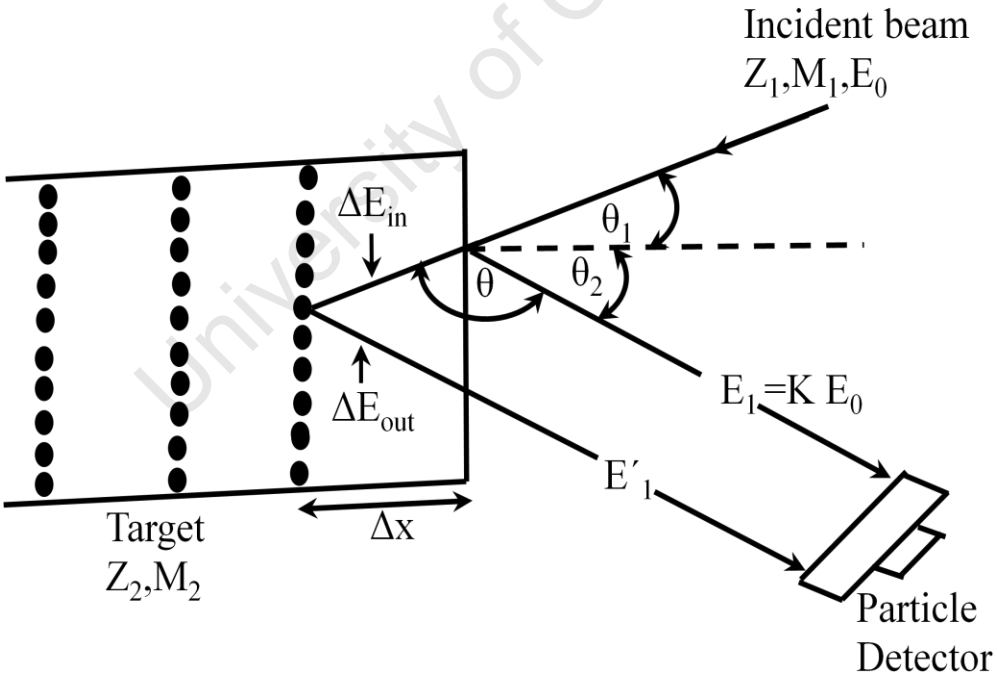

Figure 2.14: Schematic diagram for the energy loss of the incident particle in a target [51]

The energy loss factor is related to the thickness of the sample according to the following expression:

$$[S] = \frac{\Delta E}{\Delta x} = \frac{(KE_0 - E_1)}{dx} = \left[\frac{K}{\cos\theta_1} \left(\frac{dE}{dx} \right)\Big|_{in} + \frac{1}{\cos\theta_2} \left(\frac{dE}{dx} \right)\Big|_{out} \right] \qquad 2.3$$

Where: θ_1 and θ_2 are the angles between the surface normal and the outgoing particle direction, respectively, and "in" and "out" are for the values of the stopping power $\frac{dE}{dx}$ along the inward and outward paths, respectively.

In this study, the RBS experiments were performed in order to determine the interaction (diffusion) between Pt and Mo, compounds composition and coating thickness using a mono-energetic beam of 2 MeV alpha particles, a beam spot size of 2 mm in a vacuum of $5x10^{-6}$ mbar. The RBS data was collected using a surface barrier detector and the samples were titled at -10° with respect to the incident beam. All RBS experiments were performed at iThemba LABS. The RBS data was interpreted or analysed for compound composition and coating thickness determination using RUMP software.

CHAPTER 3 RESULTS FROM ELECTRON BEAM EVAPORATED SAMPLES

The effects of annealing on phase transformation in Pt coated Mo systems have been investigated using XRD, RBS, SEM, EDX and TEM. Three coated systems have been investigated; the 0.2 µm Pt single layer coatings deposited by electron beam evaporation (EBE) and systems with 0.3 µm and 0.5 µm Pt layer deposited using sputtering coating techniques. This chapter presents the results of the 0.2 µm Pt single layer coatings while the results of the thick coatings are presented in chapter 4.

3.1 The characterisation of 0.2 µm Pt layer coatings

3.1.1 X-ray diffraction (XRD)

X-ray diffraction was performed on 0.2 µm Pt coatings, for the as-deposited and after annealing at 900°C for 1, 2, 4 and 8 hours. The phase analysis was found to be challenging due to the following reasons. Firstly, there is no general consensus regarding the Pt-Mo phase diagram presently used and secondly, there are discrepancies between the current Pt-Mo phase diagram and the identified phases in the XRD data base for Pt-Mo system. Rooksby *et al.* **[10]** identified two Pt-rich phases in the Pt-Mo system, namely Pt_3Mo and Pt_2Mo. However, in the XRD data base the Pt_2Mo phase has been deleted and replaced by PtMo compound after it was found that the compound has 1:1 Pt to Mo compositional ratio, instead of 2:1 **[11, 14-16]**. The researchers **[14-16]** also found that a compound with this Pt and Mo compositions (i.e. 2:1) exists with similar diffraction patterns to that of Pt_3Mo phase, also reported by Rooksby *et al*. **[10].** A further proposal to replace Pt_3Mo phase with Pt_2Mo was then made **[15]** and following this the Pt-Mo phase diagram, depicted in Fig. 1.1, was constructed. The formation of the compounds, either

Pt_3Mo **[10]** or Pt_2Mo **[15]**, was reported to be "an ordered form of terminal f.c.c. Pt solid solution phase". However, the confusion is that in the currently used Pt-Mo phase diagram the phase appears as Pt_2Mo while in the XRD data base the phase is still presented as Pt_3Mo.

The identification of diffraction peaks in the X-ray patterns of the current investigation, Fig.3.1 (a-b), is based on the latest interpretation of Pt-Mo system which considers Pt_2Mo to be the phase to form, not Pt_3Mo. However, the Pt_2Mo phase diffraction peaks could not be identified in terms of Miller indices as the available hkl values in the XRD database used in this analysis were for Pt_3Mo phase. The presence of two intermetallic compounds (Pt_2Mo and PtMo) was detected after annealing at 900°C for 1, 2 and 4 hours. It was noticed that the diffraction peaks assigned to Pt_2Mo phase appeared at slightly high 2θ angles when compared to pure Pt peaks, see at $2\theta \approx 39.7°$ and 40° for Pt and Pt_2Mo phases, respectively, Fig. 3.1 (b). Although an alternative interpretation of the spectra shown in Fig. 3.1 (b) is that the peak at position 40.0° is merely the Pt signal shifted due to thermal stresses. However, RBS spectrum from this sample presented later in Fig. 3.4, table 3.1, show no pure Pt presence in the sample. It is believed, therefore, that the more correct interpretation is that the peak represents the presence of the Pt_2Mo phase. Several diffraction peaks were found which have not been assigned to any existing Pt-Mo phases. These additional reflections were also observed by Rooksby *et al.* and Ocken *et al.* **[10, 15]** when reporting the formation of Pt_3Mo and Pt_2Mo phases, respectively.

No additional phases were observed when the annealing time was increased to 2 and 4 hours. It was observed, however, that the intensity of the PtMo phase increased with time implying the continuous growth of this (PtMo) phase. In addition, other weak intensity peaks for the PtMo phase appeared after annealing for 4 and 8 hours at $2\theta \approx 18.0°$, 32.9° and 44.6°. The growth of the PtMo phase resulted in the decrease and after 8 hours the final disappearance of the Pt_2Mo

diffraction peaks, also shown in Fig. 3.1 (b). In addition, the unidentified reflections vanished together with diffraction peaks of Pt_2Mo phase, Fig. 3.1 (a). It therefore seems reasonable to suspect that there is a close relationship between Pt_2Mo phase and unidentified reflections.

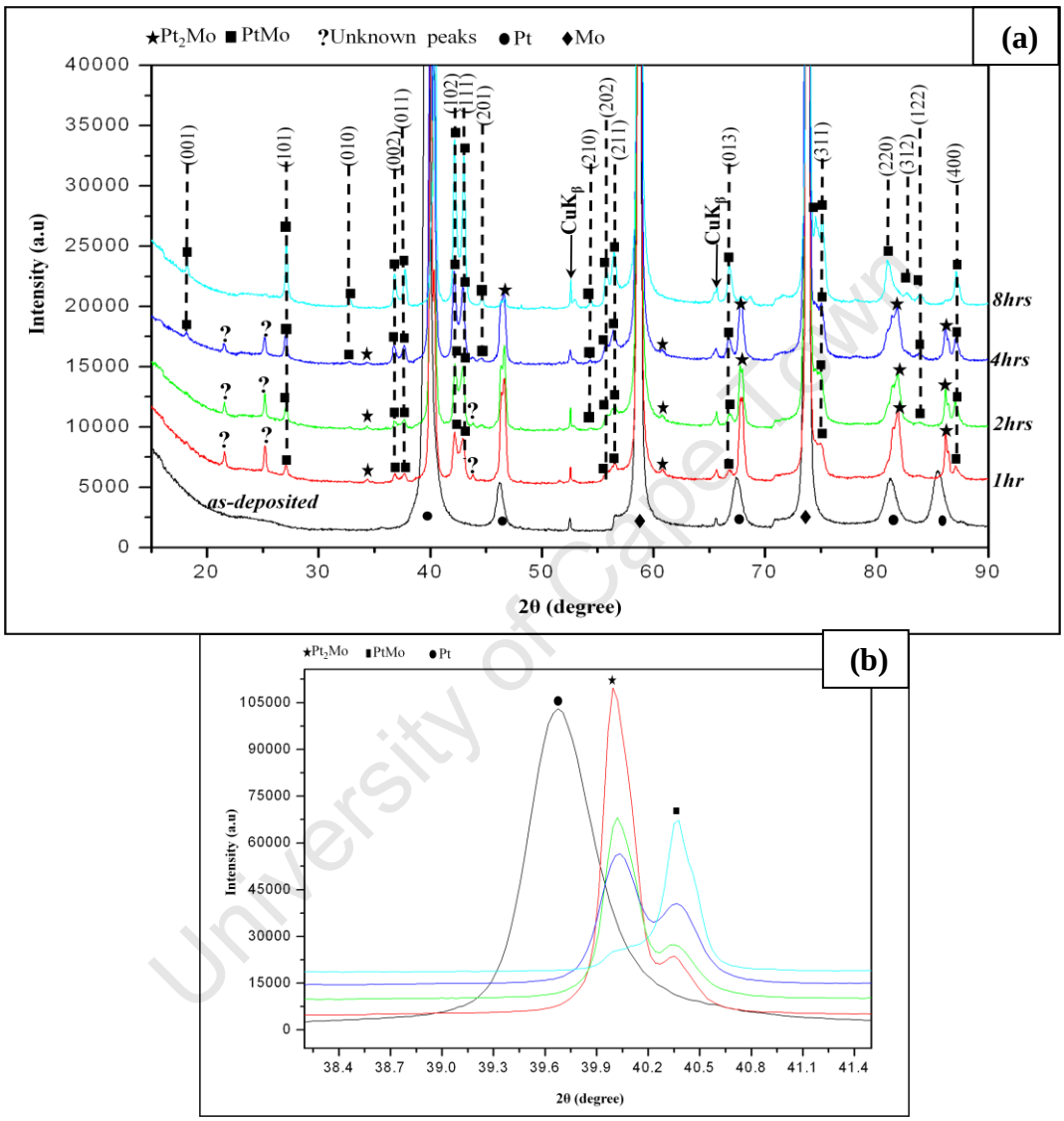

Figure 3.1: (a) X-ray diffraction patterns of 0.2 µm Pt coatings in as-deposited and annealed (at 900°C for 1, 2, 4 and 8 hours) conditions. (b) XRD patterns at 2θ=38.2°-41.5° range. CuK_β line was also diffracted and detected due to the strongest intensities of Mo peaks at 2θ = 58.61° and 73.68°

The results obtained are consistent with the PtMo phase growing at the expense of the Pt_2Mo phase in the Pt-Mo system. The XRD results therefore suggest that the Pt_2Mo phase was not stable, and as the annealing progresses it converted to the PtMo phase which appears to be the stable phase at 900°C. The stability of this compound (PtMo) was further investigated by extending the annealing time to 24 hours at 900°C, Fig. 3.2, but no additional phases were observed at these annealing conditions.

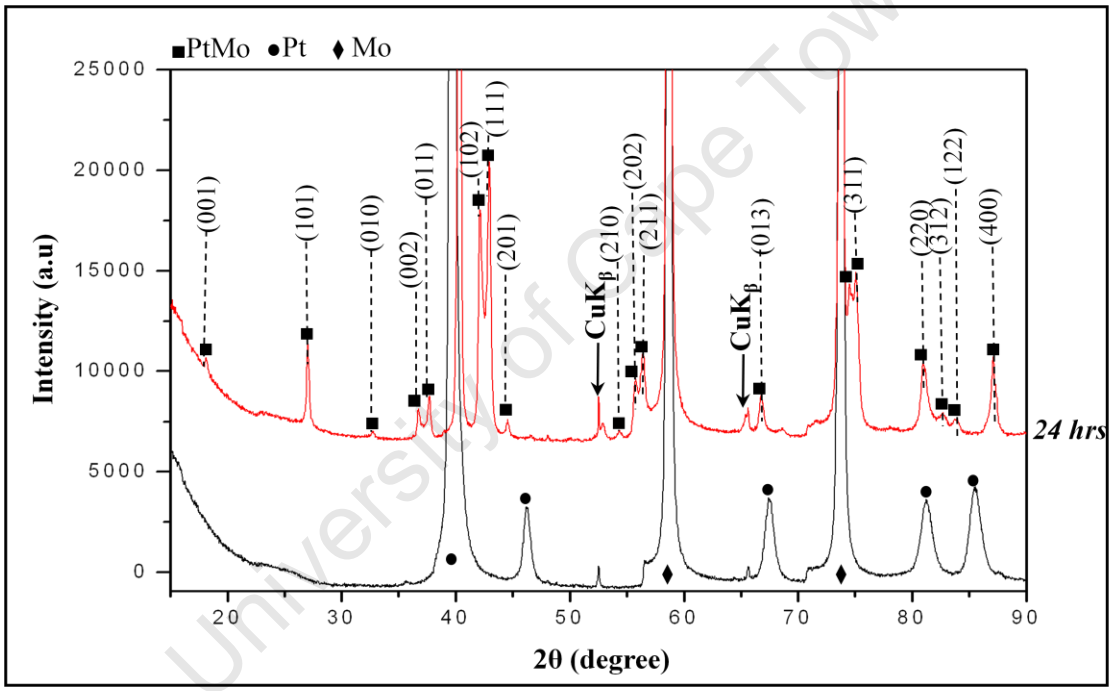

Figure 3.2: X-ray diffraction patterns of 0.2 µm Pt as-deposited and annealed at 900°C for 24 hours. CuK_β line was also diffracted and detected due to the strongest intensities of Mo peaks at 2θ = 58.61° and 73.68°

With the availability of the PtMo (orthorhombic) phase structural information, e.g. Miller indices as shown by dashed lines in Fig. 3.1 (a) and 3.2, it was therefore possible to calculate its lattice parameters (*a*, *b* and *c*) using equation 3.1 **[45]**.

$$\frac{1}{d^2} = \frac{h^2}{a^2} + \frac{k^2}{b^2} + \frac{l^2}{c^2} \qquad 3.1$$

Where: *d* is the separation of the periodical arrangement of atoms, hkl are Miller plane indices and *a*, *b* and *c* are lattice parameters.

The following Miller plane indices (200) at 2θ = 40.49°, (010) at 2θ = 32.80° and (002) at 2θ = 36.75°, Fig. 3.1 (a) and 3.2, were used to calculate *a*, *b* and *c*, respectively. In addition, the *d* spacing for each Miller plane indices was calculated using equation 2.1 prior to the calculation of lattice parameters. The obtained lattice parameters were equals to 4.452 (*a*), 2.728 (*b*) and 4.888 (*c*). These results are comparable to the published lattice parameters for the PtMo phase given in table 1.1. They are also in agreement with the following PtMo phase parameters, 4.475 (*a*), 2.729 (*b*) and 4.914 (*c*) given in XRD database, file number 00-019-0809.

X-ray diffraction can only identify phases, not composition, and since Pt-Mo phases reportedly exist over a large compositional range (*at%* Pt) the RBS technique was used to complement the XRD findings. The information from the RBS measurement provides composition of the Pt-Mo compounds present after annealing and therefore leads to a better understanding of the Pt-Mo system.

3.1.2 Rutherford Backscattering Spectrometry (RBS)

The RBS Spectrum from the 0.2 µm as-deposited coating is given in Fig. 3.3. In this figure, energy channel refers to the energy of backscattered alpha particles, channel refers to the channel number of the analogue digital convertor (ADC) in which the spectrum is stored and Normalized Yield is propotional to the number of particles backscattered at that particular energy.

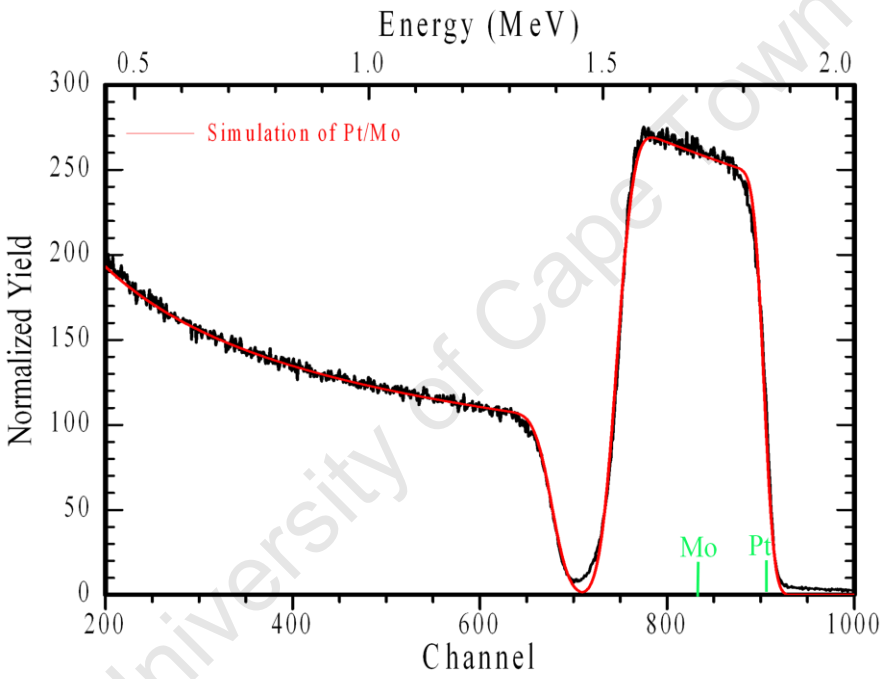

Figure 3.3: RBS spectrum of as-deposited 0.2 µm Pt coating and simulation obtained by RUMP

The back interface of the as-deposited sample appeared to be broader than the surface edge and this was attributed to the non-uniform coating layer which was deposited onto unpolished/non-uniform Mo substrate shown in Fig. 3.6 (a). The surface positions of Pt and Mo in the RBS

spectrum are indicated by green lines, at 920 and 840 channel positions, respectively. Pt is expected to appear at high energy channel because of its high atomic number (78) as compare to Mo (42). The front surface of the Pt signal appears at its surface position. However, Mo signal was found at around channel position 675 which is not unexpected as Mo was underneath the 0.2 µm Pt layer which gave rise to the energy loss before reaching the Mo substrate. It was observed, however, that Mo signal moved towards its surface channel position at about channel 840 after annealing, see Fig. 3.4 and 3.5 (a-b). This indicates that during the annealing, Mo atoms diffused towards the surface during the interaction with Pt and the formation of the Pt-Mo compounds as detected by XRD in these coatings.

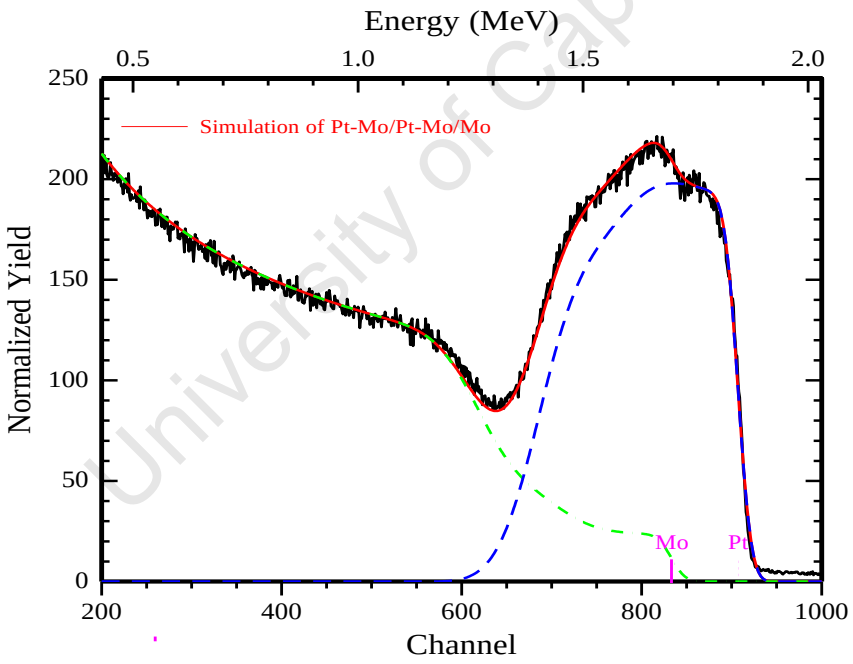

3.4: RBS results of 0.2 µm Pt annealed at 900°C for 1 hour. The blue and green dash lines illustrate the distribution of Pt and Mo, respectively

The simulation of the RBS spectrums using RUMP software is indicted by the red line. The contribution of Mo in the coating layer is shown by the green broken line while the distribution of Pt in the coating layer is illustrated by the blue broken line. All RBS spectra, including as-deposited, were simulated to determine the coating thickness and compound compositions, and the results are summarised in table 3.1. The coating thickness obtained after simulation of the as-deposited coating, Fig. 3.3, was 1450×10^{15} atoms/cm^2, which is approximately 0.22 µm Pt, and is comparable to the coating thickness indicated by crystal monitor during deposition (0.2 µm Pt). The RBS spectrum of the coating sample annealed at 900°C for 1 hour is shown in Fig. 3.4. The simulation of this spectrum required the existence of two layers of different Pt and Mo composition. In addition, fuzz command (amount: 200 and iterations: 10) was applied to obtained the best simulated spectrum. The first layer contained more Pt (73 *at%*) than in the second layer (53 *at%*), also see table 3.1. These results suggest that the ratio of Pt to Mo in the first layer is approximately 3:1 which corresponds roughly to the stoichiometry of Pt_3Mo phase. This implies, therefore, that if the information in the current literature about Pt-Mo phases, which identifies the Pt_2Mo instead of Pt_3Mo phase, is correct then our RBS analysis suggests that the Pt_2Mo phase detected by XRD in this sample is rich in Pt or possibly the excess Pt composition comes from the Pt-solid solution phase as the two-phase structure (Pt_2Mo plus Pt-solid solution) was reported in the Pt region between 70 *at%* and 80 *at%* **[15]**. The ratio of Pt to Mo in the second layer is in the region of 1:1 suggesting the presence of PtMo phase which complements the XRD results.

Table 3.1: The thickness and composition of the as-deposited and annealed (900°C for different times) 0.2 µm Pt coatings obtained by RUMP simulation

Sample	Coating thickness ($\times 10^{15}$ atoms/cm^2)	Coating thickness (µm)		Coating layer/s	Compound composition (*at%*)
As-deposited	**1450**	**0.22**		**1**	**Pt (100)**
0.2 µm Pt/Mo 900°C/1 hour	**1300**	**0.22**	**0.37**	**1**	**Pt(73) and Mo(27)**
	950	**0.15**		**2**	**Pt(53) and Mo(47)**
0.2 µm Pt/Mo 900°C/8 hours	**2820**	**0.45**		**1**	**Pt(50) and Mo(50)**
0.2 µm Pt/Mo 900°C/24 hours	**3050**	**0.47**		**1**	**Pt(49) and Mo(51)**

The second and third column of table 3.1 shows the thicknesses of the coating layer/s in atoms per cm^2 and in microns, respectively. The thickness conversion of the as-deposited sample was made based on the atomic density of Pt which is approximately 6.60×10^{22} atoms/cm^3. The mass densities of Pt_2Mo and PtMo compounds are 16.05 g/cm^3 and 15.7 g/cm^3 **[17]**, respectively, and corresponds to approximately 5.97×10^{22} atoms/cm^3 and 6.5×10^{22} atoms/cm^3. These atomic densities were used to calculate the thickness of layer 1 and 2 of the sample annealed for 1 hour in microns and the overall thickness of the two layers was found to be approximately 0.37 µm, see column 3 of table 3.1. After annealing for 8 and 24 hours, Fig. 3.5 (a) and (b), respectively, only one layer was observed by simulating the RBS spectrums of these coating samples.

No considerable difference between the compound compositions of the two samples (annealed for 8 and 24 hours) was detected, table 3.1. The RBS simulation gave approximately 1:1 Pt to

Mo compositional ratios for both samples, which was completely consistent with the XRD results of these coating samples which detected only the PtMo phase on both coating samples, Fig. 3.1 and 3.2. The only noticeable slight difference was the thickness of these two coatings which were obtained in atoms per cm^2 from RBS simulation and converted to microns using atomic density of PtMo phase (6.5×10^{22} atoms/cm^3).

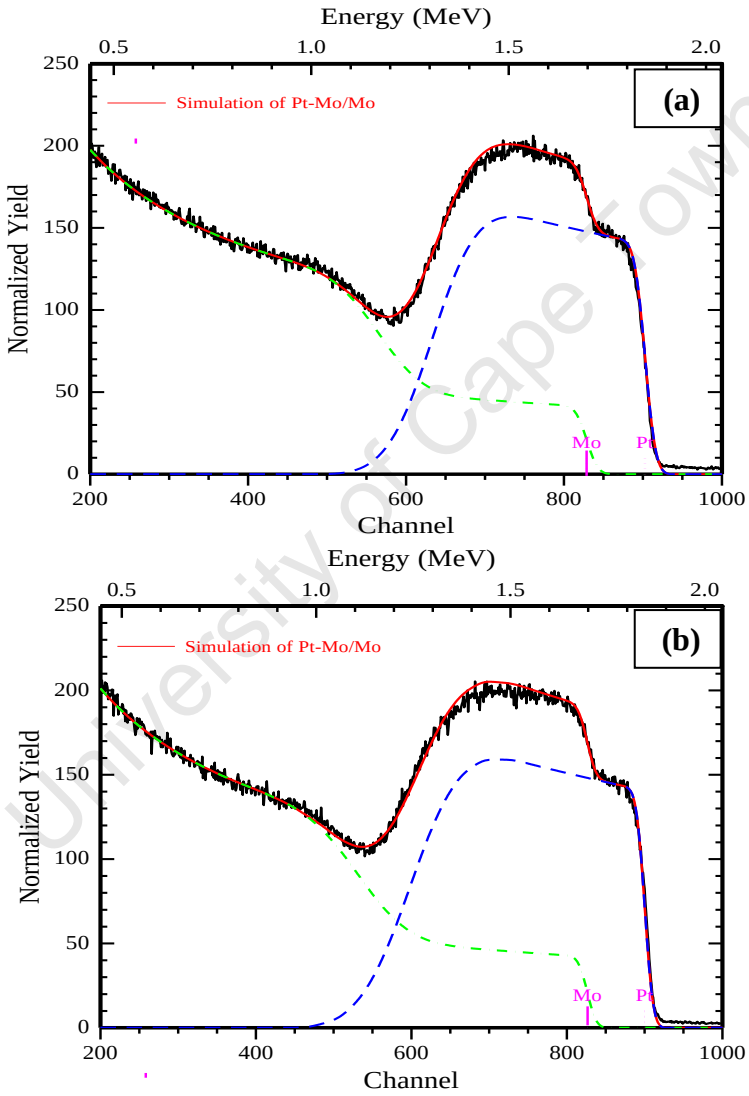

Figure 3.5: RBS results of 0.2 µm Pt annealed at 900°C for: (a) 8 hours and (b) 24 hours. The blue and green dash lines illustrate the distribution of Pt and Mo, respectively

It can be seen that the thickness of the film increases with reaction, but this is as expected as Mo is incorporated into the film. In the formation of PtMo phase, the original 0.22 µm Pt grows to a final thickness of approximately 0.46 µm which is not unreasonable since Pt and Mo atoms are roughly of the same size (2.8 Å) **[1]**, and the final composition is roughly 1:1 ratio. It should be noted that the total number of Pt atoms/cm^2 remains roughly constant e.g. 1450×10^{15}atoms/cm^2 in as-deposited and ½(2820×10^{15}atoms/cm^2) Pt in the sample annealed at 900°C for 8 hours.

3.1.3 Scanning Electron Microscopy (SEM)

The effect of annealing on coating morphology was investigated using the SEM operated in the secondary electron mode. The micrographs of the Mo substrate used in this investigation and of the as-deposited 0.2 µm Pt coating are shown in Fig. 3.6 (a-b).

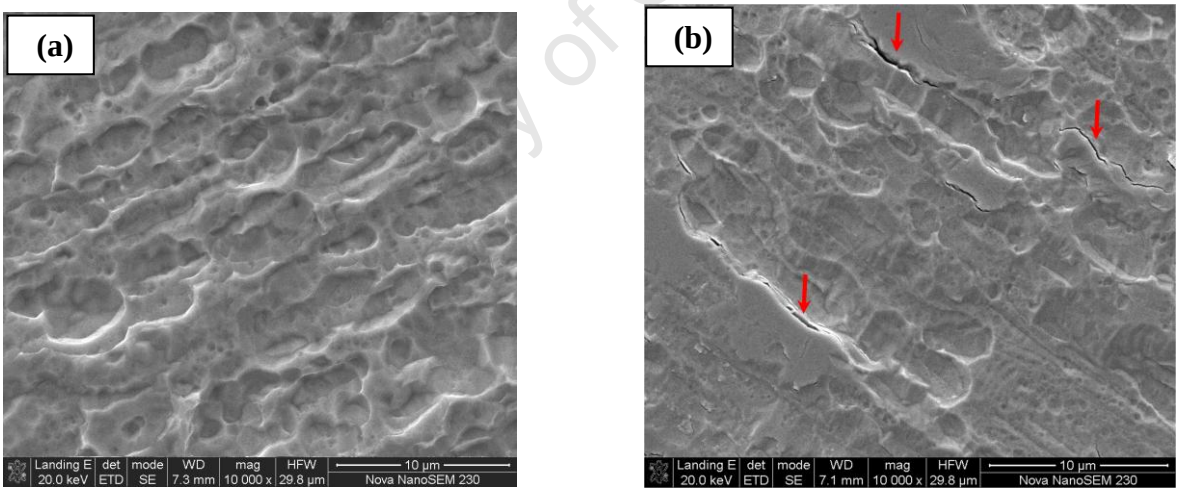

Figure 3.6: SEM images of: (a) Molybdenum substrate (b) as-deposited 0.2 µm Pt layer

It should be noted that the Pt layers were deposited onto unpolished molybdenum substrate, Fig. 3.6 (a). Consequently, the thin Pt coating layer followed the substrate morphology, Fig. 3.6 (b).

The surface morphology of the as-deposited coating also shows a number of cracks on the Pt layer as indicated by red arrows. The SEM analysis showed that the surface morphology of the 0.2 µm Pt coatings changed significantly after annealing at 900°C for 1, 2, 4 and 8 hours, Fig. 3.7 (a-d) when compared to the as-deposited.

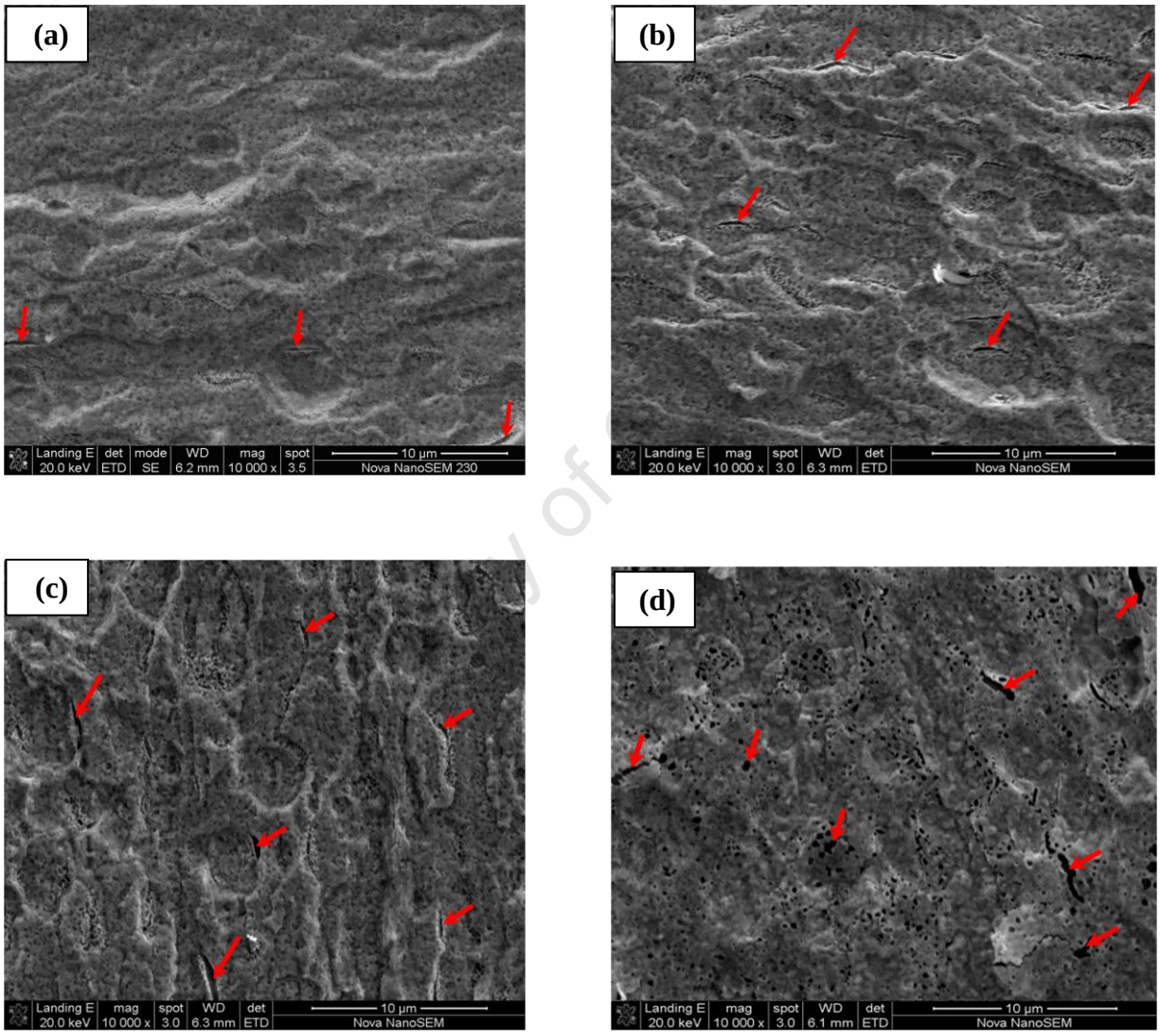

Figure 3.7: SEM images of 0.2 µm Pt coatings annealed at 900°C for: (a) 1 hour, (b) 2 hours, (c) 4 hours and (d) 8 hours

The presence of "spongy looking" coating surfaces were observed on the annealed coatings. In addition, surface cracks indicated by red arrows were also noticed across the coating surfaces of the annealed samples and were more pronounced on the sample annealed for 4 and 8 hours, Fig. 3.7 (c-d). The EDX analysis, table 3.2, was performed on the as-deposited and annealed samples for elemental composition determination in an attempt to use EDX to compare with the compound compositional results obtained by means of RBS. The data was obtained using EDX software (INCA software) and each spectrum was acquired for 30 seconds at 20 kV. The following X-ray emission lines were used: $PtM_{\alpha 1}$, $PtL_{\alpha 1}$, $PtL_{\beta 1}$, $MoL_{\alpha 1}$ and $MoL_{\beta 1}$ (see appendix, Fig. A and B).

Table 3.2: The elemental composition of the as-deposited and annealed (900°C for 1, 2, 4 and 8 hours) 0.2 µm coating systems obtained by EDX attached to the SEM at the excitation energy of 20keV in selected areas

Sample	Molybdenum (*at* %)	Platinum (*at* %)
0.2 µm Pt/Mo as-deposited	**23**	**77**
0.2 µm Pt/Mo 900°C/1 hour	**49**	**51**
0.2 µm Pt/Mo 900°C/2 hours	**53**	**47**
0.2 µm Pt/Mo 900°C/4 hours	**53**	**47**
0.2 µm Pt/Mo 900°C/8 hours	**57**	**43**

The chemical composition was obtained by selecting an area of approximately 30 μm^2 with the interest to probe the average composition of Pt and Mo on the coating layers. The results presented in table 3.2 indicate a higher Mo content than that obtained by RBS, and even indicate the presence of Mo in the as-deposited film. As the detection of Mo in the as-deposited sample is most likely due to the penetration of the electron beam through the film and into the substrate, the penetration depth of electrons in platinum and molybdenum was calculated. The energy of the beam of electrons used during EDX analysis was 20 keV. The depth of electron penetration was calculated using the following expression **[42]**:

$$R = \frac{4120}{\rho} E^{(1.265-0.0954 \ln E)} \qquad 3.2$$

where: R is the depth of electron penetration in microns, E is the primary electron energy in MeV and ρ is the absorber density in g/cm^3.

The penetration of the electrons in the Pt layer was determined to be approximately 0.32 μm and that of Mo about 0.67 μm. Based on the determined depth of electron penetration in Pt (0.32 μm), it is clear that the 20 keV electron beam penetrated through the as-deposited (0.2 μm Pt layer) film to the Mo substrate, as a result the Mo content was detected, table 3.2. Although the thickness of the Pt-Mo coating increases on annealing due to compound formation, the fact that the penetration depth in Mo is approximately twice that of Pt means that it is likely that the beam still penetrates through to the Mo substrates even for the thickest films, which goes some way to explaining why the higher Mo content was detected in the annealed samples as shown in table 3.2.

Given that the average elemental composition analyses of the 0.2 µm Pt coatings could not be obtained by EDX in order to make comparison to the compound compositions obtained from RBS analysis, it was decided to perform cross-sectional transmission electron microscopy (TEM) analysis on the annealed 0.2 µm Pt coating system so as to determine the Pt and Mo composition across the cross-section of the coating and ultimately make comparison with RBS.

3.1.4 Transmission Electron Microscopy (TEM)

Transmission electron microscope image of the cross-section of the coating annealed at 900°C for 1 hour shows the coating (region A) and the substrate (region B), Fig. 3.8.

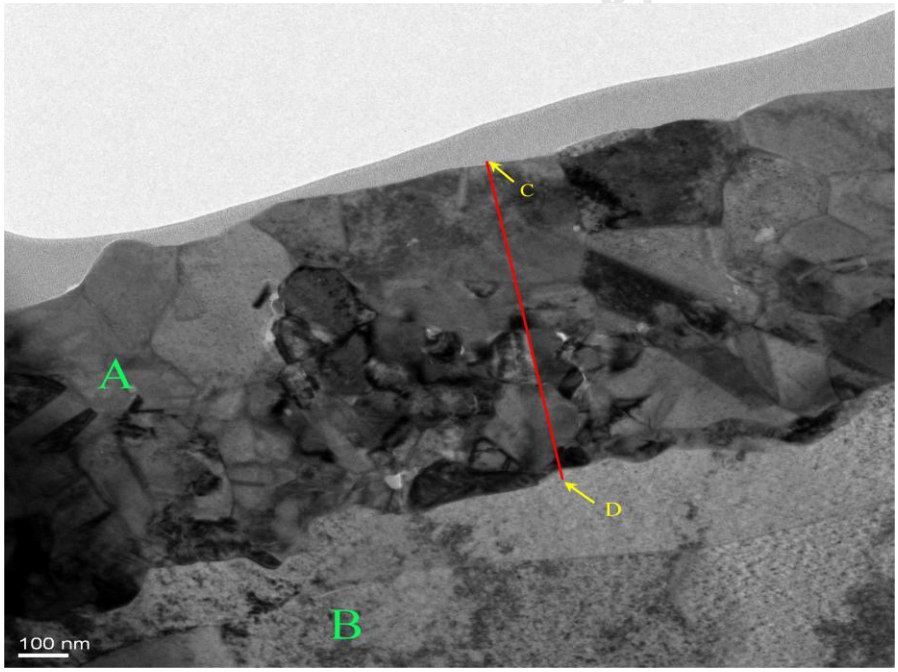

Figure 3.8: Cross-section image of 0.2 µm Pt coating annealed at 900°C for 1 hour showing coating (region-A) and Mo substrate (region-B) obtained by TEM. The points for compositional analysis were taken along the red line C-D

The average coating layer thickness in the regions analysed by TEM was calculated based on the scale bar to be approximately 0.68 µm with 10% uncertainty. This thickness is, however, not in agreement to the thickness obtained from RBS simulation of the same sample (0.37µm). Possible reasons for this discrepancy are as follows: firstly, the density of the compounds present in the sample. RBS measures atoms per cm^2, and to get the thickness in microns one needs to know the atomic density of each compound present in the sample. The atomic density of the Pt_2Mo phase, detected in this sample, is not well known because RBS showed that the phase contained about 3:1 Pt to Mo ratio. The RBS thickness in microns was, however, calculated using the atomic density of 2:1 composition available in the literature **[17]**. Secondly, the size of the area where TEM and RBS experiments were performed was different. During TEM analysis a small area of a few microns was examined. In addition, the coating layer was not uniform. RBS, on the other hand, takes the coating average of about 2 mm in diameter.

The microstructure of the coating region shows the presence of grains of different size. The grain size varied between 60 nm to 270 nm. The distribution of Pt and Mo elements across the cross-section of the coating was obtained by means of EDX attached to the TEM (Tecnai G2 F20 X-Twin) instrument. The line scan was performed as shown by the red line drawn across the coating to the substrate, Fig. 3.8. The results of the eighteen equally spaced depth (from C to D) taken along the line, with an electron beam of 1 micron spot size, are plotted in Fig. 3.9.

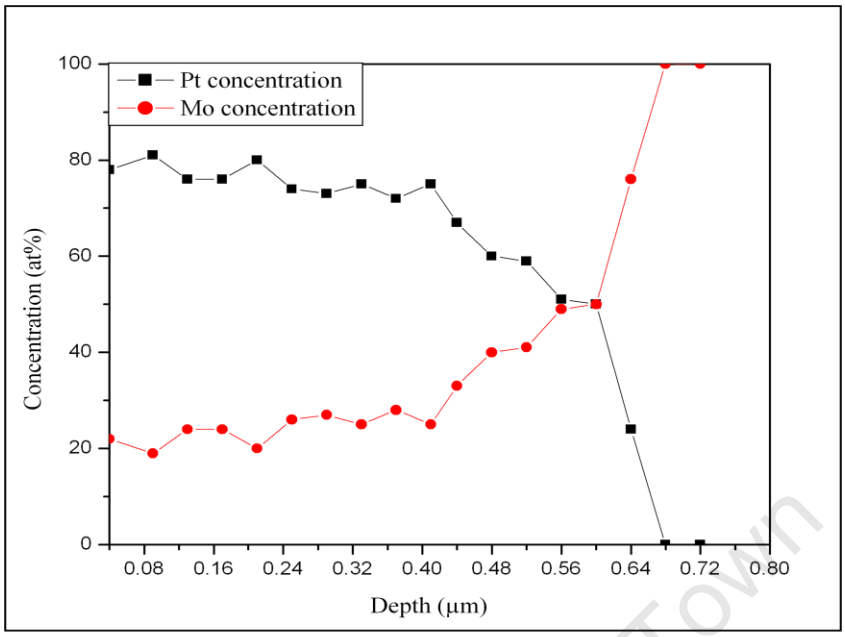

Figure 3.9: The distribution of Pt and Mo from the surface across the coating through the substrate in the 0.2 μm coating annealed at 900°C for 1 hour determined by EDX attached to TEM

It was found that about 60% of the coating has a Pt composition of approximately 74 *at%*. These results are in reasonable agreement with RBS results obtained from the analysis of the same coating (table 3.1). It can be reported, therefore, that both RBS and TEM analyses showed that in this sample the Pt_2Mo phase detected by XRD is Pt rich or possibly Pt-solid solution also exist in the sample. The ratio of Pt to Mo in this coating sample (annealed for 1 hour at 900°C) found to be close to 3:1 which is in the region where two-phase structure was reported.

The remaining part of the coating layer, according to TEM, contained comparable Pt and Mo composition of about 50 *at%*, in agreement with the findings by other techniques, XRD and

RBS. XRD detected PtMo compound while RBS simulation gave compound composition, in the second layer of the sample annealed for 1 hour, having 53 *at%* Pt and 47 *at%* Mo, see table 3.1.

3.2 Co-deposited samples with approximately 2:1 and 3:1 Pt to Mo ratios

The Pt-Mo phase analysis was also investigated on co-deposited coating samples. The samples were designed to have different Pt and Mo stoichiometries in the region of a single phase Pt_2Mo (about 2Pt: 1Mo) and two-phase region (about 3Pt: 1Mo). These coating samples were prepared at Lehigh University (USA) using PVD sputtering.

3.2.1 Rutherford Backscattering Spectrometry (RBS)

The compound compositions and the thicknesses of the co-deposited systems were analysed using RBS technique. The controlled compositional ratio of Pt to Mo in the prepared co-deposited sample was designed to be 2:1, corresponding to the Pt_2Mo phase, while the compositional ratio of Pt to Mo in the other sample was prepared to be in the range of 3:1 which corresponds to a Pt_3Mo stoichiometry or the reported two-phase region. The RBS simulation of the as-deposited and annealed (at 750°C for 1 hour) Pt_2Mo samples are given in Fig. 3.10 (a-b) and the compound compositional and thickness results are summarised in table 3.3. The annealing temperature (750°C) was chosen based on the findings of Roocksby *et al.* **[10]** that there is no Pt-Mo phase formation occurred below 800°C. It can be reported that the compound composition obtained on both co-deposited systems, as-deposited and annealed, was the same. The Pt and Mo compositions was 65 *at%* and 35 *at%*, respectively, which corresponds approximately to a 2:1 ratio of Pt to Mo composition controlled during the co-deposition of the system. The thickness of the samples which was measured from the back edge of the spectrums

was unchanged (1.16 µm) confirming that no reaction took place between the substrate and the coating layer during the annealing. However, the thickness was found to be slightly greater than, but comparable to, the thickness set for deposition (1.0 µm).

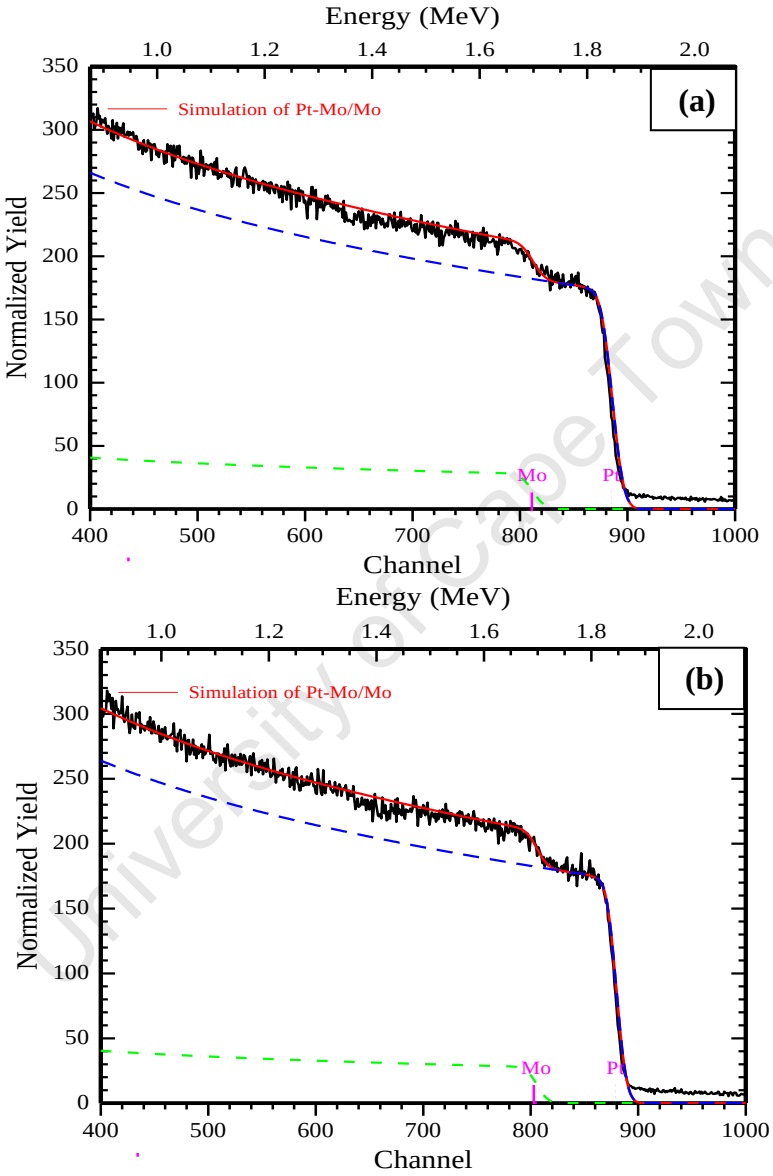

Figure 3.10: RBS results of co-deposited Pt and Mo (Pt_2Mo) samples: (a) as-deposited condition and (b) annealed at 750°C for 1 hour. The blue and green dash lines illustrate the distribution of Pt and Mo, respectively

The Pt_3Mo (3:1) system, as-deposited and annealed, were also analysed for compound composition and thickness determination using RBS, Fig. 3.11 (a-b). The simulation of the as-deposited sample, Fig. 3.11 (a), and the annealed sample at 750°C for 1 hour, 3.11 (b), gave same Pt and Mo compound composition and thickness.

Table 3.3: Compound composition of as-deposited and annealed Pt_2Mo and Pt_3Mo coating samples

Sample	Coating thickness ($\times 10^{15}$ atoms/cm^2)	Coating thickness (µm)	Phase composition (*at%*)
Pt_2Mo alloy as-prepared	**7540**	**1.16**	**Pt (65) and Mo (35)**
Pt_2Mo alloy 750°C/1 hour	**7540**	**1.16**	**Pt (65) and Mo (35)**
Pt_3Mo alloy as-prepared	**7010**	**1.06**	**Pt (80) and Mo (20)**
Pt_3Mo alloy 750°C/1 hour	**7010**	**1.06**	**Pt (80) and Mo (20)**

The Pt composition was, however, found to be 80 *at%* Pt and 20 *at%* Mo, see table 3.3. The expected Pt to Mo ratio in this system was 3:1 and the analysis by RBS, however, showed that the ratio is 4:1. It should be pointed out, however, that the composition was still in the compositional range where two-phase Pt_2Mo plus Pt-solid solution was reported by Ocken *et al*. **[15]**. In addition, the thickness which was measured from the back of the spectrums was found to be comparable to the control thickness during deposition (1.0 µm), see table 3.3.

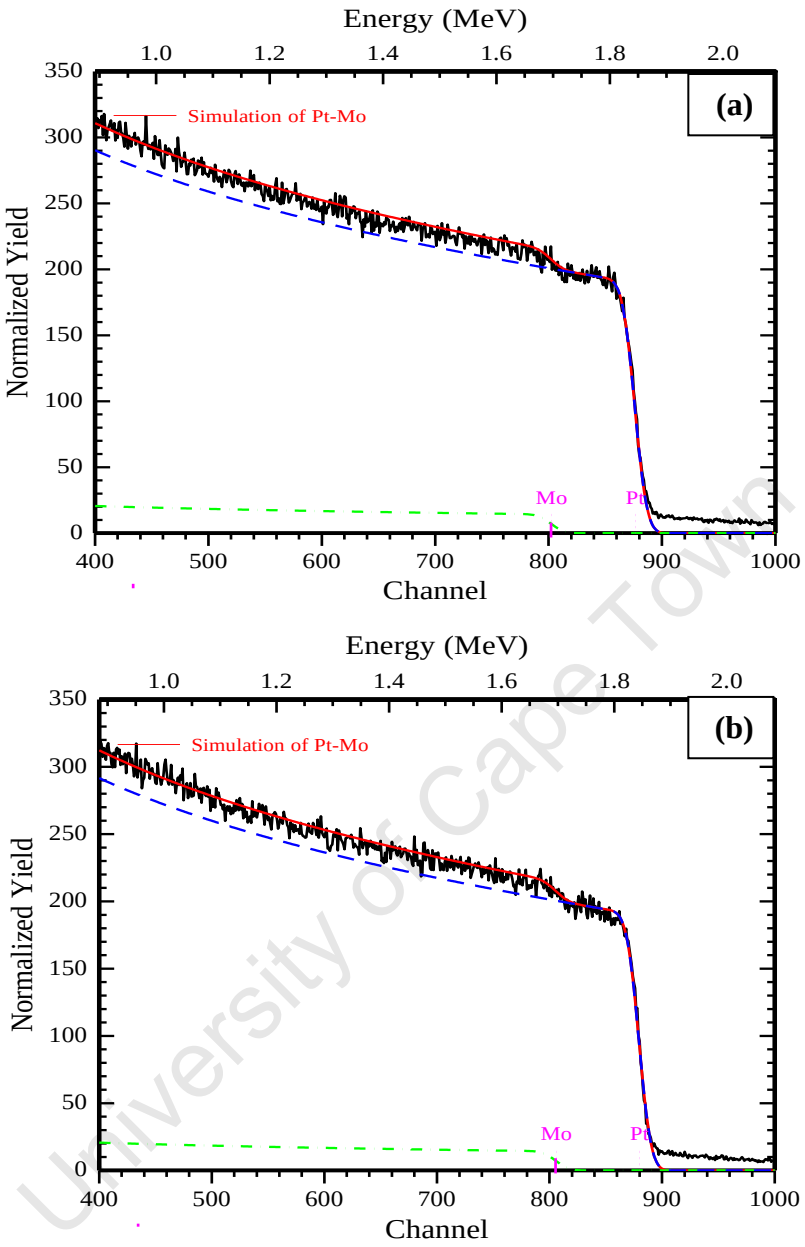

Figure 3.11: RBS results of co-deposited Pt and Mo (Pt_3Mo) samples: (a) as-deposited condition and (b) annealed at 750°C for 1 hour. The blue and green dash lines illustrate the distribution of Pt and Mo, respectively

3.2.2 X-ray diffraction (XRD)

The XRD results of the co-deposited samples are given in Fig.3.12 and 3.13. Both coatings were annealed at 750°C for 1 hour and compared with the as-deposited.

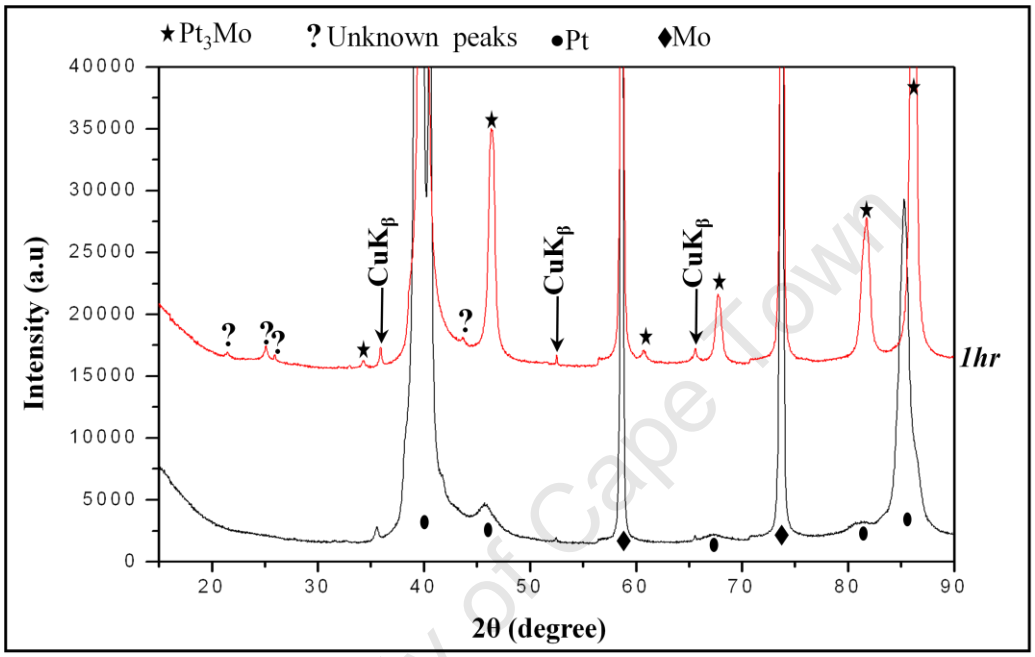

Figure 3.12: X-ray diffraction patterns of the co-deposited Pt and Mo (Pt_2Mo) in as-deposited and annealed (750°C for 1 hour) conditions. CuK_β line was also diffracted and detected due to the strongest intensities of Mo peaks at 2θ = 58.61° and 73.68° and Pt at 2θ = 39.7°

The XRD results of the as-deposited samples showed diffraction peaks of only Pt and Mo on both co-deposited samples. On the other hand, the diffraction peaks associated to an ordered form of terminal f.c.c. Pt solid solution phase (Pt_2Mo) were detected on both heat treated

samples. No pure Pt diffraction peaks were observed after annealing. In addition, the Mo diffraction peaks, from the substrate, were still detected at this annealing temperature and time.

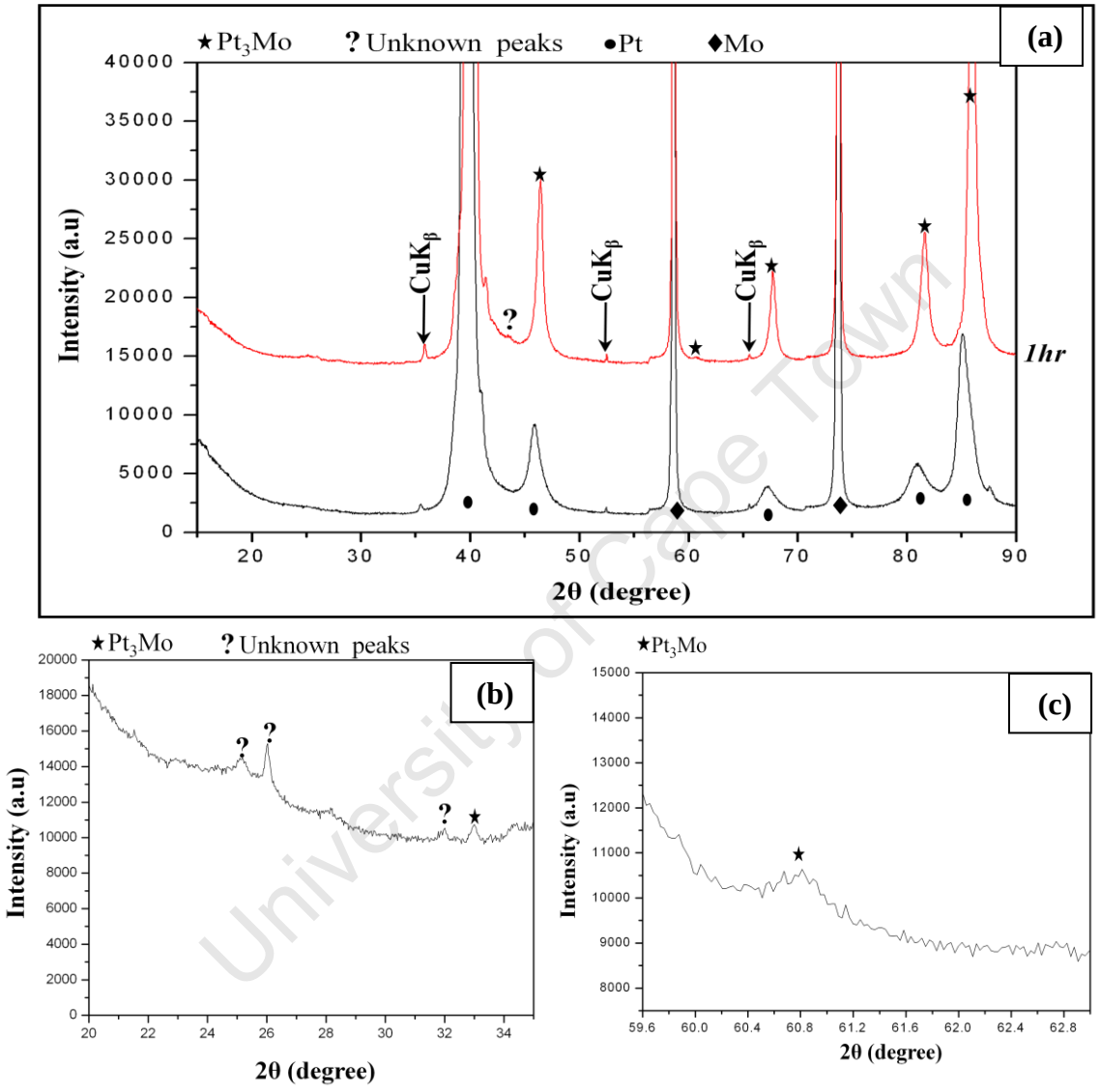

Figure 3.13: (a) X-ray diffraction patterns of the co-deposited Pt and Mo (Pt_3Mo) coatings in as-deposited and annealed (750°C for 1 hour) conditions (b) short range scan at 2θ = 20 - 35° and (c) short range scan at 2θ = 58.5° - 63°. CuK_β line was also diffracted and detected due to the strongest intensities of Mo peaks at 2θ = 58.61° and 73.68° and Pt at 2θ = 39.7°

The unknown diffraction peaks, believed to be related to Pt_2Mo compound, were observed on the annealed coating samples. In the sample with 4:1 Pt to Mo ratio the intensity of the unknown diffraction peaks was, however, very weak. Therefore in order to reveal these diffraction peaks a short range 2θ scan, at 2θ = 20-35°, was performed and the peaks were then clearly observed, Fig. 3.13 (b). The other weak intensity peak, assigned to Pt_2Mo phase at 2θ = 60.05°, was also revealed by a short range 2θ scan between 58.5° and 63°, Fig. 3.13 (c).

It can be concluded, therefore, that XRD diffraction patterns of the two co-deposited systems, having different Pt and Mo stoichiometries and annealed at 750°C for 1 hour, showed that the Pt_2Mo compound exists over a large Pt compositional range up to at least 80 *at%*. However, if the interpretation of the currently existing Pt-Mo phase diagram is accepted this suggest that at Pt composition above 70 *at%* the Pt_2Mo coexist with Pt-solid solution which could not be detected by XRD.

3.3 First phase formation in Pt-Mo system

It has been predicted by the EHF model that the phase formation sequence in Pt-Mo coating system starts from Pt rich phase/phases to Mo rich phases (section 1.3.2.2). The earlier investigation, however, showed the presence of two Pt-Mo compounds (Pt_2Mo and PtMo) in Pt-Mo coatings annealed at 900°C for 1, 2 and 4 hours. It was believed, therefore, that the annealing temperature of 900°C was high enough for the nucleation of the second phase, PtMo. In order to investigate the first phase formation, the annealing temperature was reduced below 900°C. Annealing in the range 800°C to 880°C, in steps of 20°C, for 1 hour showed no phase formation was observed until 840°C. The sample annealed for 1 hour at 840°C showed the presence of only one phase, Pt_2Mo, Fig. 3.14.

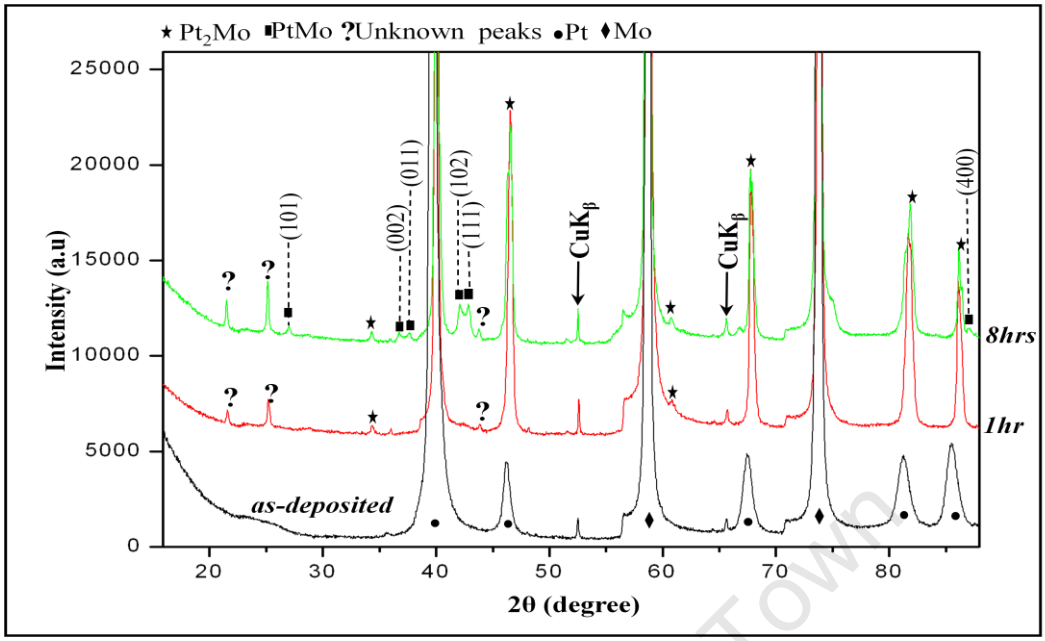

Figure 3.14: X-ray diffraction patterns of 0.2 µm Pt coatings annealed at 840°C for 1 and 8 hours. CuK_β line was also diffracted and detected due to the strongest intensities of Mo peaks at 2θ = 58.61° and 73.68°

The appearances of unknown diffraction peaks, which have been reported to be related to Pt_2Mo phase, were also observed in this sample. No diffraction peaks matching the PtMo compound were observed after 1 hour. This indicates that Pt_2Mo phase has been detected by XRD to be the phase that nucleate first in Pt coated Mo systems. XRD results of this coating, annealed for 1 hour, were compared to the XRD results of the coating annealed for 8 hours at the same annealing temperature. It can be seen that the PtMo compound was detected in this sample. The XRD pattern indicates that the Pt_2Mo phase was still present at these annealing conditions (840°C for 8 hours). The RBS analysis was also performed on these two coatings for compound composition determination, Fig. 3.15 (a-b).

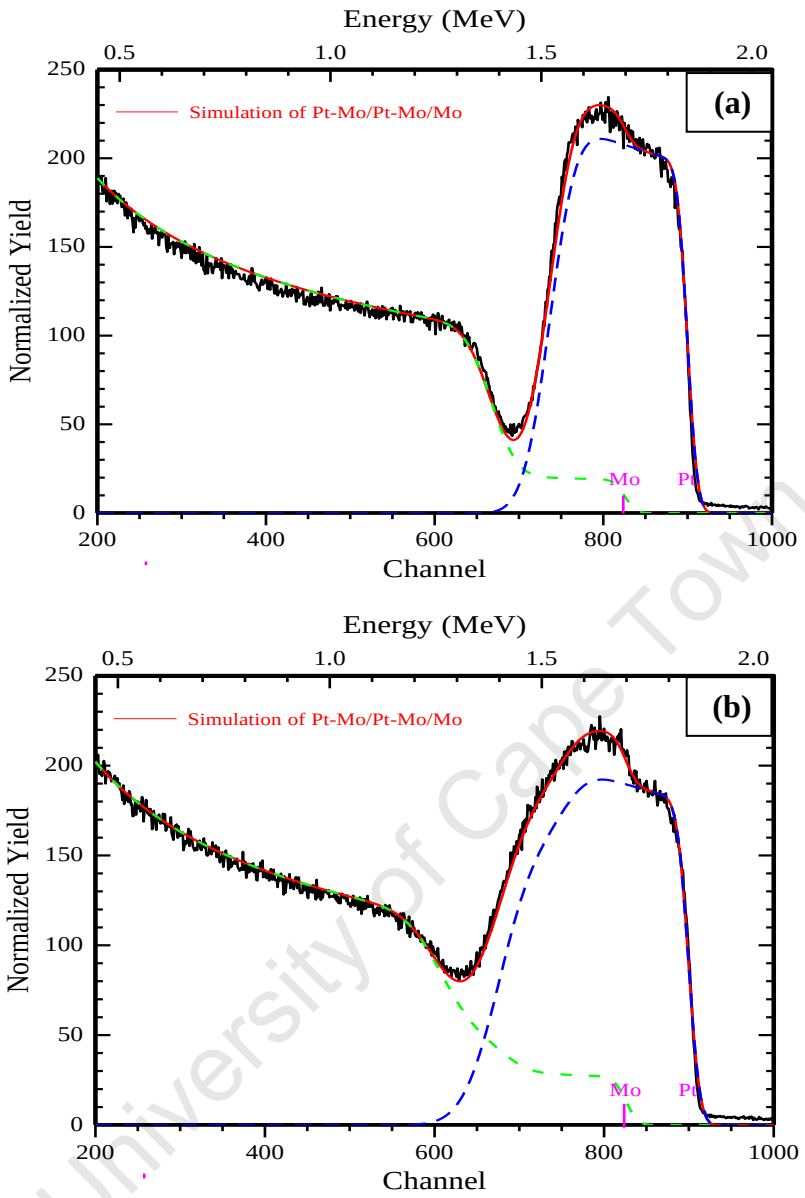

Figure 3.15: RBS spectra of 0.2 µm Pt annealed at 840°C for: (a) 1 hour and (b) 8 hours. The blue and green dash lines illustrate the distribution of Pt and Mo, respectively, obtained by simulation

Table 3.4 shows the results of the simulation performed on the RBS spectrums of these coatings. The RBS analysis of the sample annealed at 840°C for 1 hour gave only one layer having 77 *at%* Pt and 23 *at%* Mo compositions. It can be noted, while RBS indicated a compound composition of 77 *at%* Pt and 23 *at%* Mo, XRD detected only Pt_2Mo compound in this coating sample which again confirms that the phase exists at high Pt composition. It should also be noted that EHF values for Pt_2Mo phase and Pt-solid solution, given in table 1.2, are very close suggesting that the two phases have equal probability to form first in Pt-Mo system. Based on the compound compositional analysis of the sample annealed for 1 hour, more Pt composition than the one of Pt_2Mo phase was confirmed by RBS. This has been attributed to the presence of Pt-solid solution in this sample which XRD could not detect. Therefore, these results are in good agreement with EHF predictions. In addition, the results seem to be in reasonable agreement with the two-phase region (Pt_2Mo and Pt-solid solution) reported to exist in the Pt-Mo phase diagram.

Table 3.4: Composition and thickness of the coating samples annealed at 840°C for 1 and 8 hours (initial coating thickness was 0.22 µm from RBS) obtained by simulation

Sample	Coating thickness ($\times 10^{15}$atoms/cm^2)	Coating thickness (µm)		Coating layer/s	Phase composition (*at%*)
0.2 µm Pt/Mo 840°C/1 hour	1750	0.29		1	Pt(77) and Mo(23)
0.2 µm Pt/Mo 840°C/8 hours	1500	0.25	0.37	1	Pt(69) and Mo(31)
	800	0.12		2	Pt(53) and Mo(47)

A two layers coating was obtained after simulating the sample annealed for 8 hours, Fig. 3.15 (b). The layers contained different Pt and Mo compound compositions. The first layer contained 69 *at%* Pt and 31 *at%* Mo while the second layer contained 53 *at%* Pt and 47 *at%* Mo, table 3.5. These results complement the XRD analysis performed on this coating system where two phases were detected, Pt_2Mo and PtMo. Given that the Pt_2Mo phase detected in this sample, RBS suggested that the phase has Pt to Mo ratio of approximately 2:1. Therefore, these results further confirm that the Pt_2Mo phase exist over a broad compositional range. The broadening of the coating layers after annealing, showing the intermixing of Pt and Mo atoms and the formation of Pt-Mo compounds, was observed in these coatings.

CHAPTER 4 RESULTS FROM SPUTTERED SAMPLES

The characterization of the 0.2 μm coatings, heat treated at different temperatures and periods, by XRD, RBS, SEM, TEM and EDX has been carried out and the results were found to be reasonably consistent. The RBS results showed that Pt_2Mo and Pt-solid solution coexist in the Pt compositional range 70 *at%* to 80 *at%* which is in agreement with EHF prediction and the two-phase structure reported in the literature. Therefore, the Pt_2Mo phase exists over a wide Pt compositional range. The second compound observed to nucleate is PtMo phase which has been observed to grow at the expense of Pt_2Mo compound. The phase formation investigation has been extended to coating systems of thickness 0.3 μm and 0.5μm, which were prepared by the sputtering coating technique.

4.1 The characterisation of 0.3 μm Pt layer coatings

4.1.1 X-ray diffraction (XRD) results

The results of XRD analysis of 0.3 μm coating systems are shown in Fig. 4.1. The diffraction patterns showed the formation of two compounds, Pt_2Mo and PtMo, after annealing at 900°C for 1, 2 and 4 hours. These compounds were also detected in 0.2 μm coating systems, deposited by EBE, after annealing under the same conditions. It was also observed that annealing for longer periods (8 and 24 hours) resulted in the consumption of Pt_2Mo compound during the growth of PtMo phase in both coating systems (0.2 μm and 0.3 μm). It can be reported, therefore, that no differences were observed by increasing the coating thickness from 0.2 μm to 0.3 μm in terms of phase formation.

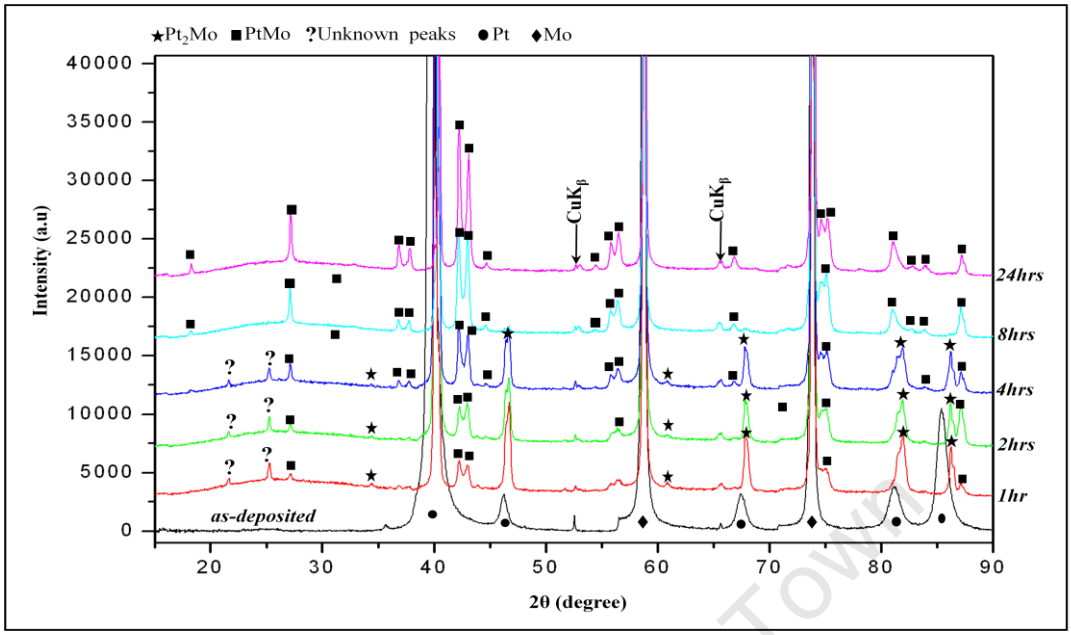

Figure 4.1: X-ray diffraction patterns of 0.3 μm Pt layer deposited on Mo substrate in as-deposited and annealed (900°C for 1, 2, 4, 8 and 24 hours) conditions. CuK_β line was also diffracted and detected due to the strongest intensities of Mo peaks at 2θ = 58.61° and 73.68°

The compound composition and the thickness of 0.3 μm layer coatings were then investigated by means of RBS and the results are presented in the following section.

4.1.2 Rutherford Backscattering Spectrometry (RBS)

The RBS analysis of the as-deposited 0.3 μm layer coating is shown in Fig. 4.2. It was observed that increasing the thickness of the coating system, from 0.2 μm to 0.3 μm, increased the width of Pt signal which resulted in the Mo signal shifting to a lower channel position (about 600) when compared to the Mo channel position of the as-deposited 0.2 μm coating (675), see Fig.

3.3. The thicker Pt layer increases the number of Pt atoms on the surface of the coating which then contributed to the energy loss of the incident beam during interaction with the Pt coating layer, causing the energy of the beam reaching the substrate to be further reduced.

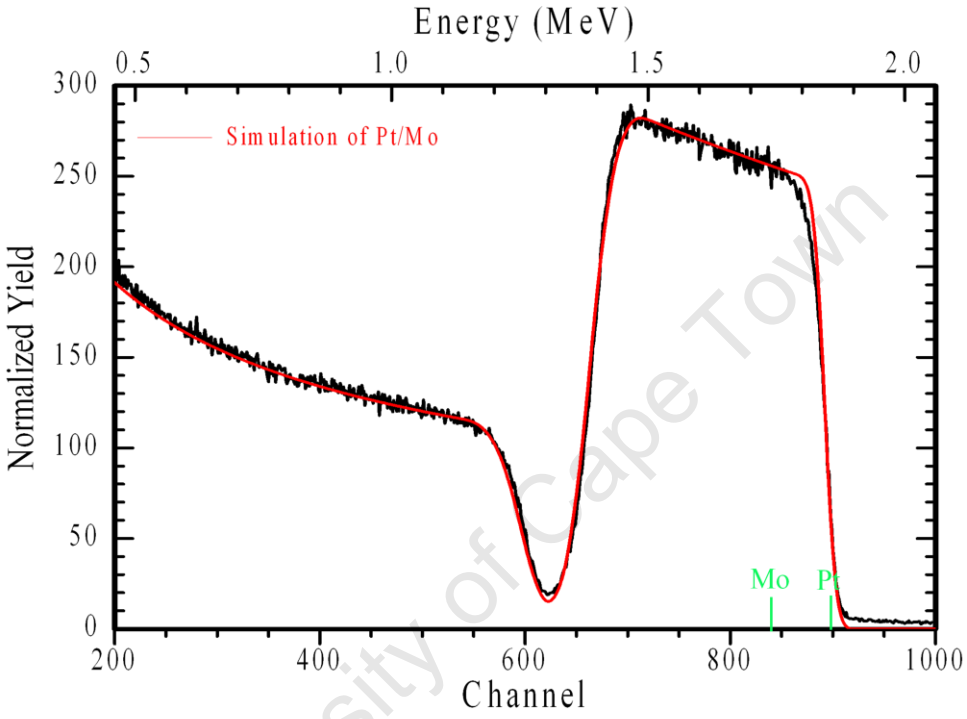

Figure 4.2: RBS results of as-deposited 0.3 µm coating deposited by sputtering

The spectra of as-deposited coating and those annealed at 900°C for different times were simulated for thickness as well as compound compositions. The results of the simulations are summarised in table 4.1.The thickness of the as-deposited 0.3 µm coating was found to be 2180×10^{15} atoms/cm^2 (0.32µm). The simulation of the RBS spectrum of the sample annealed at 900°C for 1 hour, Fig. 4.3 (a), reveal the presence of two layers with different compositions.

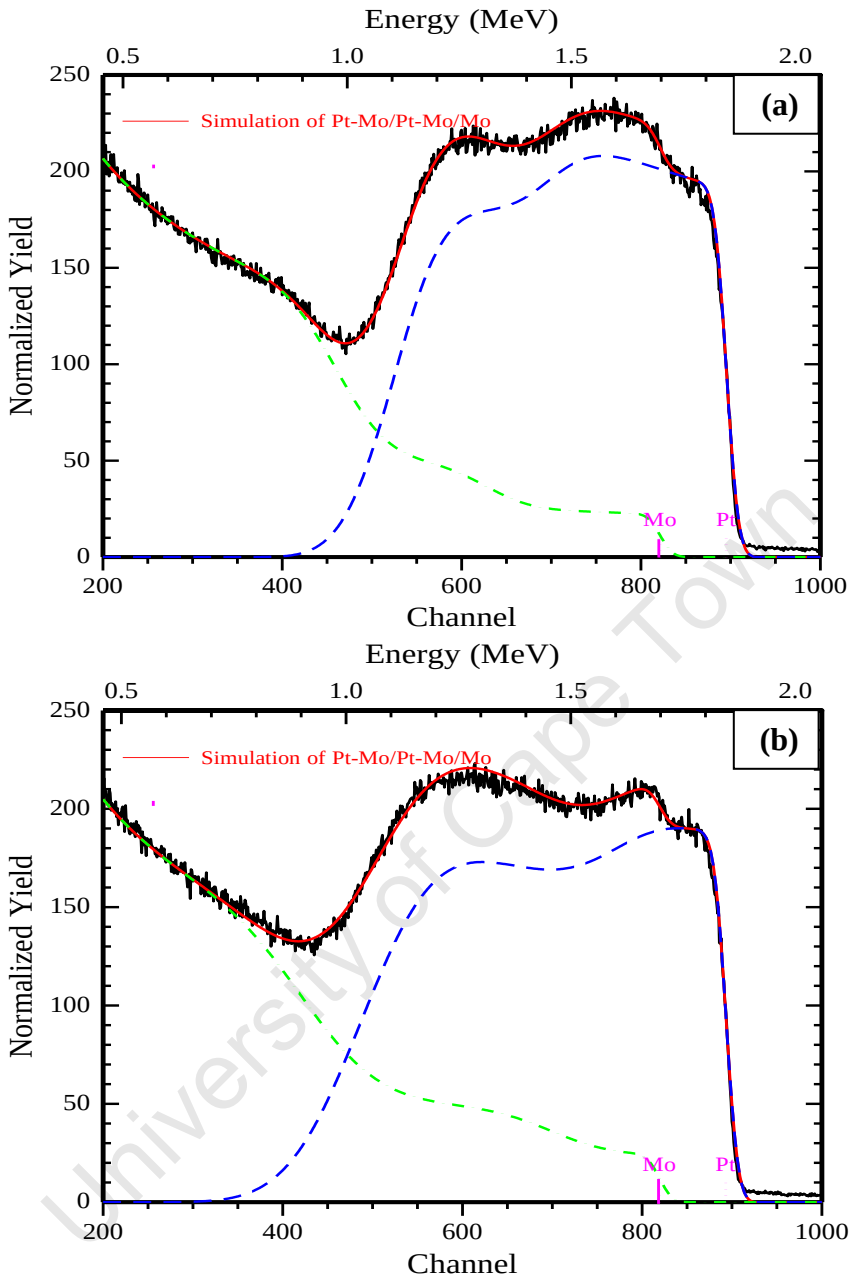

Figure 4.3: RBS results of 0.3 µm Pt coatings annealed at 900°C for (a) 1 hour and (b) 4 hours. The blue and green dash lines illustrate the distribution of Pt and Mo, respectively

The Pt and Mo concentrations in the first layer were 73 *at%* and 27 *at%*, respectively. The composition of the second layer (53 *at%* Pt and 47 *at%* Mo) corresponds to the phase with 1:1 Pt to Mo ratio (PtMo) which is in agreement with the results obtained by XRD, Fig. 4.1. The RBS spectrum of the coating annealed for 4 hours is presented in Fig. 4.3 (b). The simulation results of this sample also show the presence of two layers with different compositions. However, the compound compositions as well as thicknesses of the layers were different from the ones obtained by simulating the coating annealed for 1 hour, see table 4.1.

Table 4.1: Coating thickness and phase composition of 0.3 µm Pt coatings in as-deposited and annealed (900°C for different times) conditions

Sample	Coating thickness (atoms/cm2)	Coating thickness (µm)		Coating layer/s	Phase composition (*at%*)
As-deposited	**2180**	**0.32**		**1**	**Pt (100)**
0.3µmPt/Mo 900°C/1 hour	**1970**	**0.33**	**0.57**	**1**	**Pt(73) and Mo(27)**
	1620	**0.24**		**2**	**Pt(53) and Mo(47)**
0.3µmPt/Mo 900°C/4 hours	**1250**	**0.21**	**0.65**	**1**	**Pt(68) and Mo(32)**
	2840	**0.44**		**2**	**Pt(50) and Mo(50)**
0.3µmPt/Mo 900°C/8 hours	**4400**	**0.68**		**1**	**Pt(50) and Mo(50)**
0.3µmPt/Mo 900°C/24hours	**4600**	**0.71**		**1**	**Pt(49) and Mo(51)**

The ratio of Pt to Mo in the first layer of the coating annealed for 1 hour was approximately 3:1 while the ratio of Pt to Mo in the first layer of the coating annealed for 4 hours was found to be

closer to 2:1. It should be pointed out that XRD detected Pt_2Mo compound on both coatings, therefore, these observations further suggest that Pt_2Mo compound can exist over a wide compositional range. However, at high Pt compositional range (70 *at%* to 80 *at%*) the phase is believed to coexist with Pt-solid solution. The ratio of Pt to Mo in the second layers of both coatings (annealed for 1 and 4 hours) was 1:1 and it is consistent with the phase analysis results of these coatings by XRD. In addition, the thickness of the second layer increased after annealing for 4 hours, table 4.1. This is associated with the growth of PtMo phase as XRD results showed an increased intensity of this phase after 4 hours, Fig. 4.1.

The RBS results of coated systems annealed for 8 and 24 hours, Fig. 4.4 (a-b), show the formation of one layer with Pt to Mo ratio of 1:1, also see table 4.1. These results are consistent with XRD analyses of these coatings; the formation of only the PtMo phase was detected with both annealed conditions (900°C for 8 and 24 hours), Fig. 4.1. The simulation of these coating samples gave comparable compositional and thickness results. Due to the diffusion of Mo atoms from the interface to the surface of the coating, the broadening of the coating thickness from 0.3 µm (as-deposited) to approximately 0.7 µm (annealed coatings) was observed, table 4.1.

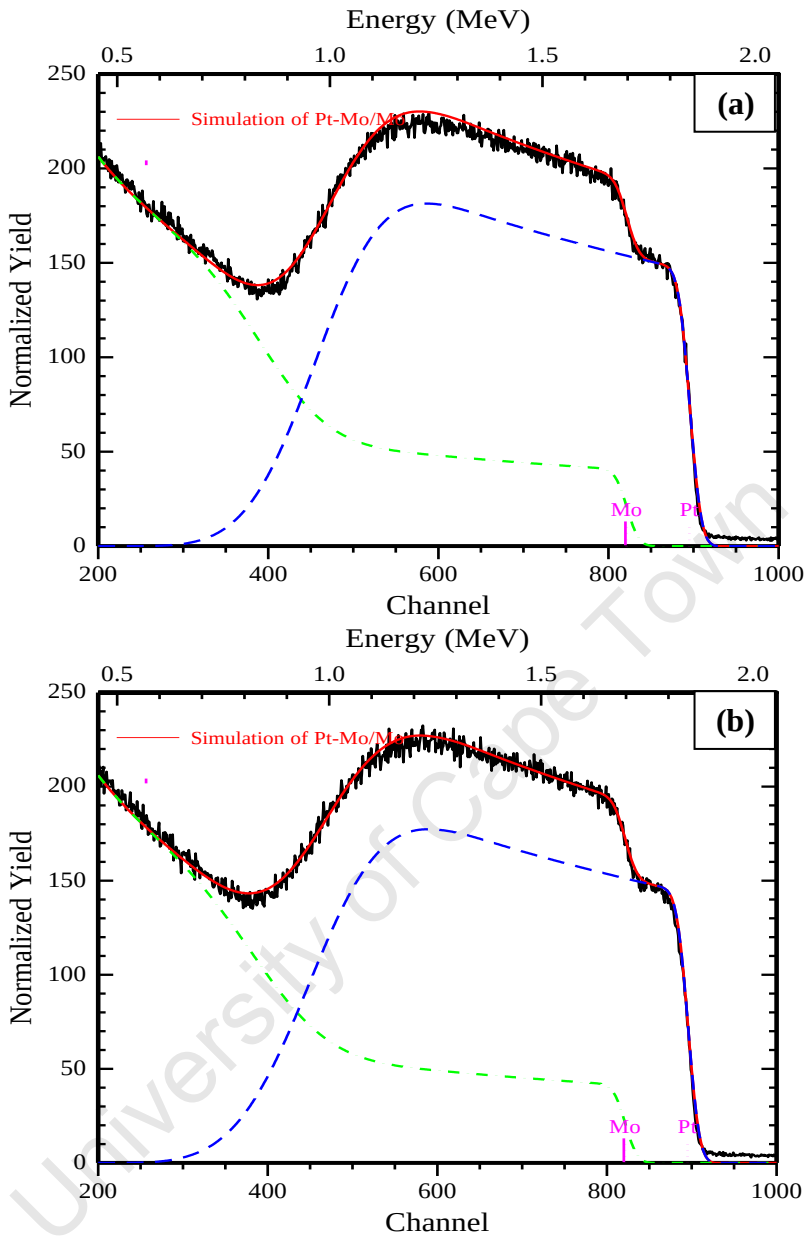

Figure 4.4: RBS results of 0.3 µm Pt coating annealed at 900°C for: (a) 8 hours and (b) 24 hours. The blue and green dash lines illustrate the distribution of Pt and Mo, respectively

4.1.3 Scanning Electron Microscopy (SEM) and EDX

Surface morphology of as-deposited and annealed 0.3 µm coating system was also investigated by scanning electron microscope (SEM), Fig. 4.5 to 4.6. The scanning electron microscope images revealed the change in coating morphology as a consequence of annealing. It was observed that deposited Pt layer followed the substrate morphology, Fig. 4.5, while the surface roughness increased with annealing time, Fig. 4.6 (a-c). No cracks in the as-deposited Pt film deposited by sputtering when compared to the as-deposited Pt film prepared by EBE.

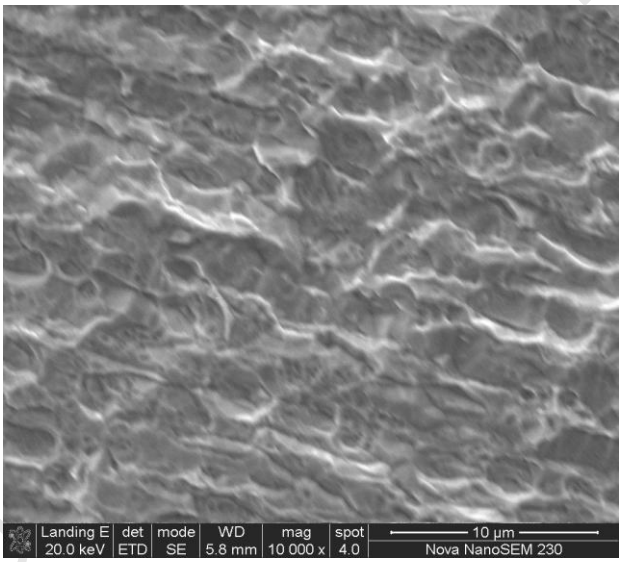

Figure 4.5: SEM image of the as-deposited 0.3 µm Pt layer

The longer annealing time of 8 and 24 hours caused insignificant changes on the coating morphologies as "spongy looking areas", indicated on the images, were observed on the coating surfaces. The compositional analysis was performed on both as-deposited and annealed coated

systems using EDX. The data was acquired on the areas of the micrographs, approximately 30μm^2, and the results are given in table 4.2.

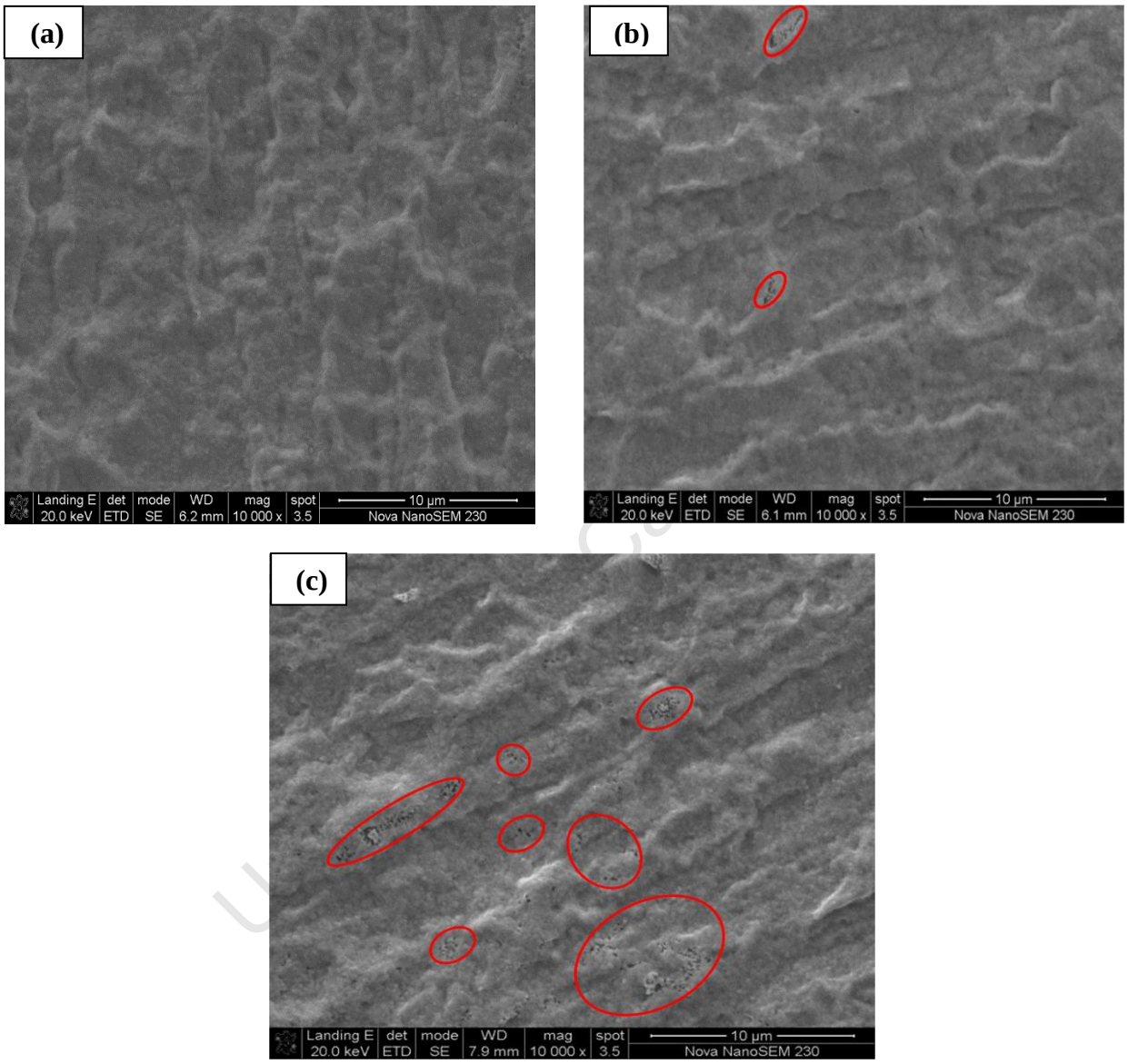

Figure 4.6: SEM images of 0.3 μm Pt coatings annealed at 900°C for: (a) 1 hour, (b) 8 hours and (c) 24 hours. The red ellipses show the spongy looking regions

The result of the as-deposited sample shows that only Pt was detected on the surface of the coating indicating that the electron beam had not penetrated the film to the Mo substrate. This was not entirely unexpected as the depth of X-ray penetration in Pt, calculated using equation 3.3, was found to be 0.32 μm. The average Pt composition on the coating annealed for 1 hour was 61 *at%*. These results are consistent with the RBS results which gave the average Pt concentration of approximately 63 *at%*, table 4.1.

Table 4.2: Elemental composition of 0.3 μm Pt coatings in as-deposited and annealed (900°C for 1, 8 and 24 hours) conditions

Sample	Molybdenum (*at* %)	Platinum (*at* %)
0.3 μm Pt/Mo as-deposited	**0**	**100**
0.3 μm Pt/Mo 900°C/1 hour	**39**	**61**
0.3 μm Pt/Mo 900°C/8 hours	**53**	**47**
0.3 μm Pt/Mo 900°C/24 hours	**54**	**46**

The Pt content in the samples annealed for 8 and 24 hours was reduced to the range of 46 *at%* to 47 *at%*, see table 4.2. This compositional range is also comparable to RBS results of the same samples, table 4.1, as RBS simulation also revealed the presence of only one layer with approximately 1:1 Pt to Mo ratio on both coatings.

4.2 The characterisation of 0.5 µm Pt layer coatings

4.2.1 X-ray diffraction (XRD) results

The XRD results of the 0.5 µm Pt coated system are shown in Fig. 4.7. The analysis showed the presence of two Pt-Mo compounds, Pt_2Mo and PtMo, after annealing at 900°C for 1, 2, 4 and 8 hours. The Pt_2Mo phase was not detected after annealing the 0.2 µm and 0.3 µm systems at 900°C for 8 hours. However, in 0.5 µm system the Pt_2Mo phase and unknown reflections associated with it were still present after annealing for 8 hours, Fig. 4.7. With more Pt to react, one expects the Pt_2Mo phase to be present for a longer time.

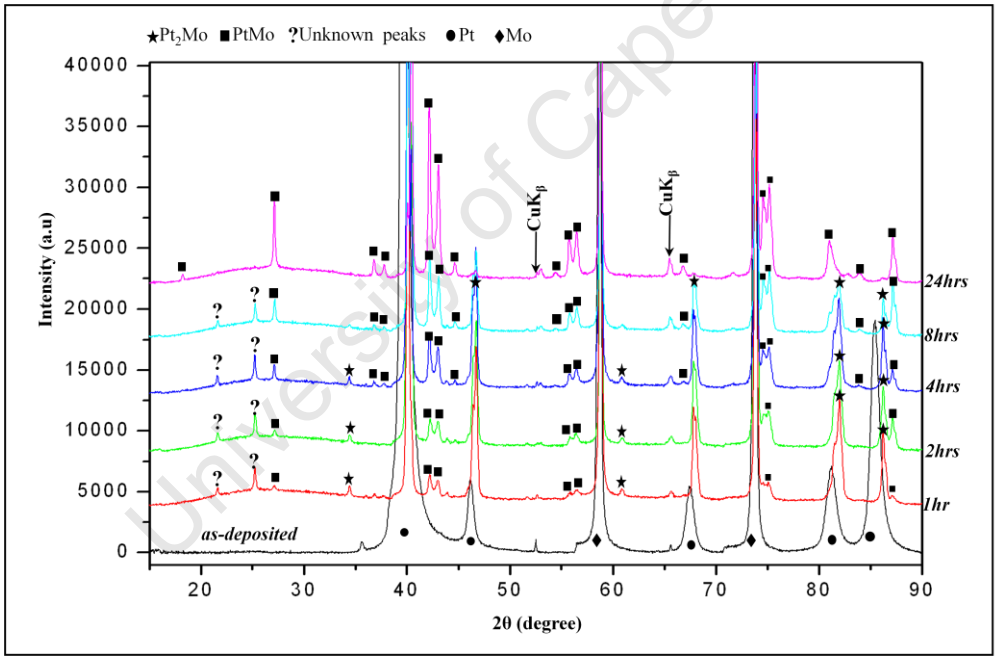

Figure 4.7: X-ray diffraction patterns of 0.5 µm Pt layer deposited on Mo substrate in as-deposited condition and annealed at 900°C for 1, 2, 4, 8 and 24 hours. CuK_β line was also diffracted and detected due to the strongest intensities of Mo peaks at 2θ = 58.61° and 73.68°

This phase, Pt_2Mo, disappeared after annealing the 0.5 µm system for 24 hours while the intensity of the diffraction peaks of the PtMo phase increased significantly, Fig. 4.7. RBS analytical technique was employed to study compound composition that results after annealing the 0.5 µm thick system at a fixed temperature for different times.

4.2.2 Rutherford Backscattering Spectrometry (RBS)

The RBS results of the 0.5 µm coated system are given in Fig. 4.8 to 4.10. The simulation of the as-deposited 0.5 µm is shown in Fig. 4.8.

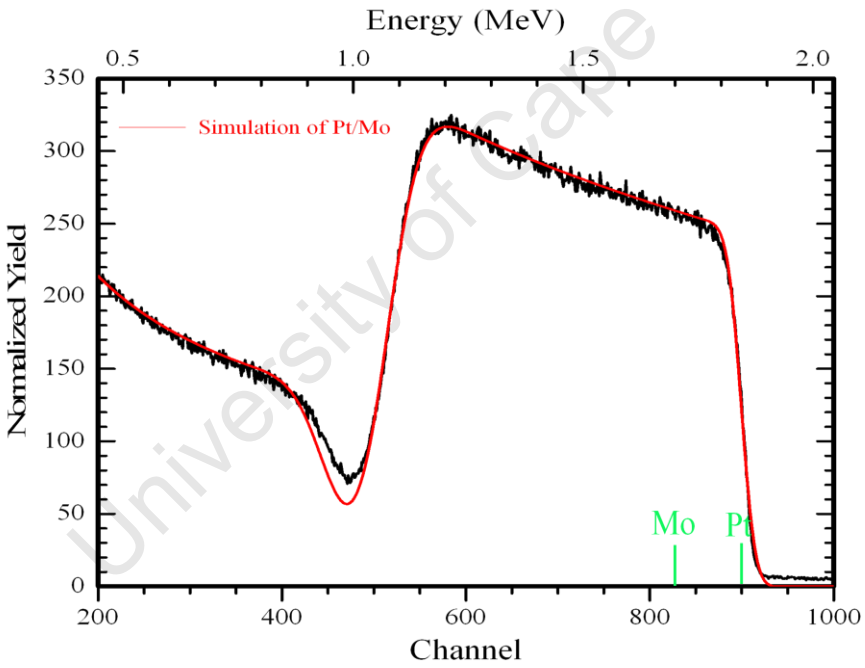

Figure 4.8: RBS results of the as-deposited 0.5 µm Pt layer

The thickness of the as-deposited coating was found, by simulation, to be 3600.00×10^{15} atoms/cm^2 (0.54 µm) which is comparable to the coating thickness given by thickness monitor

during sputtering deposition (0.5 µm), table 4.3. Two layers were obtained by simulating the spectrum of the coating annealed at 900°C for 1 hour with 3:1 and 1:1 Pt to Mo ratios in the first and second layer, respectively, Fig. 4.9 (a).

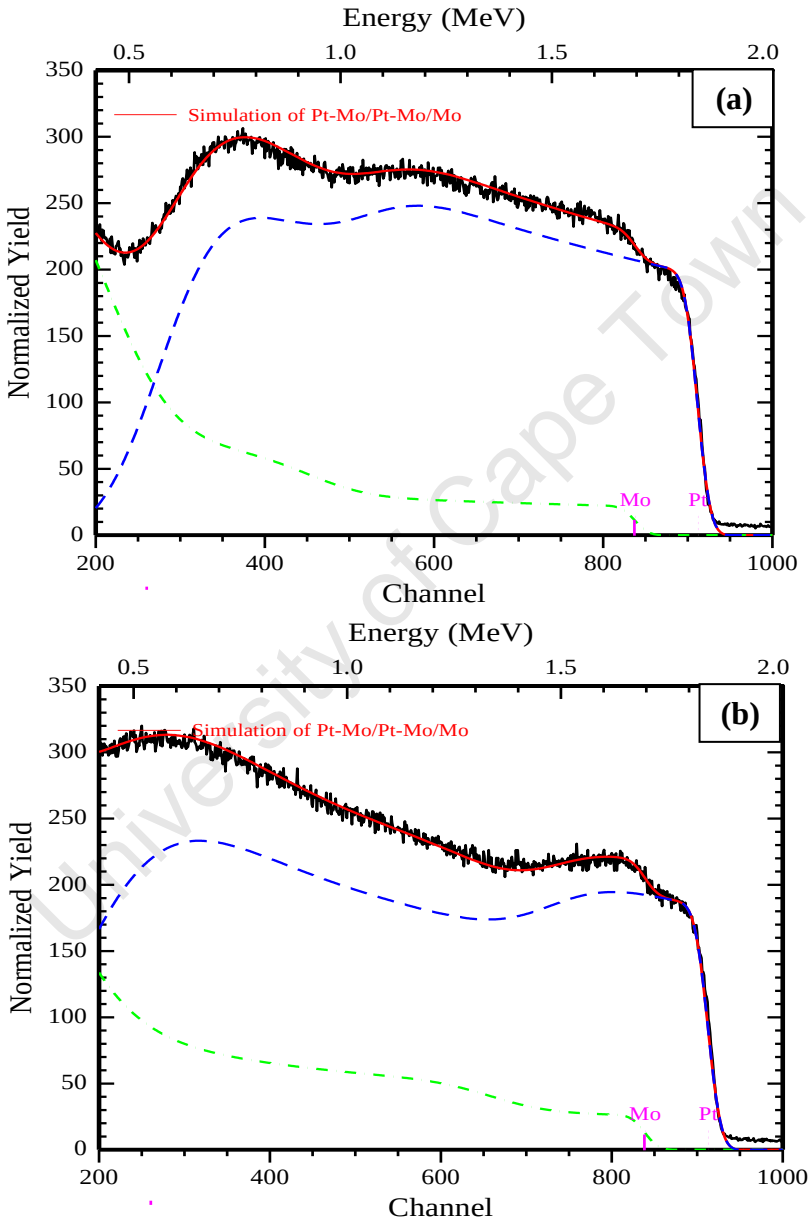

Figure 4.9: RBS results of 0.5 µm Pt coatings annealed at 900°C for: (a) 1 hour and (b) 8 hours. The blue and green dash lines illustrate the distribution of Pt and Mo, respectively

These results complement the XRD findings as two phases, Pt_2Mo and PtMo, were detected in this coating system. The phase analysis performed on the 0.5 µm coating annealed for 8 hours still revealed the presence of the Pt_2Mo phase. Therefore, RBS was carried out in order to obtain the compound composition of this phase at these annealing conditions (900°C for 8 hours). The coating was simulated and two layers were obtained having different compositions, Fig. 4.9 (b). These phases were also obtained in the coating annealed for 1 hour. However, the compositions of Pt and Mo as well as the thickness of the layers were not the same, see table 4.3.

Table 4.3: Coating thickness and phase composition of 0.5 µm Pt coatings in as-deposited and annealed (900°C for different times) conditions

Sample	Coating thickness (atoms/cm2)	Coating thickness (µm)		Coating layer/s	Phase composition (*at%*)
As-deposited	**3600.00**	**0.54**		**1**	**Pt (100)**
0.5 µm Pt/Mo 900°C/1 hour	**3800.00**	**0.63**	**0.98**	**1**	**Pt(73) and Mo(27)**
	2300.00	**0.35**		**2**	**Pt(53) and Mo(47)**
0.5 µm Pt/Mo 900°C/8 hours	**1780.00**	**0.30**	**1.15**	**1**	**Pt(68) and Mo(32)**
	5570.00	**0.85**		**2**	**Pt(50) and Mo(50)**
0.5 µm Pt/Mo 900°C/24hours	**7550.00**	**1.19**		**1**	**Pt(49) and Mo(51)**

The ratio of Pt to Mo in the second layer was approximately 1:1 after annealing for 1 and 8 hours. It was observed that the Pt to Mo ratio in the first layer was approximately 3:1 after 1 hour and 2:1 after 8 hours. Despite different Pt to Mo compositional ratios, XRD detected one Pt rich

compound, Pt_2Mo, on both coating samples. Therefore, these results are still consistent with the observation made earlier in this investigation that Pt_2Mo phase exist over a broad compositional range. These results also confirm that Pt_2Mo phase was present after annealing for 8 hours in the thick coating (0.5 μm) which is not the case in the thin coatings (0.2 μm and 0.3 μm). It can be mentioned that the disappearance of this compound, Pt_2Mo, was detected by XRD to only have taken place after 24 hours in the 0.5 μm thick coating system. Therefore, the RBS analysis was performed in order to study the compound composition present in this sample, Fig. 4.10.

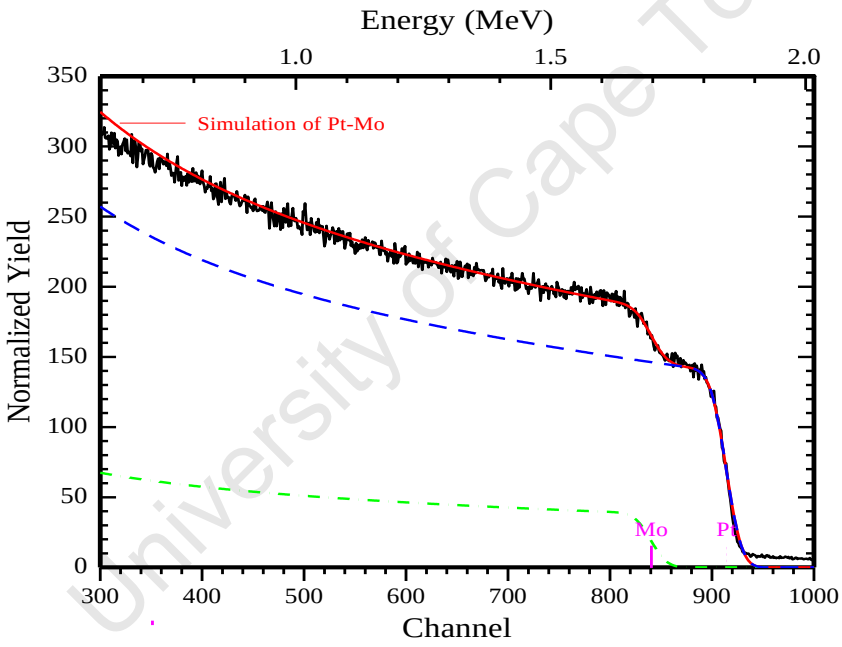

Figure 4.10: RBS results of 0.5 μm annealed at 900°C for 24 hours. The blue and green dash lines illustrate the distribution of Pt and Mo, respectively

One layer was obtained after simulating the RBS spectrum of this sample. The composition of this layer corresponds to the stoichiometry of PtMo phase, see table 4.3, which complements the

XRD results of the same coating. It should be pointed out that the coating thickness in this system, 0.5 µm, increased to approximately 1 µm after annealing, table 4.3.

4.2.3 Scanning Electron Microscopy (SEM) and EDX

The surface morphologies of thick Pt coatings (0.5 µm) before and after annealing have been analysed, Fig. 4.11 to 4.12. No noticeable differences between the morphology of the as-deposited 0.5 µm, Fig. 4.11, and the substrate morphology in which the coating system was deposited on, Fig. 3.6 (a).

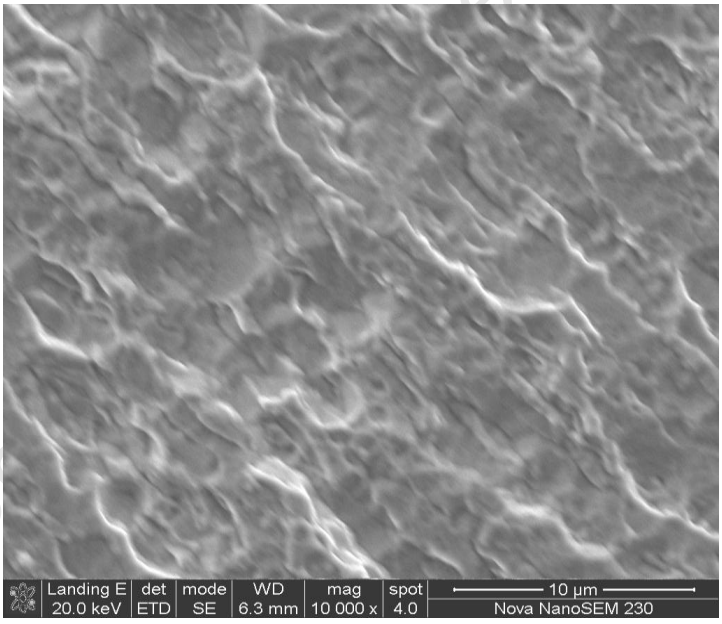

Figure 4.11: SEM image of 0.5 µm Pt layer in as-deposited condition

The coating morphology changed significantly after annealing. The scanning electron microscope images revealed the presence of "precipitates" evenly distributed across the coating surface. The size of the precipitates was approximately 5-10 nm.

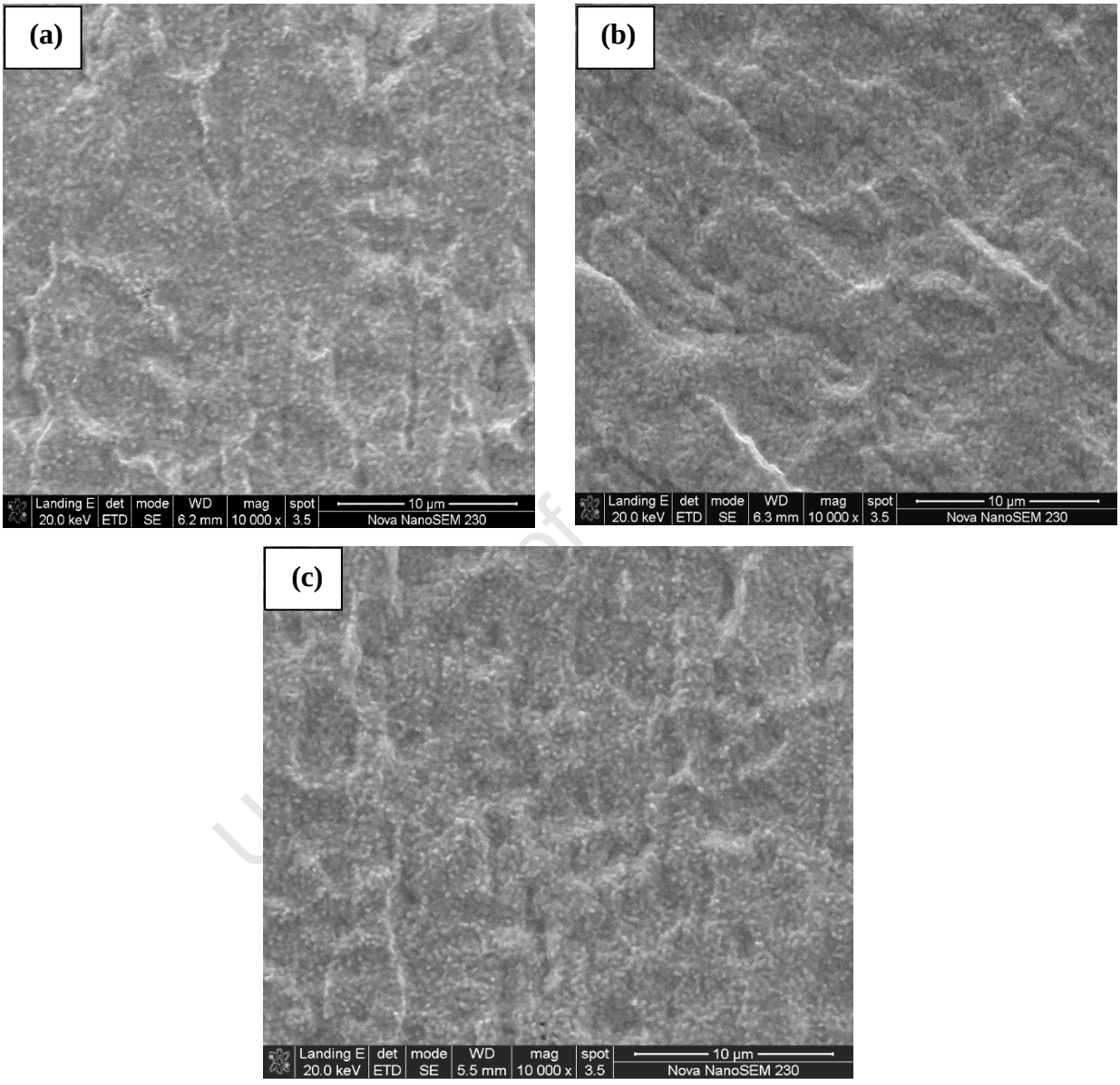

Figure 4.12: SEM images of 0.5 µm Pt coatings annealed at 900°C for: (a) 1 hour, (b) 8 hours and (c) 24 hours

The elemental composition analysis was performed by means of EDX on all annealed and as-deposited coatings and the results are summarised in table 4.4. The composition of Pt on the annealed samples, at 900°C for 1, 8 and 24 hours, was 65 *at%*, 55 *at%* and 46 *at%*, respectively. These results are consistent with RBS results of these coatings, table 4.3. The average Pt concentration of the two layers obtained from RBS simulation of the coating annealed at 900°C for 1 hour is about 65 *at%* which is consistent with EDX results of the same sample (65 *at%*).

Table 4.4: Elemental composition of 0.5 µm Pt coatings in as-deposited and annealed (900°C for 1, 8 and 24 hours) conditions

Sample	Molybdenum (*at* %)	Platinum (*at* %)
0.5 µm Pt/Mo as-deposited	**0**	**100**
0.5 µm Pt/Mo 900°C/1 hour	**35**	**65**
0.5 µm Pt/Mo 900°C/8 hours	**45**	**55**
0.5 µm Pt/Mo 900°C/24hours	**54**	**46**

The other coatings annealed for 8 and 24 hours had Pt concentration, from RBS simulation, equals to 54 *at%* and 49 *at%*, respectively, which are also in reasonable agreement with EDX results, 55 *at%* and 46 *at%*.

4.3 The formation of Mo rich compound

It has been observed that the phase transformation in Pt-Mo system starts from Pt rich region to Mo rich region of the phase diagram. It was predicted by EHF model that Mo rich compounds (Pt_2Mo_3 and $PtMo_6$) are the last compounds to nucleate in Pt-Mo phase sequence (section 1.3.2.2). Therefore, one selected system (0.3 µm Pt layer) was annealed at a temperature of 1200°C for periods of 2 and 24 hours. The formation of the Mo rich phase, Pt_2Mo_3, was observed in both samples, see Fig. 4.13.

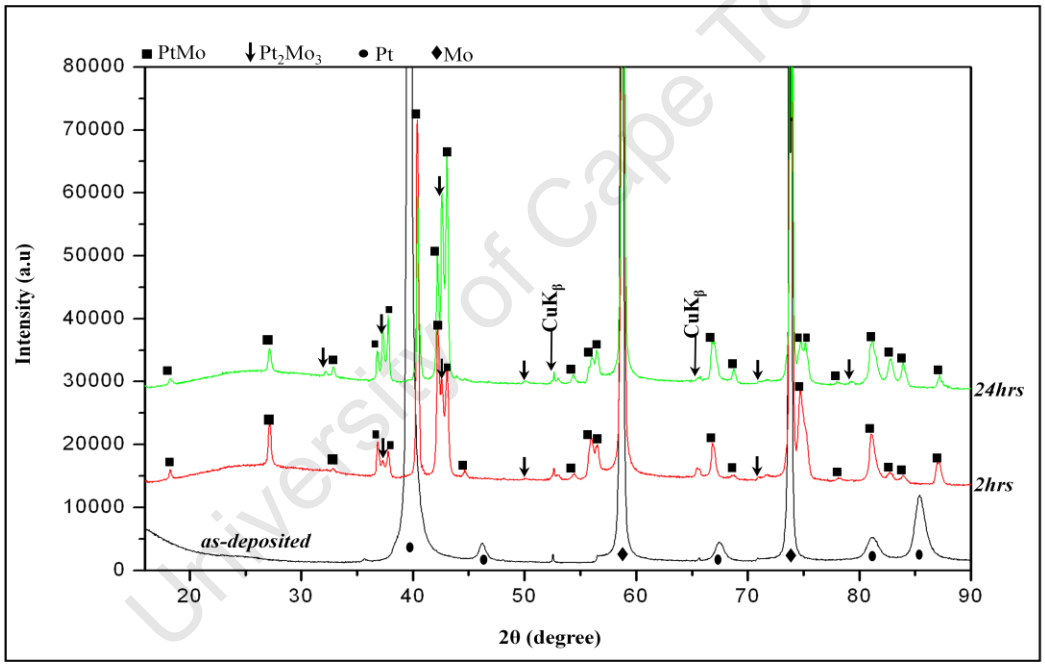

Figure 4.13: X-ray diffraction patterns of 0.3 µm Pt layer deposited on Mo substrate: as-deposited sample and annealed samples at 1200°C for 2 and 24 hours. CuK_β line was also diffracted and detected due to the strongest intensities of Mo peaks at 2θ = 58.61° and 73.68°

The major noticeable difference between the two annealing periods (2 and 24 hours) is that some diffraction peaks of Pt_2Mo_3 phase were more pronounced after annealing for 24 hours. This indicates that the phase continued to grow as the annealing period was extended. It can be said, therefore, that Pt_2Mo_3 compound is indeed the third phase to nucleate in the phase sequence of Pt-Mo system as predicted by EHF model. In addition to Pt_2Mo_3 phase, XRD also detected PtMo compound in these annealing conditions (1200°C for 2 and 24 hours). Therefore, PtMo phase was observed to be a stable phase at the temperatures 900°C and below, and the Pt_2Mo_3 phase appears to require a temperature of approximately 1200°C in order to nucleate.

CHAPTER 5 SUMMARY AND DISCUSSION

Several complementary techniques have been used to study the effects of annealing on phase transformation in the Pt coated Mo systems. Phase analysis was performed by X-ray diffraction (XRD) while the Rutherford backscattering spectrometry (RBS) was used to determine the compounds composition and coating thickness. The changes in coating morphology caused by annealing treatment and subsequent formation of Pt-Mo intermetallics were investigated by scanning electron microscopy (SEM). The changes caused by high temperature were investigated as a function of coating thickness, the deposition method and annealing conditions (temperature and time). Variety of coated systems were investigated in this study: (i) 0.2 µm Pt layer, (ii) 0.3 µm Pt layer, (iii) 0.5 µm Pt layer, (iv) co-deposited 2Pt:1Mo layer, and (v) co-deposited 4Pt:1Mo layer deposited on Mo-substrates.

This project studied the phase formation sequence in the Pt-Mo system. The EHF model predicted that the phase formation in the Pt-Mo system starts from Pt rich region to Mo rich region of the phase diagram. In order to confirm these predictions, the selected 0.2 µm Pt coating system was annealed at a temperature of 840°C and analysed by means of XRD and RBS and the following findings can be discussed: One phase, Pt_2Mo, was detected by XRD in the sample annealed for 1 hour while two phases (Pt_2Mo and PtMo) were detected in the sample annealed for 8 hours suggesting that Pt_2Mo is the first phase to form. The simulation of the RBS spectrum of the sample annealed for 1 hour revealed the presence of one layer with the stoichiometry of approximately 3:1 Pt to Mo indicating that there was more Pt composition than the expected 2:1 Pt to Mo compositional ratio of the Pt_2Mo phase detected by XRD. The detected Pt_2Mo phase by XRD and the excess Pt composition given by RBS analysis is in reasonable agreement with the

two-phase region (Pt_2Mo plus Pt-solid solution) reported in the region above 70 *at%* of Pt-Mo phase diagram. It is also in agreement with EHF prediction, see table 1.2. In the sample annealed for 8 hours, the RBS analysis revealed the presence of two layers containing approximately 2:1 and 1:1 Pt to Mo ratios which was in good agreement with Pt_2Mo and PtMo phases detected by XRD in the same sample.

The phase analysis was also investigated at high annealing temperature of 900°C for different annealing periods (1, 2, 4, 8 and 24 hours) in 0.2 µm system. The phase analysis showed the presence of two phases after annealing for 1 hour (Pt_2Mo and PtMo) and no changes, in terms of the phase formation, were observed until 8 hours. Only the PtMo phase was present after annealing for 8 and 24 hours and the results were consistent to RBS analysis, see table 5.1.

Table 5.1: Comparison of XRD and RBS results of 0.2 µm Pt coatings annealed at 900°C for 1, 8 and 24 hours

Sample	XRD: Phase detected	RBS: Phase composition (*at%*)
0.2 µm Pt/Mo 900°C/1 hour	**Pt_2Mo and**	**Pt(73) and Mo(27)**
	PtMo	**Pt(53) and Mo(47)**
0.2 µm Pt/Mo 900°C/8 hours	**PtMo**	**Pt(50) and Mo(50)**
0.2 µm Pt/Mo 900°C/24hours	**PtMo**	**Pt(49) and Mo(51)**

Phase analysis also found a number of unidentified diffraction peaks. These diffraction peaks were later concluded to be related to the Pt_2Mo phase due to the observation that the peaks

disappeared together with the diffraction peaks assigned to Pt_2Mo phase after annealing for 8 and 24 hours. These results indicated that PtMo phase was growing at the expense of Pt_2Mo phase.

It should be pointed out that the XRD results for phase analysis were not entirely in agreement with RBS analysis for compound composition based on the formation of the Pt_2Mo phase after annealing at 840°C and 900°C for 1 hour. The expected stoichiometry of Pt_2Mo phase is 2:1 Pt to Mo and RBS simulation of these samples gave about 3:1 stoichiometry. Therefore, the Pt_2Mo phase detected by XRD at low annealing time (1 hour) was more Pt rich according to RBS. However, this has also been attributed to XRD inability to detect the presence of Pt-solid solution phase. RBS also revealed the existence of a second layer in the sample annealed at 900°C for 1 hour. The layer had a composition of approximately 1:1 Pt to Mo which complimented the stoichimetry of PtMo phase detected by XRD in the same sample. In addition, the compound composition analyses of the two coatings, annealed at 900°C for 8 and 24 hours, revealed the presence of one layer with roughly 1:1 Pt to Mo ratio, which was also consistent with PtMo phase detected by XRD in these coating samples. The thickness analyses by RBS of this coating system (0.2 µm) showed an increase to about 0.4 µm after annealing. This was approximately the expected thickness, particularly in the samples containing 1:1 stoichiometry, due to the comparable atomic size of Pt and Mo (≈ 2.8 Å) **[1]**.

The existence of the Pt_2Mo phase over a wide compositional range was confirmed by the co-deposition of Pt and Mo with stoichiometry of approximately 2:1 and the sample was analysed by XRD and RBS. In addition, the sample with 4:1 ratio of Pt to Mo was also included for comparison. XRD analyses revealed only the diffraction peaks of Pt and Mo on the as-deposited samples. All co-deposited samples were then annealed at a temperature below the formation of

Pt-Mo phases (750°C) for 1 hour. RBS analyses showed no changes in terms of compound composition and thickness when compared to the as-deposited sample. After annealing, XRD analysis revealed the presence of Pt_2Mo phase detected on both co-deposited samples. These results confirmed the existence of Pt_2Mo phase over a wide Pt compositional range from 65 *at%* to 80 *at%*. It should be noted that this phase (Pt_2Mo) at high Pt composition is believed to coexist with Pt-solid solution.

The SEM results of 0.2 µm system showed that the coatings were affected by annealing conditions used in this study. The spongy looking surface morphologies were observed on the annealed coatings. Surface cracks were also observed on these coatings and were more pronounced after extending the annealing time to 4 and 8 hours. The cracks observed in this coating system (0.2 µm Pt) were attributed to the difference in the coefficient of thermal expansion of Pt and Mo which are $9.1\times10^{-6}/^{\circ}C$ and $4.9\times10^{-6}/^{\circ}C$, respectively **[1]**. The EDX analysis was performed on the 0.2 µm coating systems for average composition. The results, however, proved that the energy of the electron beam (20 keV) was too high to probe not only the coating layer, but also penetrated through to the substrate (Mo). Therefore the EDX results could not be used to compare with compound composition analysis by RBS. The EDX attached TEM analysis was alternatively used for elemental composition across the cross-section of the coating annealed at 900°C for 1 hour. The EDX results obtained were reasonably consistent to the results of the RBS technique. RBS and TEM analyses showed, therefore, that Pt_2Mo phase which was detected by XRD in this sample (annealed for 1 hour at 900°C) has more Pt composition, approximately 3:1 Pt to Mo ratio, than expected 2:1 Pt to Mo stoichiometry.

The focus was also placed on the investigation of the effect of increasing Pt coating thickness on the phase formation in Pt-Mo system. The thick coatings (0.3 µm and 0.5 µm) were prepared

onto Mo substrate using sputtering. The annealing of the 0.3 µm systems showed similar phase formation as observed in 0.2 µm system annealed at the same conditions. RBS and EDX results of 0.3 µm system also gave comparable results to XRD, see table. 5.2.

Table 5.2: Comparison of XRD, RBS and EDX results of 0.3 µm Pt coatings annealed at 900°C for 1, 8 and 24 hours

Sample	XRD: Phase detected	RBS: Phase composition (*at%*)	EDX: Average Pt and Mo coating composition (*at%*)
0.3 µm Pt/Mo 900°C/1 hour	**Pt_2Mo and**	**Pt(73) and Mo(27)**	**Pt (61) and Mo (39)**
	PtMo	**Pt(53) and Mo(47)**	
0.3 µm Pt/Mo 900°C/8 hours	**PtMo**	**Pt(50) and Mo(50)**	**Pt (47) and Mo (53)**
0.3 µm Pt/Mo 900°C/24hours	**PtMo**	**Pt(49) and Mo(51)**	**Pt (46) and Mo (54)**

In addition, the phase analysis showed that annealing the Pt coated systems (0.2 µm, 0.3 µm and 0.5 µm) at 900°C for 1 hour, same Pt-Mo compounds nucleated (Pt_2Mo and PtMo). However, in 0.2 µm and 0.3 µm Pt coating systems the Pt_2Mo phase was no longer present after annealing for 8 hours, while in 0.5 µm system the phase was still present. The Pt_2Mo phase only disappeared after annealing the thick coating at 900°C for 24 hours. These results were complemented by RBS and EDX analyses, table 5.3.

It should be noted that the Pt_2Mo phase detected after 1 hour had 3:1 Pt to Mo ratio while a 2:1 stoichiometry of Pt_2Mo phase was detected after 8 hours of annealing (table 5.3). This verified that the Pt_2Mo phase can exist over a broad compositional range.

Table 5.3: Comparison of XRD, RBS and EDX results of 0.5 µm Pt coatings annealed at 900°C for 1, 8 and 24 hours

Sample	XRD: Phase detected	RBS: Phase composition (*at%*)	EDX: Average Pt and Mo coating composition (*at%*)
0.5 µm Pt/Mo 900°C/1 hour	Pt_2Mo and	Pt(73) and Mo(27)	Pt (65) and Mo (35)
	PtMo	Pt(53) and Mo(47)	
0.5 µm Pt/Mo 900°C/8 hours	Pt_2Mo and	Pt(68) and Mo(32)	Pt (55) and Mo (45)
	PtMo	Pt(50) and Mo(50)	
0.5 µm Pt/Mo 900°C/24 hours	PtMo	Pt(49) and Mo(51)	Pt (46) and Mo (54)

The SEM images showed that the morphology of the coating changes with increase in annealing time as well as the thickness of the coating. SEM analysis revealed that the coating surface deteriorated by increasing annealing time in 0.2 µm coating system. However, as the coating thickness was increased to 0.3 µm and 0.5 µm and annealed at similar conditions the SEM analysis showed no significant surface defects. The deterioration of the coating surface of the 0.2 µm system might not only be due to the thin layer of Pt, however, because the thick (0.3µm and 0.5 µm) coating systems were prepared by sputtering method while the thin (0.2 µm) system was prepared by EBE. In sputtering coating technique, the sputtered atoms arrive at the substrate surface with much higher energies than evaporated atoms **[35]**. This therefore improves the bonding between the substrate and the coating material and the formation of a coating layer which sticks firmly on the substrate surface.

A molybdenum rich phase (Pt_2Mo_3) was detected by XRD after annealing one coating system (0.3 µm) at high temperature (1200°C) for 2 and 24 hours. The intensity of diffraction peaks corresponding to this phase was more pronounce after 24 hours which was associated to the growth of the phase at this annealing period. Our results, therefore, verified that Pt_2Mo_3 phase is the third phase to nucleate in Pt-Mo phase sequence, as predicted by EHF model.

CHAPTER 6 CONCLUSION

The aim of this research project was to investigate the first phase formation as well as phase sequence in the Pt-Mo system as a function of annealing parameters (temperature and time) by complementary techniques. Based on the EHF model predictions which predicted Pt_2Mo/Pt-solid solution, PtMo, Pt_2Mo_3 and $PtMo_6$ phases to form sequentially during the annealing of a Pt coated Mo system, see fig. 6.1 (a), the following can be concluded:

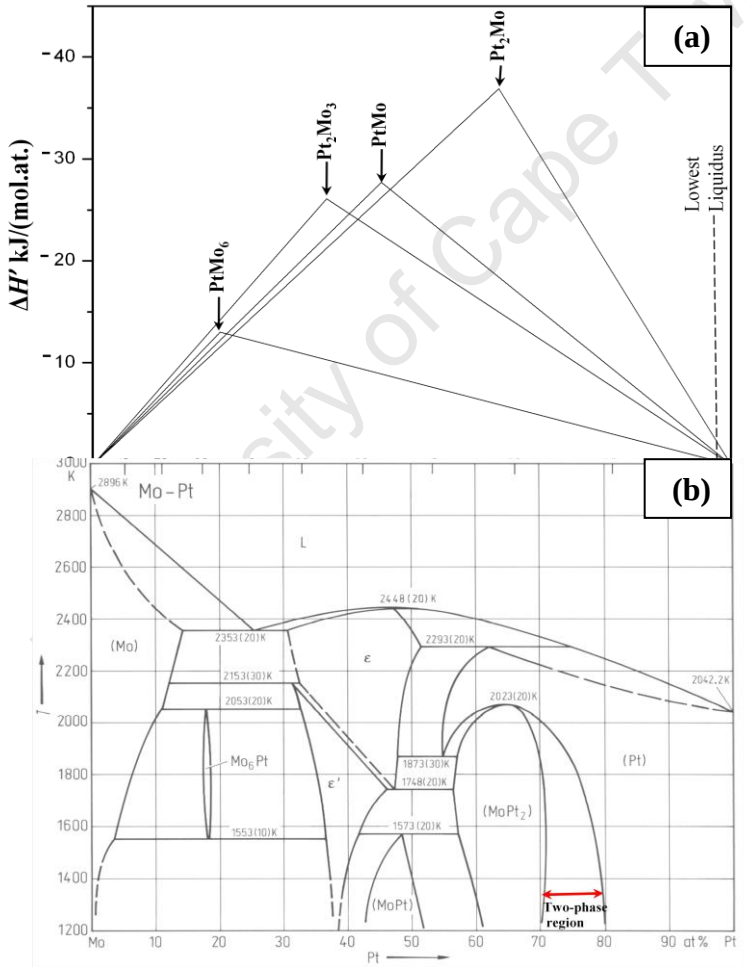

Figure 6.1: (a) The effective heat of formation (*ΔH'*) diagram for compound formation and (b) the Pt-Mo phase diagram

i. The Pt_2Mo phase was observed to be the first compound to nucleate after annealing the 0.2 µm Pt coated Mo system at 840°C for 1 hour, according to XRD analysis. However, the excess Pt composition obtained by RBS analysis of the same sample, table 3.4, was believed to be contributed by the presence of Pt-solid solution, and with EHF model predicting the possibility of the Pt_2Mo phase and Pt-solid solution nucleating simultaneously, it can therefore be said that the results are in reasonable agreement with the EHF model predictions. In addition, the results are also in good agreement with the two-phase structure existing in the 70 *at%* to 80 *at%* Pt range of the Pt-Mo phase diagram, Fig. 6.1 (a).

ii. The second phase is PtMo which is also in good agreement with the EHF predictions and the phase was observed to form as the annealing time was extended to 8 hours at 840°C. In addition, the Pt_2Mo phase was also detected in these annealing conditions, however, with a reduced Pt composition and thickness (table 3.4). It appears, therefore, that initial composition shows when the Pt_2Mo phase form is in the excess of Pt which is in agreement with the proposed two-phase Pt_2Mo plus Pt-solid solution. The fact is that, as the reaction continues the composition in the excess phase reacts to form the PtMo phase leaving behind the Pt_2Mo phase with the expected composition. This observation was also confirmed when comparing the 0.3 µm system annealed at 900°C for 1 and 4 hours, table 4.1, as well as 0.5 µm system annealed at 900°C for 1 and 8 hours, table 4.3.

iii. The third phase in Pt-Mo phase sequence is Pt_2Mo_3 which was detected after annealing the 0.3 µm coating system at high temperature (1200°C) for different periods (2 and 24 hours). The Pt_2Mo_3 phase, therefore, appears to only form at high temperature of about 1200°C.

The phase analysis results show that the phases determined in the Pt coated Mo systems are in reasonable agreement with the phase sequence predictions made by effective heat of formation (EHF) model. The phase formation sequence results of this investigation are believed to be of great importance to the material scientists when targeting a particular phase or phases with special properties for a specific application.

REFERENCES

1. W.D. Callister. Jr., Material Science and Engineering (6th edition), John Wiley and Sons, (2003).

2. A.J. Ardell and K. Janghorban, F.V. Nolfi, Jr., Phase Transformations during irradiation, Applied Science Publishers, (1982).

3. G.L. Selman, Platinum Metals Rev., 11 (1967) 132-137.

4. D. Stojic, T. D. Grozdic, M. P. Marceta Kaninski, A. D. Maksic, N. D. Simic, International J. Hydrogen Energy, 31 (2006)841-846.

5. D. Stojic, T. D. Grozdic, M. P. Marceta Kaninski, V. D. Stanic, International J. Hydrogen Energy, 32 (2007)2314 – 2319.

6. A.S. Darling, and G. L. Selman, Platinum Metals Rev., 12 (1968) 92.

7. M. Carelse, C.I. Lang, Scripta Materialia, 54 (2006) 1311.

8. T. Biggs, S.S Taylor, E. Van der Linden, Platinum Metals Rev., 49 (2005) 2.

9. R.P. Elliot, Constitution of Binary Alloys, First Supplement, McGraw-Hill, New York, (1965) 63.

10. H.P. Rooksby and Lewis, J. Less-Common Metals, 6 (1964) 451-460.

11. A.E. Dwight, R.A. Conner, Jr. and J.W. Downey, Acta Crystallogr., 18 (1965) 835

12. V. Sadagopan, H.C. Gatos and B.C. Giessen, J. Phys. Chem. Solids, 26 (1965) 1687.

13. E. Raub and E. Roschel, Naturwiss, 53 (1966) 17.

14. A. Maldonaldo and K. Schubert, Z. Metallik., 55 (1964) 619-626.

15. H. Ocken and J. H. N. Van Vucht, J. Less-Common Metals, 15 (1968) 193-199.

16. R. Flukiger, K. Yvon, C.P. Susz, R. Roggen, A. Paoli, J. Muller, J. Less-Common Metals,32 (1973) 207-225.

17. L. Brewer, R.H. Lamoreaux, Bull. Alloy Phase Diagrams, 1 (1980) 89-91.

18. R.P. Walters, B.S. Covino, Jr., Metallurgical transactions, 19A (1988) 2164-2165.

19. M.Y. Benarchid, N. David, J. M. Fiorani, M. Vilasi, T. Benlaharche. J. Chem. Thermodynamics, 41 (2009) 383-385.

20. J.M. Jaksic, L. Vracar, S.G. Neophytides, S.Zafeiratos, G. Papakonstantinou, N.V. Krstajic, M.M. Jaksic, Surface Science, 598 (2005) 156-173.

21. P.G. Shewmon, Diffusion in solids, McGraw-Hill Book, (1963).

22. C. Kittel, introduction to solid state physics, 8th edition, John Wiley and Sons, (2005).

23. J.S. Kirkaldy and D.J. Young, Diffusion in the condensed state, Maney Pub,(1988).

24. J.H. Westbrook and R.L. Fleischer, Intermetallic Compounds (Volume 1-Principles), John Wiley and Sons, (1995).

25. R.M. Walser and R.W. Bene, Appl. Phys. Lett., 28 (1978) 624.

26. B.Y. Tsaur, S.S. Lau, J.W. Mayer, and M.A. Nicolet, Appl. Phys. Lett., 38 (1981) 922.

27. R.W. Bene, Appl. Phys. Lett., 41 (1982) 529.

28. R. Pretorius, Mater. Res. Soc. Symp. Proc., 25 (1984) 15.

29. R. Pretorius, C.C. Theron, A.C. Vantomme, J.C. Mayer, Crit Rev Solid State Mater Sci., 24 (1999) 1–62.

30. R. Pretorius, R.de Reus, A.M. Vredenberg and F.W.Saris, Mater. Lett., 9 (1990) 494.

31. R. Pretorius, A.M. Vredenberg and F.W.Saris, R.de Reus, J. Appl. Phys., 70 (1991) 3636-3646.

32. R. Pretorius, T.K. Marais and C.C. Theron, Mater. Sci. Eng., 10 (1993) 1.

33. C.C. Theron, O.M. Ndwandwe, J.C. Lombaard, R.Pretorius, first phase formation at Interfaces, Materials Chemistry and Physics, 46 (1996)238-247.

34. A.M. Brown and M.F. Ashby, Acta Metall., 28 (1980) 1085.

35. C. Hood, Coating methods for use with the Platinum metals, Platinum Metals Rev., 20 (1976) 48-52.

36. J. Li, T. Malis, S. Dionne, Materials Characterization, 57 (2006) 64-70.

37. J. Mayer, L.A. Giannuzzi, T. Kamino, J. Michael, TEM sample preparation and FIB-induced Damage, MRS Bulletin, 32 (2007) 400-406.

38. M. Clancy, M.J. Pomeroy, S. Belochapkine, Microns, 43 (2012) 627-630.

39. T. Mahrtens, S. Bley, P. V. Satyam, A. Rosenauer, Microns, 43 (2012) 902-909.

40. M.T. Posterk, K.S. Howard, A.H. Johnson, and K.L. McMichael, Scanning Electron Microscopy, Ladd research Industries, (2001).

41. P.J. Goodhew and F.J.Humphreys, Electron Microscopy and Analysis (2^{nd} edition), Taylor and Francis, (1988).

42. J.I. Goldstein, D.E. Newbury, P. Echlin, D.C. Joy, A.D. Roming, Jr., C.E. Lyman, C. Fiori, and E. Lifshin, Scanning Electron Microscopy and X-Ray Microanalysis (2^{nd} edition), Plenum Press, New York and London, (1992).

43. T.E. Everhat, Simple theory concerning the reflection of electrons from solids. J.App.Phys., 31(1960).

44. K.G. Cox, N.B. Prince, and B.Harte, An introduction to the practical study of crystals, minerals and rocks, McGraw-Hill, (1968).

45. B.D. Cullity, Elements of X-ray Diffraction (2^{nd} edition), Addison-Wesley,(1978).

46. E.W. Nuffield, X-ray Diffraction Methods, John Wiley and Sons, (1966).

47. R.J.W. Weiss, Physics of Materials, Hemisphere, (1990).

48. D. McLachlan, Jr., X-ray crystal structure, McGraw-Hill, (1957).

49. W.G. Marburger and C. W. Hoffman, Physics for our Times, McGraw-Hill, (1958).

50. W. Chu, J. W. Mayer and M. Nicolet, Backscattering Spectrometry, Academic Press, New York, (1978).

51. H.R. Verma, Atomic and Nuclear Analytical Methods, Springer-Verlag Berlin Heidelberg, (2007).

Appendix

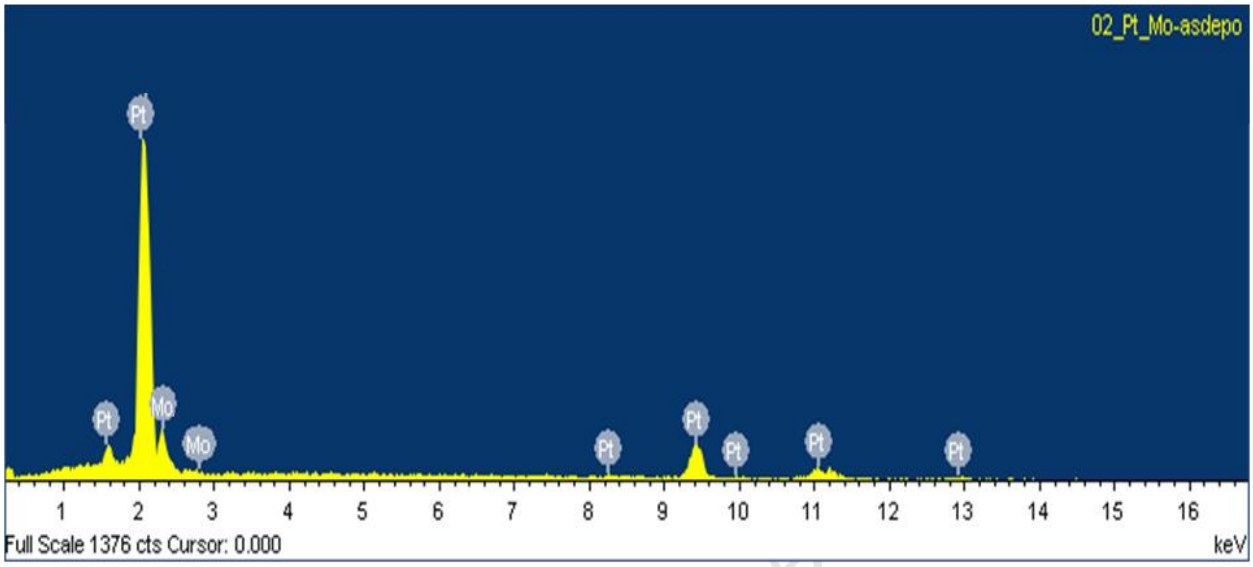

Figure A. EDX spectrum of as-deposited 0.2 µm Pt coating. The spectrum shows the X-ray emission lines for Pt and Mo elements

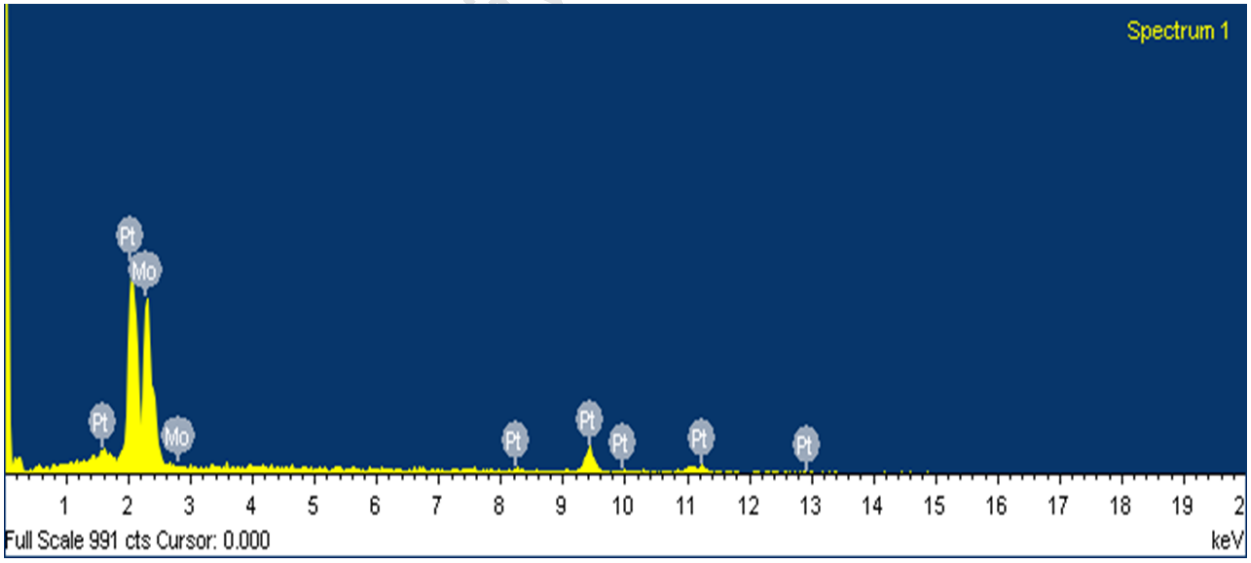

Figure B. EDX spectrum of 0.2 µm Pt coating annealed at 900°C for 8 hours. The spectrum shows the X-ray emission lines for Pt and Mo elements